2017

Nanoscale Studies of Proteins and Thin Films Using Scanning Probe Microscopy

Zachary Lane Highland
Louisiana State University and Agricultural and Mechanical College

NANOSCALE STUDIES OF PROTEINS AND THIN FILMS USING SCANNING PROBE MICROSCOPY

A Dissertation

Submitted to the Graduate Faculty of the
Louisiana State University and
Agricultural and Mechanical College
in partial fulfillment of the
requirements for the degree of
Doctor of Philosophy

in

The Department of Chemistry

by
Zachary Lane Highland
B.S., Longwood University, 2012
May 2017

Dedicated to my family and friends with love and appreciation.

ACKNOWLEDGEMENTS

First and foremost, I want to thank my professor, Dr. Jayne C. Garno for allowing me in her group. During my graduate school career, I have learned and grown immensely as a scientist and as an individual because of her guidance. Through the opportunities you have provided me, I truly have had a memorable career here at Louisiana State University.

I would like to thank all of my committee members for the insightful discussions that we have had. Your guidance has truly helped me along the way and prepared me to tackle the challenges of being a scientist in an environment that is ever changing. Your insights into my projects have helped me do the very best that I could have done.

To my friends, church members, and tailgate buddies you have truly made this journey memorable and enjoyable. With all of our laughs, day trips, and time shared together, we truly made this a memorable experience. These memories will forever be held in my heart. The encouragement you have given me through this time has gotten me through the hard parts and kept me going with a smile. From every home game to Mardi Gras parade, we were there together. The love we shared will never be forgotten. We have worked through the tough times together and have made each other stronger throughout this entire journey. We are all made better by these experiences.

To my family and my especially my parents Lynn and Craig Highland, I owe all of this to you. Without your encouragement growing up, I would not have the confidence or the determination and the discipline to complete this doctoral degree. To my grandparents: Granny Helen, Granny Sue, and Grandpa, thank you for always being there for me and encouraging me along the way. Grandpa, you instilled a love of science and always seeking the truth and discovering the unknown from an early age. You are the reason I wanted to become a scientist.

Granny Sue, you are the one who never got mad as a kid for always asking "why?" Even now, I still ask that question in search for the truth and answers. Granny Helen, thank for inspiring in me the determination to keep going, for the encouragement through the hard times. Moreover, thank you for instilling in me the love of music for when times are tough. Finally thank you for the steadfast life of following God and learning to listen. These lessons from all of my family have not gone unnoticed, nor have they gone unappreciated. Of course I could not forget my wonderful sister, Lesleigh Hope Highland. Her continued comedy has seen me through some of the hard times throughout my life. She always keeps situations real. Here's to you, Lesleigh.

TABLE OF CONTENTS

LIST OF FIGURES

ABBREVIATIONS

ABBREVIATION	NAME
AC	Alternating current
AFM	Atomic force microscope
BSA	Bovine serum albumin
DLFM	Dynamic lateral force modulation
DPN	Dip-pen nanolithography
EBL	Electron beam lithography
EDC/NHS	1-ethyl-3-(3-dimethylaminopropyl)carbodiimide · HCL/ N-hydroxysuccinimide
FITC	Fluorescein isothiocyanate
FMM	Force modulation microscopy
GFP	Green fluorescent protein
HIV	Human immunodeficiency virus
IgG	Immunoglobulin G
kHz	Kilohertz
m	Meter
MHA	16-mercaptohexadecanoic acid
MPTMS	(3-mercaptopropyl)trimethoxysilane
N	Newton
NSOM	Nearfield scanning optical microscope
OTS	Octadecyltrichlorosilane
PBS	Phosphate buffered saline

PEG	Polyethylene glycol
PDMS	polydimethylsiloxane
PMMA	Poly(methyl methacrylate)
MPT-silane	2-[methoxy(polyethyleneoxy)$_{6-9}$propyl]trichlorosilane
SAM	Self-assembled monolayer
SPL	Scanning probe lithography
SPM	Scanning probe microscopy
UV	ultraviolet

ABSTRACT

Nanostructures of organosilanes, thin metal films, and protein nanopatterns were prepared and analyzed with atomic force microscopy (AFM). Organosilanes with designed functional groups were used to selectively pattern green fluorescent protein at the nanoscale using protocols developed with particle lithography. Mesospheres are deposited onto a substrate to produce a surface mask. Organosilanes are deposited to form a matrix film surrounding nanopores for depositing proteins. The nanopatterns were characterized using AFM, after steps of particle lithography for directly visualizing surface changes. Studies with AFM also provide a compelling tool for teaching undergraduates to introduce concepts of nanoscience.

An undergraduate laboratory was developed with particle lithography to introduce the concepts of nanoscience and surface chemistry. Nanopatterns of organosilane films are prepared using protocols of particle lithography. An organic thin film is applied to the substrate using steps of either heated vapor deposition or immersion in solution. At the molecular level, two types of sample morphology can be made depending on the step for depositing organosilanes. Experience with advanced AFM instrumentation is obtained for data acquisition, digital image processing and analysis. Skills with chemical analysis are gained with bench methods of sample preparation. Concepts such as the organization of molecules on surfaces and molecular self-assembly are demonstrated with the visualization of nanopatterns prepared by students. Experiments with particle lithography can be used as a laboratory module or for undergraduate research projects, and are suitable for students with a multidisciplinary science background.

The kinetics and properties of thin gold films during dewetting were studied using AFM. Thin films of gold with varying initial thickness were first deposited onto fire polished glass slides and imaged with AFM. Next, the films were annealed for two hours, and then imaged after

annealing. Gold islands with varying degrees of separation were formed. Surface plasmon spectroscopy was also used to analyze the gold films. To further this study, a kinetic study was done. Two gold thin films of 10 nm each were imaged after being annealed for 15, 30, 45, 60 and 120 minutes. It was found that after the first 15 minutes of annealing, gold islands were observed.

CHAPTER 1. INTRODUCTION

Protocols were developed for investigations with patterned nanomaterials including organic thin films, protein nanopatterns and gold films using scanning probe microscopy (SPM). Nanopatterns of organosilanes can be prepared to define exquisite nanopatterns for the development of well-defined surfaces. Selected imaging modes were used during the course of the dissertation research to characterize samples, including tapping mode, contact mode and force modulation microscopy. In addition, a nanoscale laboratory module was developed for undergraduate students to open opportunities with nanopatterning and the atomic force microscope for the undergraduate curriculum.

Nanopatterning of proteins have been applied to create biochips, biosensors,[3, 4] and tissue engineering, [5] as well as for the study of cells.[6] Protein-protein interactions can be studied at the nanoscale using SPM in nondestructive, ambient and liquid environments. Methods used for the study of proteins at the nanoscale include microcontact printing, [7-10] nanoimprint lithography, [11-13] electron beam lithography[14-16] and scanning probe microscopy. [17, 18]

1.1 Surface Studies at the Molecular Level with Atomic Force Microscopy

Research in fields including biology, electronics, medical diagnostics, and organic films have been advanced by the sensitive measurement capabilities of SPM instruments. One of the main studies used with an AFM are performed on organic thin films. [19-22] Electronic properties of surfaces can also be ascertained from AFM measurements.[23-25] Magnetic properties of surfaces can be investigated from AFM data as well.[26, 27]

A chemically or mechanically sharpened probe is used with AFM to scan over the sample to provide detailed information of the forces between the sample and the tip. Resolution of the AFM is not limited by the diffraction of light when compared to traditional light microscopes;

resolution can be achieved at the molecular level. At least 50 measurement modes of AFM have been invented which measure the forces between the tip and the sample. There are three general imaging modes: contact, non-contact, and intermittent contact depending on how the tip is operated to scan over the sample. Detailed discussion on these selected modes will be presented in Chapter 2.

1.2 Experimental Approaches for Patterning and Imaging at the Nanoscale

Details of the imaging modes used in this dissertation are presented in Chapter 2 as well as details of the methods used for nanopatterning with particle lithography. Particle lithography with organosilanes was used to prepare nanopatterns on silicon substrates. High throughput patterning of substrates can be achieved with small amounts of dilute reagents. With particle lithography, substrates can be patterned with a resist and an active area for the selective patterning of proteins. The instrument set-up and operation for force spectroscopy and *in situ* sample modulation also will be described in Chapter 2.

1.3 Protein Patterning using Organic Thin Films

A number of methods have been reported for patterning proteins for the interface of sensing surfaces and testing platforms. An overview of protein patterning methods is presented in Chapter 3. Methods reported for protein patterning include photolithography, colloidal lithography, electron-beam lithography, microcontact printing, nanoimprint lithography, stencil lithography, biased induced lithography and nanografting. Patterning proteins can also be done with an atomic force microscope (AFM) tip, such as with dip-pen nanolithography. Examples for each method will be described.

1.4 Nanopatterning of Green Fluorescent Protein using Particle Lithography [28]

Nanoscale surface patterning of green fluorescent protein (GFP) was achieved using particle lithography as detailed in Chapter 3. During the initial step a film of (3-mercaptopropyl) trimethoxysilane with a reactive sulfhydryl head group was deposited onto the substrates (microscope glass coverslips). Next a solution of size-sorted mesospheres was deposited on top of the film and dried in ambient conditions. During the drying process, capillary action as the solvent dries draws the mesospheres together into a hexagonal arrangement. Treatment with UV-ozone exposure was used to etch away areas of the silane film that were not protected by the mesospheres. The samples were then placed into a solution of 2-[methoxy(polyethyleneoxy)6-9propyl] trichlorosilane (MPT-silane) to form a resist to prevent protein binding. Subsequently, GFP was covalently linked to the prepared nanopatterns to generate an array of protein nanopatterns.

1.5 Undergraduate Laboratory for the Preparation of Organosilane Nanopatterns[29]

An undergraduate laboratory module for the preparation of nanopatterns of octadecyltrichlorosilane is presented in Chapter 4. A few basic steps are described for preparing reproducible arrays of silane nanopatterns. Monodisperse size-sorted mesospheres (latex or silica) can be used to create arrangements of rings or holes with nanoscale dimensions. Areas of the substrate in direct contact with the mesosphere masks are protected from silane deposition. Silanes are deposited surrounding the mesospheres to form a film with nanopatterns.

1.6 Investigations of Gold Island Dewetting[30]

Atomic force microscopy studies was performed on thermally induced island formation in thin gold films deposited on fire-polished glass substrates. High-resolution AFM was used to determine the morphology of Au films prepared by electron beam deposition onto fire-polished

glass slides. The microstructure of films with a nominal thickness in the range of 2 nm to 15 nm was measured before and after annealing at 550 °C in an argon/hydrogen atmosphere for 1 hour. In addition, the films were probed using surface plasmon resonance spectroscopy in order to obtain a secondary characterization of the effects of annealing. Although annealing induced granularity in all of the films studied, films with thicknesses of 5 nm or less where found to be somewhat more resilient to the anneal treatment. These thin films exhibited a close-packed grain structure that almost completely covered the substrate. In contrast, films having thicknesses of 7 nm and greater exhibited well defined post-anneal island separation. Our observations suggest that thermally induced de-wetting is suppressed in the thinner films.

1.7 Conclusions and Future Directions

The AFM provides a tool to characterize the properties of surfaces and to conduct experiments at the nanoscale using new measurement modes. Conclusions are presented in Chapter 6 for the dissertation. Particle lithography when combined with organosilanes deposition can be used to prepare exquisite arrangements of nanopatterns on surfaces. Particle lithography can also be used as an educational tool for undergraduates to learn basic chemistry techniques for nanoscience studies. Learning methods of particle lithography provides hands on laboratory skills that can be used in future research and careers.

CHAPTER 2. EXPERIMENTAL APPROACHES WITH SCANNING PROBE MICROSCOPY FOR THIN FILM AND PROTEIN INVESTIGATIONS

Studies at the nanoscale were accomplished using measurement and imaging modes of scanning probe microscopy (SPM). Advantages of using an SPM system include imaging in ambient conditions where an ultra-high vacuum environment is not needed. Experiments can also be done in liquid environments to simulate biological conditions and *in situ* processes.

2.1 Overview and History of SPM

The atomic force microscope is part of the scanning probe microscope family that includes the scanning tunneling microscope (STM) as well as the nearfield optical scanning microscope (NSOM). The class of microscopes have an ultra-sharp tip or probe to scan across the surface in a raster pattern. During scans, a computer is used to control and monitor the position of the tip as it is placed on or near the surface. The STM was invented by Gerd Binning and Heinrich Rohrer in 1981 at IBM Laboratories.[31] Later came the invention of the NSOM which was reported in 1984.[32] In 1986, the AFM was introduced by Gerd Binning, Calvin Quate, and Christopher Gerber.[33] Since its invention, the AFM has become an invaluable tool for studies at the molecular and micron scale. New modes have been developed with AFM for measuring forces and accomplishing AFM-based nanolithography.[34-36]

2.2 Imaging Principle of AFM

Samples that can be analyzed with AFM include organic thin films,[23, 37-39] biological specimens,[40, 41] polymers,[42] and solid state materials.[43] A major advantage of using an AFM is that samples do not have to be conductive or magnetic as required for electron microscopy. Additionally, the AFM can be operated in a range of environments including ambient, vacuum, and liquid. Resolution limits for the AFM have been reported to be roughly 0.01 nm vertically and 0.1 nm laterally when using an ultra-sharp tip.[44]

A representation of the basic set up is shown in Figure 2.1 for a tip-mounted AFM scanner. A laser diode is focused onto the back of the cantilever near the tip. The laser light deflects off the reflective coating on the backside of the tip to a position sensitive photodetector. A feedback loop is maintained between the computer and the piezoceramic scanner. As the tip is scanned across the surface, the movement in relation to the surface topography and other forces that are incurred between the tip and the sample is tracked by the detector. A feedback loop continuously adjusts the piezoceramic scanner to maintain either a constant force (contact mode) or constant amplitude (intermittent contact mode) during imaging. Digital signals from the photodiode are then sent to the controller and to a computer for processing and real time adjustments during the scanning process.

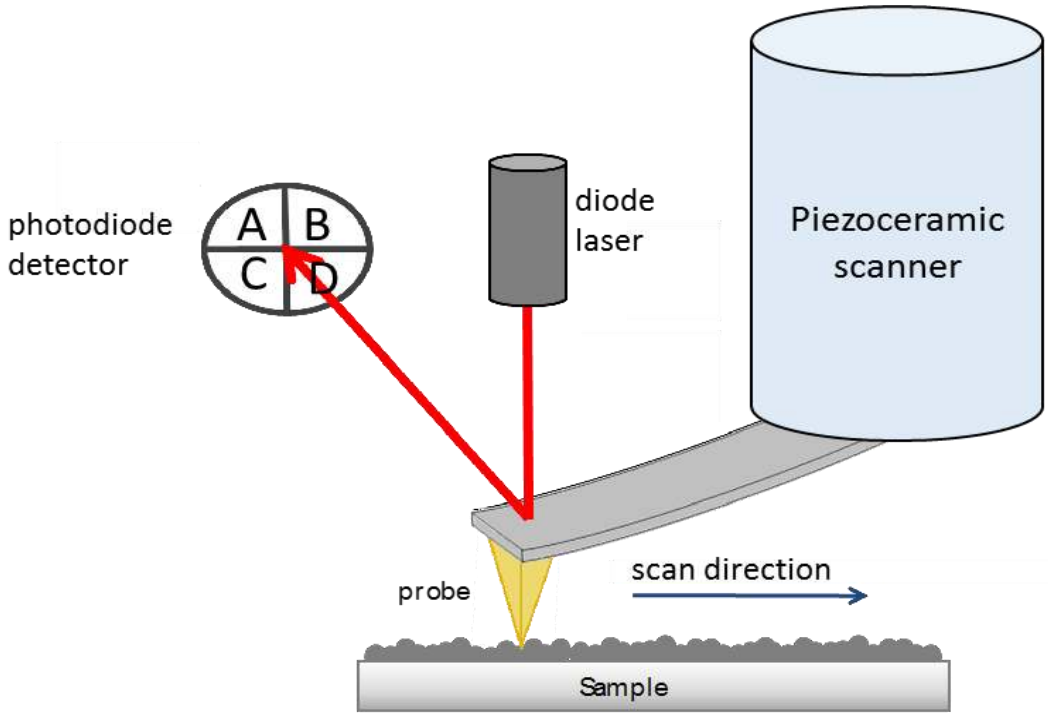

Figure 2.1**:** Basic setup of a tip-mounted AFM.

There are several types of AFM probes that can be used to investigate sample properties, depending on the selected imaging mode and instrument configuration. Most probes are made from silicon (Si) or from silicon nitride (Si_3N_4) and either have a pyramid shaped tip or a stylus probe

shaped tip. The apex of the tips can be made from carbon nanotubes, certain metals or even diamond, depending on the needs of the experiment. Typically the apex of a tip is ~10 nm. The tips are attached to a flexible cantilever. The backside of the cantilever has a thin metal layer of either gold or other reflective metal that will deflect the laser signal.[45] For magnetic imaging modes, the tip is constructed with a magnetic metal coating.

2.3 Contact and Frictional Force Modes of AFM

Contact mode and frictional force microscopy are the two main modes used with an AFM operated in continuous tip-surface contact. For contact mode, a tip is placed on a surface and continuously scanned in contact with the sample. Using a force setpoint determined by the operator, the tip and the sample force is adjusted during scanning by the feedback loop and adjustments to the z piezo. As the tip moves up and down on the surface, the laser spot moves up and down in a likewise fashion on the position sensitive photodiode to produce a topography image. When the tip moves up, the z piezo will move the tip away from the surface. However, when the tip is scanned over a depression, the laser spot will move downwards on the position sensitive photodiode. To counteract the tip movement the z piezo feedback loop will change the force applied between the tip and sample.

The incremental changes to the x, y, and z piezo are controlled during the entire scanning process using the feedback loop of the software and the instrument. Using the quadrants of the photodiode represented in Figure 2.1 a mathematical representation for topography is (A+B)-(C+D). Simultaneously an error or deflection image is produced and shows the amount of voltage the instrument has to apply to the piezo to return the forces back to the original force set point. In addition to moving up and down during scanning, the tip will move side to side as repulsive and attractive forces between the tip and sample. Frictional force images are produced from the signals

as the tip twists in relation to these forces and show a difference in surface chemistry. A mathematical way to present this is by using the letters of each quadrant of the photodiode presented in Figure 2.1; (A+C)-(B+D) will represent the lateral force signals.

Examples of contact mode images of nanopores within a thin film of octadecyltrichlorosilane (OTS) are shown in Figure 2.2. The topography image (Figure 2.2A)

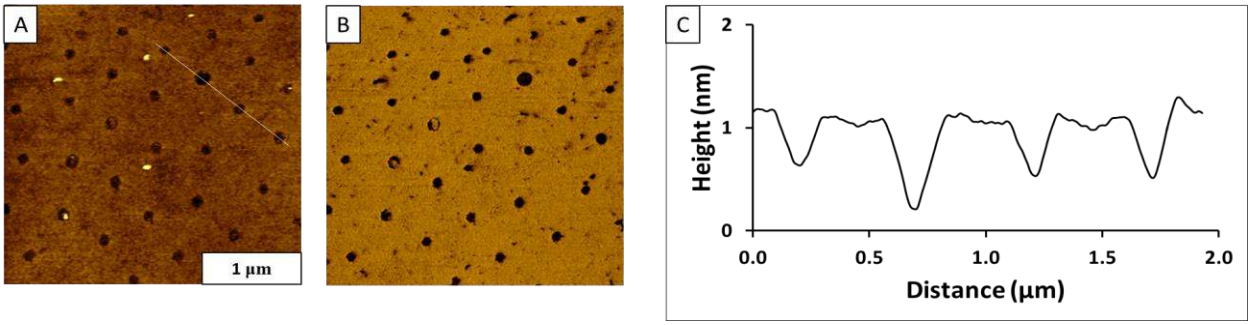

Figure 2.2: Nanopores within a thin film of octadecyltrichlorosilane viewed with contact mode AFM. (A) Topography frame; (B) Lateral force image; (C) Cursor profile for the line in A.

shows the heights of the features on the surface; the lighter color for the areas indicate taller features; whereas the areas with darker color reveal shallower features. Lateral forces images (Figure 2.2B) are simultaneously acquired during scanning and the color scale shows differences in surface chemistry for areas of the sample. The average film thickness of the OTS monolayer is roughly 1 nm high as can be seen from the cursor profile in Figure 2.2 C.

The first use of contact mode was reported in 1986 from IBM laboratories by Binning, Quate, and Gerber during which the researchers imaged aluminum oxide surfaces.[33] Subsequently atomic resolution was achieved when Binning *et. al*. reported images of a graphite surface in 1987.[44] The first biological surface imaged with contact mode was polyalanine in 1989 by Drake *et. al*.[46] Since then true atomic resolution has been obtained in previously reported studies.[47-49]

2.4 Force Spectroscopy

Force spectroscopy is used to measure the forces between the tip and the sample. Force measurements can be used to determine quantitative information about certain types of binding interactions of samples. Mechanical properties of biological systems,[50-53] polymers,[54] and thin films have been reported.[55-57] During data acquisition, a force distance curve is generated as the tip approaches the surface in the z direction. Using Hooke's Law, $F = -kx$, forces between the tip and sample can be quantified. In this law, F is the force that the tip applies to the surface; k is the spring constant of the cantilever; and x is the cantilever deflection that is measured by the instrument. The tip is approximated to be a spring and the force is assumed to be directly proportional to the tip deflection. A typical force distance curve is presented in Figure 2.3 of nanopores within an OTS matrix with the approach curve in blue and the retraction curve in red. When the tip is far away from the surface, it does not experience any long range attractive or repulsive forces (regime 1). As the tip nears the surface, long range attractive forces start to interact with the tip and the tip "snaps to" the surface (regime II). As the tip is continued to be pressed onto the sample surface, the long-range attractive forces are replaced by short-range repulsive forces and the force against the tip increases (regime III). When the tip is pulled away from the surface, after a maximum is reached, the short range repulsive forces begin to decrease (regime IV). Once the repulsive forces have dissipated, there are attractive forces that hold the tip until it "snaps away" from the sample (regime V) showing the attractive forces. Finally the tip is withdrawn far enough away from the surface that there are no net forces acting on the tip (regime VI).

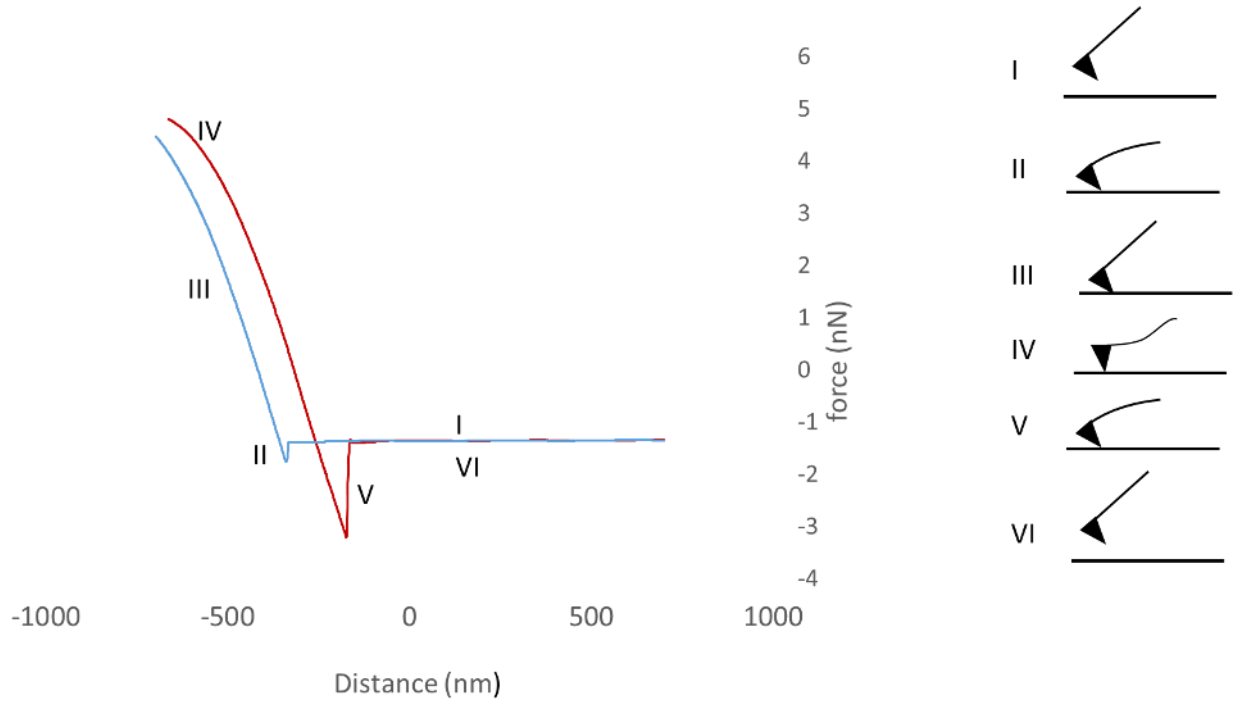

Figure 2.3: Force-distance curves obtained in air for a Si_3N_4 tip on an OTS thin film.

2.5 Tapping Mode AFM and Phase Imaging

Another primary mode of SPM used in this dissertation is tapping mode or intermittent contact mode.[58] A possible drawback for contact mode is for softer samples to be damaged when imaged due to shear forces. In tapping mode a tip "taps" the surface during scanning which minimizes the forces applied to samples.[59, 60] Intermittent contact mode has therefore been used to image samples such as proteins, [61-63] nanoparticles, [64, 65] cells, [66-68] and polymers.[59, 69] For tapping mode the tip is driven to oscillate near its resonant frequency. During scanning, an alternating current (AC) is used to drive a signal in a piezoceramic actuator that is mounted in the nosecone assembly.

Tips for tapping mode generally have a higher aspect ratio and higher spring constants than for contact mode imaging. Typical resonance frequencies of tapping mode tips can range from 50-

400 kHz with spring constants of 10-50 N/m. During scanning, a lock-in amplifier is used to monitor changes in the amplitude of the tip in relation to the driving AC signal. The feedback loop will then adjust the z piezo of the scanner to return tip amplitude back to the original driving signal. The error signal for tapping mode is generated by the difference in the amplitude of the tip from the amplitude set point of the driving signal.

During imaging, phase images are simultaneously acquired with topography and amplitude images. A difference in the phase angle between the driving AC signal and the output of the phase of tip are monitored by the lock-in amplifier and are converted into phase images. Differences of sample and tip surface adhesion and viscoelasticity can be evaluated from changes in the phase lag (Figure 2.4).

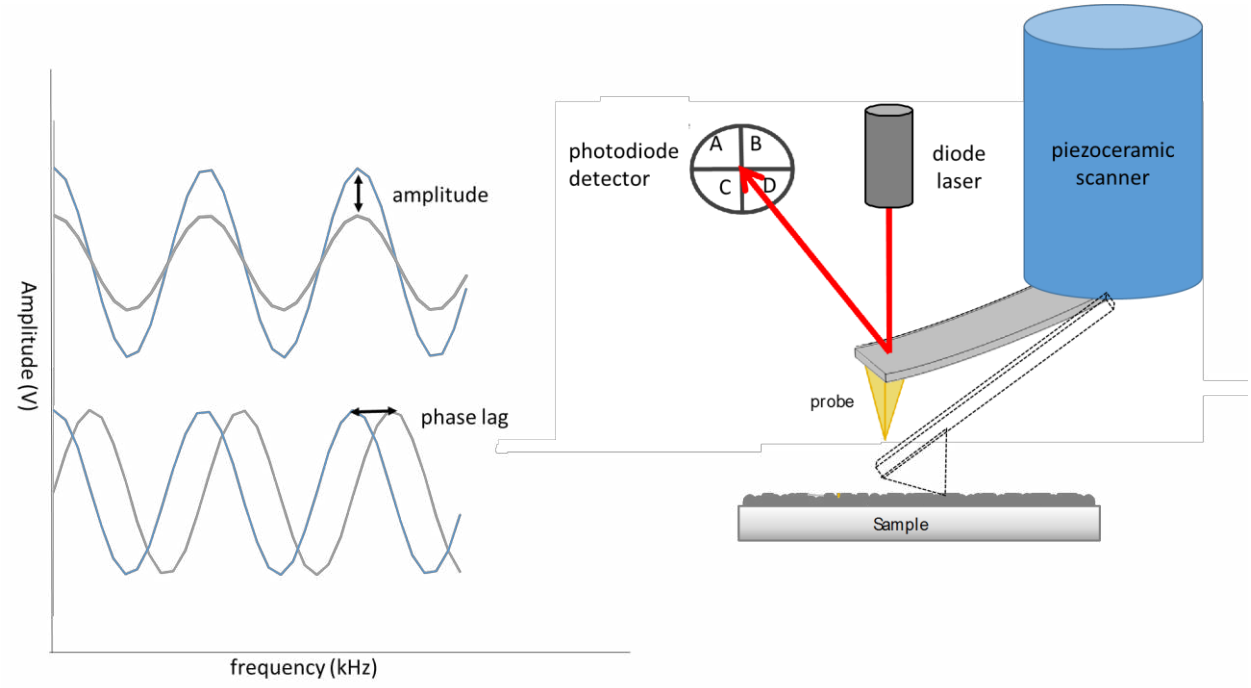

Figure 2.4: Operating principle of tapping mode atomic force microscopy.

Fibrinogen bound within nanopores formed in a film of 2-[methoxy(polyethyleneoxy)6-9 propyl] trichlorosilane (MPT-silane) are viewed with tapping mode AFM in Figure 2.5. The

heights and surface features are presented in the topography channel (Figure 2.5A). Brighter areas correspond to taller surface features while darker areas represent areas with lower topological features. In Figure 2.5B phase images show viscoelastic differences between the tip and the sample during imaging. The brighter areas reflect the bound protein to the sample while the darker areas correlate to the MPT-silane matrix. The height profile for the white line drawn in the topography image is shown in Figure 2.5C. The average heights are roughly 3.5 nm which roughly corresponds to one layer of fibrinogen in a side orientation on the surface.[70]

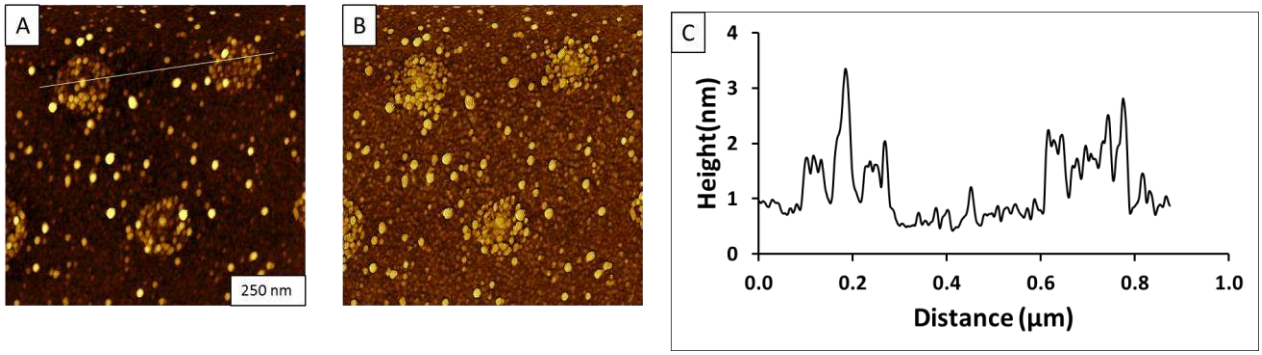

Figure 2.5: Tapping mode AFM micrographs of fibrinogen bound inside nanopores of MPT-silane viewed with tapping mode AFM.(A) Topography image of fibrinogen immobilized onto MPTMS nanopores. (B) Corresponding phase image of (A). (C) Cursor profile of the white line in (A).

2.6 Particle Lithography Combined with Silane Deposition

Particle lithography,[71] has been used to pattern self-assembled monolayers,[72] porphyrins,[73] nanoparticles,[74] metals,[75] and polymers.[76] The advantages of using particle lithography include long range ordering of the particle mask, and the use of simple benchtop techniques and basic lab equipment to reproducibly make patterns at the micro and nanoscale.[77, 78] The sizes and periodicity of the patterns can be tuned by selecting the sizes of mesospheres used for the particle mask, ranging from 50 nm to microns.[79]

For protocols with particle lithography, a surface mask is prepared on a flat substrate by drying a suspension of either latex or silica spheres. During the drying step, capillary forces pull

the mesospheres together into a close packed arrangement (Figure 2.6).[80] After drying there are trace amounts of water trapped in the meniscus sites at the base of the mesospheres. The minute amount of water defines the sites where hydrolysis and condensation of organosilanes will occur. During either vapor deposition or immersion protocols, the organosilanes will intercalate between the mesospheres and cover the unmasked areas of the surface. The mesospheres protect small local areas where direct contact provides a surface mask. The amount of water present on the substrate defines the amount of self-polymerization of the silane on the substrate.[81] Substrates that only have trace amounts of water on the surface will form a monolayer when immersed into a dilute solution of silanes, forming nanopores where the mesospheres were located.[72] Because trace amounts of water aid in the hydrolysis of the silanes, anhydrous or dry solvents are used for the immersion protocols. If excess water is present at the base of the mesospheres multilayers of OTS are observed to produce nanorings.[72, 82] Periodic arrays of nanostructures provide exposed local surface sites that can be used to bind another silane with selected head group chemistry.

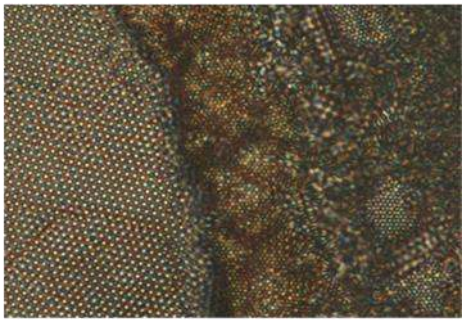

Figure 2.6: Close packed mesospheres on glass. Oil immersion micrograph (100×).

2.7 Application of Particle Lithography for Patterning Proteins

Combining particle lithography with immersion or vapor deposition of self-assembled monolayers (SAMs) enables surfaces to be tailored for selective protein attachment. Self-assembled monolayers are formed when the organothiols or organosilanes form a two-dimensional

arrangement on the surface. Organothiol and organosilane SAMS have been previously reported for the attachment of proteins.[83] Thiol SAMs have been patterned on gold, silver, and other coinage metals. The sulfur end group of thiols attach by chemisorption to metal surfaces.[84, 85] Silane SAMs have been prepared on gold, glass, mica, quartz, indium-tin oxide, as well as silicon surfaces.[72, 86] A siloxane network is formed by Si-O-Si crosslinking of the silanes to the surface (Figure 2.7).[87] Typically, for protein immobilization and patterning, a surface is functionalized with two chemistries. The first is a protein resistant layer usually having either a methyl, hydroxyl or ethylene glycol group. The second molecule will have reactive head groups for binding proteins. Organosilanes were used in protein binding experiments due to the inherent thermal stability and also for designing chemistries suitable for glass or quartz substrates.

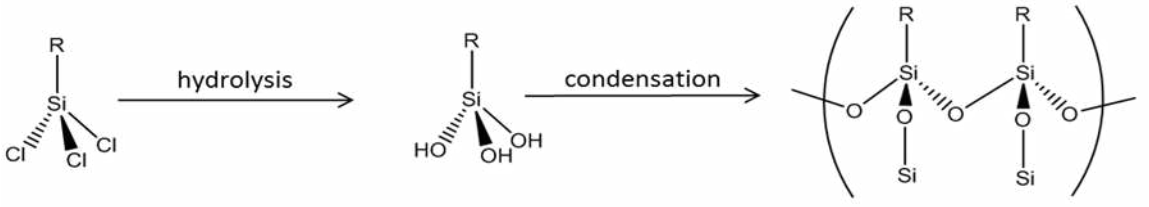

Figure 2.7 Mechanism of organosilane self-assembly on a silicon surface

A well-studied silane, octadecyltrichlorosilane (OTS), has been used to prepare SAMs on Si substrates.[87, 88] Due to the three chlorines on the OTS molecule, it is highly reactive in the presence of water and will polymerize.[88] When silanes come into contact with water either in the liquid or vapor phase, the chlorines will hydrolyze and form silanol groups. Upon exposure to a hydroxylated surface, the silanols will either react with hydroxyl groups on the surface to form covalent bonds, or horizontally polymerize and react with other silanes in solution to form Si-O-Si bridges. A densely packed OTS monolayer is formed with an orientation of approximately 12° from the surface normal.[88]

Protein patterning on surfaces was first described in 1985 by Haddon and Lamola for use as an electronic biomolecular device.[89] The first surface to be functionalized with a monolayer of protein was reported by MacAlear and Wehrung in 1978.[90] A protein layer was patterned for use as a biomolecular circuit. Methods that have been reported for generating micro and nano sized protein arrays on surfaces include microfluidic patterning,[91-93] photolithography,[94-96] electron-beam lithography,[81, 97] microcontact printing,[98-100] dip-pen nanolithography[101, 102] and particle lithography.[1, 103-105 83, 106, 107]

2.8 Force Modulation Microscopy

Force modulation microscopy (FMM), invented in 1991 by Maivald and Hansma *et. al.*,[108] is used to image changes in surface elasticities during AFM imaging. During contact mode imaging, a modulated force is applied to the surface and the response of the tip is monitored using the photodiode. Quantitative elasticity and viscoelasticity measurements can be obtained using the FMM mode. Additionally Young's modulus can be quantified for certain materials using FMM. Since its invention FMM has been used to image samples including biological,[109-111] thin organic films,[110, 112, 113] and polymers.[114-118]

For FMM the AFM is operated in contact mode. However, during imaging a driving frequency in the z direction is applied to a piezoactuator either in the tip holder assembly or in the sample stage.[62, 113, 116, 119] A variation on FMM was invented by Li *et. al.* in which an AC current was applied to the tapping mode nosecone as the tip was scanned in contact mode across the sample.[120] As the tip is raster scanned across the sample a lock-in amplifier monitors the response of the tip and sample to the driving signal. Two different channels are monitored in this mode, amplitude and phase response of the tip. Amplitude images display the elastic response of the tip

and sample contact. Phase images display the viscoelastic response of the tip and sample contact area.

2.9 Dynamic Lateral Force Modulation Atomic Force Microscopy

Dynamic lateral force modulation AFM (DLFM-AFM) or shear force modulation, is similar to FMM however, instead of the sample being modulated in the z direction, the sample is modulated in the x or y direction during scanning. Two different instrument configurations can be used for DLFM. The first uses a piezoactuator mounted in the sample stage to move the sample in the x or y direction.[121] However, the second method uses a specially designed nosecone with a piezoceramic material mounted to the side of the tip holder (Figure 2.8). Notice that at the base of the tip holder there is a grey line. This line is the piezo that is attached to the side of the tip holder. When an AC current is passed through the piezoactuators, the stage or the tip moves parallel to the scan direction of the sample. Localized shear forces can be analyzed using this method. For example, glass transition temperatures have been found for certain polymer samples,[122-124] characteristics of metal thin film contamination,[121] and viscoelasticity of cells.[125] Details and application of DLFM-AFM to image materials and instrument set up are presented in Appendices A and B.

Figure 2.8 Piezo tube scanner with DLFM nosecone attached

CHAPTER 3. PROTEIN PATTERNING USING ORGANIC THIN FILMS

3.1 Introduction

Proteins are part of the biochemical pathways for functions such as tissue construction,[126, 127] cellular functions, [128, 129] antibody and immune response,[130] and regulating osmotic pressure.[131] Protein patterns can be useful for molecular-level studies of the kinetics and properties of proteins. Protein patterns are currently used for biointerfaces, biosensors, and drug-screening.[132-135]

An inherit challenge for producing protein patterns is the fragility of proteins and a tendency to denature in chemical environments. When dispersed in a solution, protein samples dried on surfaces tend to self-aggregate and form clusters. For samples that are dried, proteins bind through attractive forces that can be ionic, hydrophobic, or van der Waals forces.[136-138] Proteins can denature and lose the tertiary structure upon drying on a surface. An example atomic force microscopy (AFM) image of protein aggregation, even at dilute concentrations as shown in Figure 3.1 as reported by Ngunjiri et al.[1] The AFM results demonstrate that even with incomplete surface coverage, proteins bind together and form aggregates on surfaces of mica. To overcome the challenges with depositing protein on surfaces, new strategies in protein patterning apply chemical approaches for surfaces with organothiol and organosilane self-assembled monolayers (SAMs). Methods have been developed for selective patterning of protein on patterns of SAMs. Two types of chemistries have been employed to pattern proteins. Organosilane SAMs bind to glass, metal oxides, mica or silicon substrates through a silanol bond. Organothiol chemistry has a sulfur group to bind to coinage metals such as gold or silver.

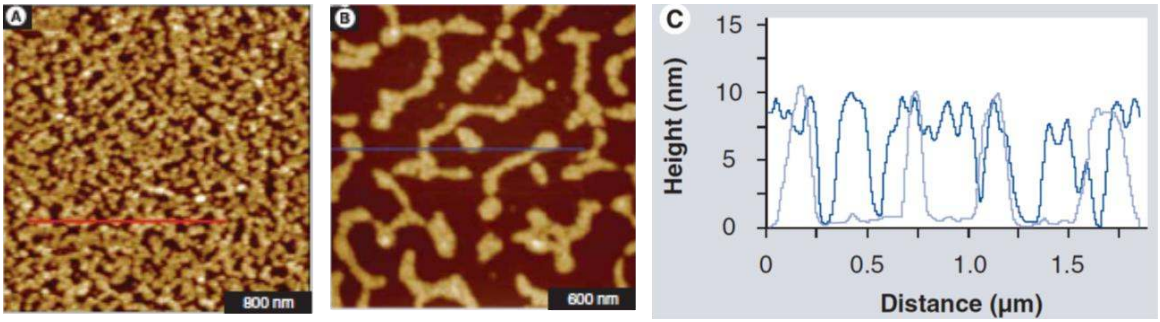

Figure 3.1: Ferritin deposited onto a mica surface, imaged in ambient conditions with tapping mode AFM. (A) At saturation surface coverage; (B) Aggregation persists with lower surface coverage. (C) Combined cursor profiles for A and B. Reprinted with permission from Ngunjiri et al.[1]

Surfaces are patterned with two distinct regions of functional SAMs, a matrix region and reactive sites of patterns. The matrix region has a protein resistant layer to prevent nonspecific adsorption of proteins. A general relationship between the wettability of the surface correlated to a stronger absorption of proteins, reported by Sigal et al.[139] Matrix surfaces can be either methyl-terminated or present oligomers of ethylene glycol at the interface.[140-143] Self-assembled monolayers that have a tripropylene sulfoxide group have also been found to resist protein adsorption.[144] The reactive layer proveds a protein attractive region to bind proteins to the surface. Surfaces presenting amino, carboxylic acid, and thiol groups have been used with linker chemistries to attach proteins to patterns of SAMs.

Techniques have been developed to produce patterns of proteins on SAM surfaces with micro- and nanometer resolution. Two approaches to this challenge are to either directly graft proteins to the surface or to use the proteins to write or inscribe the patterns. Direct grafting of proteins has been reported using methods of photolithography,[95, 145-147] colloidal lithography,[1, 27, 70] electron-beam lithography,[15, 148-150] microcontact printing,[100, 151-154] nanoimprint lithography,[96] stencil lithography,[155, 156] biased induced lithography,[157-160] and nanografting.[161-165] Patterning proteins can also be done with an AFM tip, such as with dip-pen nanolithography.[101, 166, 167] One of the early examples of preparing protein patterns was reported in 1978 by MacAlear et. al.[90] A

protein layer was deposited onto a clean silicon wafer with a native oxide layer. A photoresist was deposited onto the top of the protein layer. Micropatterns of proteins were produced using an electron beam to irradiate away areas of the sample to create patterns.

3.2 Patterning Proteins using Photolithography

Photolithography is a widely used patterning techniques used to pattern proteins. Photolithography methods use light, usually ultraviolet (UV), to make 3D structures on surfaces. A polymer is initially deposited on a substrate and then a photoresist containing the pattern is placed on top of the polymer. A glass slide with a pattern is made by depositing chromium onto the glass. When the polymer is exposed to UV light, it will react and either become etched away or the chemical functionality will change and become dissolvable in the development step. [145, 168, 169]

The ease of surface modification using a surface mask combined with light irradiation of the sample makes photolithography a practical method for protein patterning. Photolithography can be applied to change the functional groups of surfaces. For example, thiol groups on a surface can be turned to sulfonates.[170] An arylzide when exposed to light can be functionalized to a nitrene group that can bind to a CH bond in a molecule.[171, 172] Caging chemistry can also be used. When exposed to light, the cage molecule is decomposed to a ketone and a carbon dioxide.[173-176] Diazirine, which absorbs light at 350 nm, can be used to attach proteins with covalent bonds.[177, 178]

3.3 Protein Patterning with Stencil Lithography

For Stencil lithography, a stencil is used to block and control the flux of molecules. Unlike photolithography, microcontact printing, or nanoimprint lithography the stencil is not in physical

contact with the sample.[179] The method can be applied to fragile substrates such as thin glass microscope coverslips that could crack and break.

Methods of stencil lithography have been used for protein patterning. Stencil lithography was used to pattern IgG by Huang et al.[155]Stencils were prepared using low-pressure chemical vapor deposition on silicon nitride substrates. Once the stencils were made, they were placed over a substrate with PDMS. The PDMS that is not masked by the stencil was exposed to oxygen plasma treatment and became hydrophilic. Next, the solution containing the protein was put into the chamber on top of the hydroxylated PDMS. Next the solutions were analyzed using SPM and fluorescence microscopy.

Protein patterns of IgG were produced using stencil lithography.[155]A PDMS stamp was irradiated with plasma to hydroxylize areas through a stencil. Next an amino terminated silane was bound to the hydroxylated surface. Bis(sulfosuccinimidyl)suberate was used to bind the amine on the silane to the amine of anti-mouse IgG. Heights of the prepared samples displayed one protein binding to the nanodots. Subsequent immobilization of mouse IgG showed the bonding of an antibody to the anti-mouse IgG.[155]

A parylene-C membrane was used to pattern substrates for protein patterning with stencil lithography, reported by Wright et al.[180] The method is advantageous because the membrane that was used as a mask is flexible. Using the membrane enables a reusable stencil to be used. Texas Red-BSA was deposited onto the substrate through the stencil. Once the stencil was removed a second protein, FITC-BSA was incubated on the patterns. The method provided a protocol for patterning two different proteins on one substrate.

Advantages of stencil lithography for protein patterning include the ease of the procedure, the capability of the stencil to be moved while deposition takes place, as well as the reusability of the stencil Potential disadvantages are the clogging of the membrane as well as the stability of the membrane. With advances in UV and plasma treatment of substrates, stencil lithography is becoming a more viable option for routine patterning of substrates with proteins.

3.4 Patterning SAMs and Proteins using Particle Lithography

Particle lithography also referred to as colloidal lithography,[181] nanosphere lithography,[75, 182] evaporative lithography,[183] and natural lithography,[71] uses a surface template of either latex or silica spheres to create patterns onto a surface. Particle Lithography has advantages of using small volumes of dilute reagents, high throughput, and reproducibility of nanostrucres. A solution of spheres was deposited onto a surface as described in an early report by Deckman and Dunsmuir.[71] As the solvent dried and evaporated, capillary forces pulled the spheres together into close-packed arrays. The substrate area that is in contact with the base of the particle was protected from further functionalization by the surface mask of spheres. By changing the size of the particles used, the surface density of patterns can be controlled. The smaller the size of the spheres, the greater the number of nanopatterns within a certain area.[82]

Particle lithography was used to pattern ferritin onto gold, mica(111), and glass surfaces, as reported by Ngunjiri et al.[1] Nanorings of ferritin were produced on each of the substrates. At a certain protein:sphere ratio, the surface coverage of the proteins was greater for nanopatterns prepared on glass followed by mica and then gold. Changing the concentration of protein resulted in protein patterns of nanopores with a film of bovine serum albumin (BSA) that formed in the interstitial sites between the spheres (Figure 3.2 A-D). The ratio could be tuned to produce nanorings of the BSA (Figure 3.2 E-H).

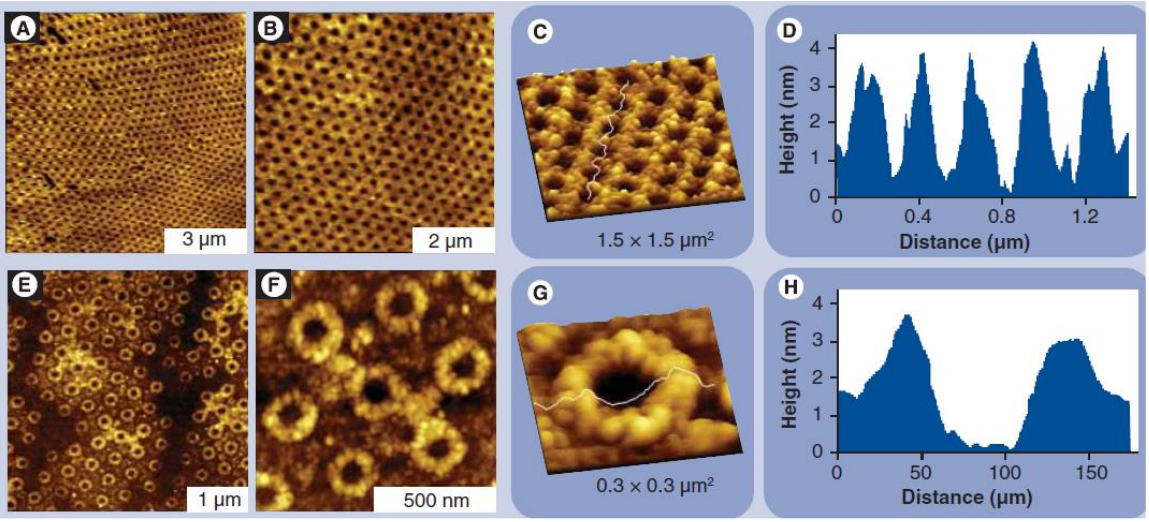

Figure 3.2: Nanostructures of IgG on mica obtained by varying the concentration of spheres to protein. (A) AFM topograph of pore-shaped nanostructures, 10 x 10 μm^2. (B) Zoom-in image of pore nanostructures, 6 x 6 μm^2. (C) View of pore morphology. (D) Cursor profile of the white line in (C). (E) Ring nanostructures produced with a lower protein to sphere ratio. (F) Zoom-in image of **E**. (G) Three dimensional view of an individual nanoring of protein. (H) Height profile along the white line in (G). Used with permission from reference 184.[184]

Colloidal lithography was used to prepare micro and nanosized protein patterns by Singh et al.[185] Colloidal suspensions formed on gold were sputtered onto glass substrates to create an area for protein binding. Areas of the glass that were protected by the spheres was used as the protein resist. Bovine serum albumin was bound to the exposed areas of the substrate and results were confirmed with fluorescence microscopy.

Gold nanodots that were patterned through a polystyrene-block-poly[2-vinylpyridine$(HAuCL_4)_{0.5}$] copolymer onto glass coverslips were used for particle lithography by Arnold et al.[186] Plasma treatment was used to remove the block copolymer leaving behind a hexagonal array of gold nanodots. By changing the composition of the copolymer, the distribution between the nanodots could be controlled. Distances between the gold nanodots were roughly 28

nm apart enabling one integrin molecule to be bound to each of the nanodots for cell patterning. Subsequently, MC3T3-osteoblasts were attached to the prepared nanostructures.

Charged polystyrene spheres were deposited on top of a thin film of gold in a study by Agheli et al.[187] The sample was then heated, leading to a deformation of the polystyrene spheres into disks. Next, an argon ion beam was used to etch away the gold that was not covered by the melted polystyrene to produce gold islands with a radius of 124 nm. Next, ferritin was bound to the exposed nanodisks that were crosslinked with laminin. The binding orientation of laminin was determined since the nanodisks were smaller than the length of laminin.

Ring patterns of ferritin were produced onto freshly cleaved mica (0001).[27] A solution of protein was mixed with a solution of mesospheres. As the solvent dries capillary action pulls the mesospheres together in a hexagonal close packed array. The proteins in the solution will form a ring around the base of the mesospheres. Individual ferritin proteins can be seen in the ring nanopattern. A new imaging mode, magnetic sample modulation, was used to image the protein nanopatterns under an applied magnetic flux.

Fibrinogen was patterned using particle lithography.[70] Three different packing densities were used to create nanostructures that were 100, 250, and 500 nm apart. In the studies it was noticed that MPT terminated silanes would cross react with another silane in the backfilling step. A novel method was developed to produce a monolayer of the protein binding silane first and then deposit the mesospheres on top of the formed monolayer. Next, UV-ozone treatment was used to irradiate the area that was not protected underneath the mesospheres. The mesospheres are left on the substrate and the sample is placed into a solution of dilute MPT-silane. The MPT-silane creates the protein resist around the active silane pillars. Surface coverage of the protein increased as the size of the mesospheres decreased.

3.5 Application of Electron Beam Lithography for Patterning Proteins

Electron beam lithography is a method to pattern substrates with high spatial resolution of approximately 5-10 nm.[188] In electron beam lithography (EBL), a high energy beam of electrons is focused onto the surface. The molecules that are on the surface can either be irradiated away or can be oxidized using EBL. [189] Electron beam lithography was used to pattern proteins by Christman *et. al.* in 2009.[81] In this method a polyethylene glycol (PEG) chain was functionalized with one of four protein linking chemistries. After subsequent binding of the functionalized PEG to the surface, areas were irritated with an electron beam which caused the PEG to crosslink.

One of the challenges of electron beam lithography is that the high energy beam needed to design the patterns can be harmful to biological molecules and could cause damage. Electron beam lithography was applied to produce patterns of antibodies on silicon substrates for protein immobilization by Lau et al.[16] Using polymers that contain a trehalose side chain can stabilize proteins in certain environmental conditions.[190-192] First a PEG-silane was deposited onto silicon substrates through immersion. Next, a solution with either anti-interleukin 6 or antitumor necrosis factor alpha as well as PolyProtek and ascorbic acid was spin-coated onto the sample. An electron beam was used to irradiate away the molecules that were not crosslinked to the surface. Multicomponent systems could be fashioned using the spin coating procedure.

Protein nanopatterns were made using EBL to create platforms to differentiate between normal and breast cancer cells, as reported by Horzum et al.[193] Indium tin oxide substrates were first coated with an amino-terminated silane to facilitate protein binding. Fibronectin binding regions with a K-casein background were used as the proteins that differentiated the surface morphology for cell attachment. It was found that breast cancer cells could grow on the non-adhesive regions better than normal mammalian epithelial cells.

Electron beam lithography has advantages including high spatial resolution, range and sizes of patterns that can be written and high resolution. However the cost of an electron beam system is relatively expensive and the deposition step must be done in a high vacuum environment.

3.6 Protein Patterning using Microcontact Printing

Microcontact printing has been used to pattern proteins at the micron scale.[127, 154, 194] Nanoscale patterning of proteins was later achieved in 2002 by Delamarche et al.[195, 196] For microcontact printing, a master pattern is made with PDMS to make the stamp. Next, the stamps are inked in a protein solution. The inked stamp is then placed on a substrate to physically transfer the protein to the surface. When the stamp is removed the transferred protein is bound by physical absorption of the protein to the substrate. Physisorption may not be a good option for studies where forces are measured between the protein and sample, such as for AFM characterizations. Advancements with microcontact printing have been done by adding a reactive silane to the surface before stamping with protein. In this approach, the protein will react with the patterns of active silane to form a covalent bond with the surface.

A pyramidal PDMS stamp was used to pattern rabbit IgG onto a silicon substrate by Filipponi et al.[197] The sample was then exposed to anti-rabbit IgG. The PDMS mold was made using photolithography and etching in basic solution. The PDMS stamp was then formed with the Si master. The stamp was incubated with rabbit IgG and placed onto a glass cover slip. Patterns of protein were confirmed using fluorescence microscopy. Subsequent binding of anti-rabbit IgG was done with an incubation step.

To understand the role of the extracellular proteins with myotube patterning, a study was done by Duffy et al using microcontact printing.[198] Glass slides coated with PDMS were placed into contact with a PDMS stamp that was coated with protein. Selected proteins were used to create

patterns for cell attachment. Patterns with a range of line widths were used to test for myotube formation after cell differentiation. The production of myotubes increased when the surfaces were patterned with laminin.

Complex features of multiple proteins were produced using microcontact printing and plasma initiated protein patterning as reported by Segerer et al.[199] Prepared templates were used to create gradient dispersions of fibronectin. By placing an inked stamp with one protein in contact with the substrate, and then treating the substrate with oxygen plasma a second protein can be placed in the area on the outside of the substrate that is exposed to a solution of the second protein. Once the stamp was removed, the areas that were protected by holes in the stamp can be filled with a third protein. A replica of the university logo was patterned using Alexa-488 and Alexa-647 fibrinogen with microcontact printing.

Methods using microcontact printing enable relatively large areas to be patterned in one step. Possible disadvantages of microcontact printing when used with protein patterning is that EBL is required to design patterns for stamps. When used to pattern proteins, force has to be applied to the stamp for the pattern to transfer which can lead to denaturation.[200] With continued use of the PDMS stamp the polymer can start to break down and the patterns can be deformed under pressure.[201]

3.7 Protein Patterning Using Imprint Lithography

For imprint lithography the stamp is not made from PDMS and id usually made of silicon. The master templates are fashioned by e-beam lithography or deep-UV photolithography to obtain nanosized patterns. Calibration gratings have been used to create imprint masters. The master is transferred to a polymer to create the stamp. A master can be hot embossed into a poly(methyl methacrylate) (PMMA) glass and then used as the transfer stamp.[200]

Nanoimprint lithography was used to pattern streptavidin onto a modified niobium oxide substrate by Falconnet et al.[96] A Si template with the pattern was placed into a PMMA polymer solution that was deposited onto the niobium oxide substrate. Once the pattern was transferred the area was opened using oxygen reactive ion etching (RIE) treatment. The sample was placed into a solution of a copolymer of PLL-g-PEG/PEG-biotin. The remaining PMMA was then removed using acetone. The surface was passivated with PLL-g-PEG as a protein resist. In the final step, streptavidin was bound to the biotin functionalized PLL-g-PEG polymer.

Nanoimprint lithography was used to pattern biotin-streptavidin to attain line patterns that were 75 nm wide, by Hoff et al.[202] A Si substrate was patterned by EBL to make a template. The template was placed against a PMMA surface and heated to 175 °C with pressure for five minutes. When the mold was separated from the PMMA surface, the excess was removed with an oxygent plasma and the uncovered areas were passivated by polymer from the passivating CHF_3 that was used in the etching process. Once the exposed areas were passivated the areas of PMMA that did not react were removed by rinsing with acetone. An aminosilane was bound to the exposed areas to facilitate protein binding.

Protein patterning with nanoimprint lithography addresses challenges with microcontact printing by advancing the resolution of the features to the nanoscale. The Si template needs to be made in a clean room environment using EBL. Removing the molds still pose challenges for nanoimprint lithography, especially when used over a larger area. Surfaces used with nanoimprint lithography need to be as flat as possible to have effective transfer of the pattern from the stamp to the substrate.[189, 200]

3.8 Protein Patterning with Microfluidic Devices

Microfluidic devices operate by taking advantage of the capillary forces of liquids.[203] A stamp with channels is placed onto a substrate and a liquid is introduced on the side of the stamp. Capillary action will pull the liquid through the channels and particles that are contained in the liquid will deposit onto the substrate. Typically the molds with the channels are made from PDMS. Microfluidic systems have advantages due to the small amount of reagent that is needed for patterns to be produced.

Microfluidic systems were used to pattern proteins such as IgG as reported by Delamarche et al.[204, 205] Surfaces of gold, glass, and polystyrene were used for patterning. The microfluidic channels were prepared using a PDMS stamp. The substrates were activated with a hydroxylsuccinimidyl ester to bind to the amino groups of the proteins. Surfaces of 1 mm^2 could be patterned with IgG by this approach.

Selected substrates were tested for protein adsorption after being transferred by PDMS or solvent-extracted PDMS, as reported by He et al.[206] Fluorescence intensity was used to determine the capability of the substrates and the channels to enable protein to move through the channels. Once conditions were optimized a two-step immunosensosr was developed. In the first step anti C-reactive protein was immobilized on the surface using microfluidic channels. Next the surfaces were cleaned and the areas that were not covered by the protein were passivated. Next, another microfluidic stamp was placed perpendicular to the first set of channels. Certain concentrations of FITC labeled C-reactive protein solution was introduced to flow through each of the channels creating a platform for evaluating concentration vs. fluorescence intensity.

Microfluidic devices have advantages since small amounts of reagents are needed to produce the protein patterns. A range of designs can be made using the microchannels.

3.9 Scanning Probe Based Approaches for Patterning Proteins

Nanoscale studies and manipulation have advanced to achieve atomic resolution with atomic force microscopy (AFM).[33, 44] There are several approaches for scanning probe lithography (SPL) at the nanoscale, including dip-pen nanolithography (DPN), bias induced lithography,[158, 159, 207, 208] and nanografting.[18, 209, 210]

To accomplish dip-pen nanolithography, a tip that is inked in a solution of analyte to be deposited onto the substrate is used to write patterns, as reported by Mirkin et al.[211] Typically the ink is a thiol molecule that will physisorb onto a gold substrate. Patterns are written using a computer program to trace the trajectory of the tip. The time that the tip is one spot controls the size of area of the transfer for the diffusion-limited process of DPN.[212]

Protein arrays were designed using dip-pen nanolithography for the detection of Human Immunodeficiency Virus Type 1 from a plasma sample by Lee et al.[213] Nanodots, (~60 nm in diameter) of 16-mercaptohexadecanoic acid (MHA) were deposited onto a gold thin film using dip pen nanolithography. The areas that were not patterned were passivated with a PEG-alkythiol film. Next, mouse anitbodies to the HIV-1 p24 antigen were deposited onto the substrate to bind to MHA. Subsequently, the sample was placed in a plasma solution containing HIV-1 p24. A sandwich assay was formed using gold nanoparticles that were functionalized with anti HIV-1 p24 antibodies to amplify the height signal.

Nanopipetting can be accomplished using a modified AFM probe for dispensing liquids. An AFM tip containing a reservoir to hold a solution to be patterned was dispensed, as reported by Fabié et al.[214]At the apex of the tip a small hole is drilled for the liquid to dispense through the tip on to the surface. The hole was produced using a focused ion beam milling procedure.

Fluorescent proteins were patterned through a tip with an aperture of 760 nm. It was estimated that there are roughly 60 proteins per spot when this tip was used.

Nanografting is an AFM-based method for patterning organothiol SAMs and proteins.[215] A gold surface was coated with a PEG-thiol or methyl-terminated thiol monolayer. When the films are imaged under high force, the molecules can be removed from the surface under the mechanical force of the tip. When this is done in liquid media containing a dilution solution of another thiol molecule patterns are produced along the scanning path of the AFM probe. After the methyl or PEG terminated thiol is removed under force, the protein binding thiol that is in solution will then replace the surface molecules. Patterns can be produced through a computer program to design the shapes and sizes of surface features. After SAM patterns are made a protein can be bound to the protein adhesive sites of nanopatterns.[18, 209]

Nanopatterns of staphylococcal protein A were produced on a gold substrate using in situ nanografting within a liquid environment, as reported by Ngunjiri et al.[209] Octadecanethiol was deposited onto gold substrates to form a protein resist. Nanografting was used to remove selected areas of octadecanethiol molecules with an AFM probe under force, and replace it with a 11-mercaptoundecanoic acid. Linking chemistry with EDC/NHS was done in a liquid cell for 30 minutes. Staphylococcal protein A was then introduced and bound to the primary amine of the protein. After the attachment of immunoglobulin G to the nanografted area characterizations were done with AFM Surface reactions were done *in situ* and monitored by AFM at each step. Sequential AFM images of the nanographting steps are shown in Figure 3.3

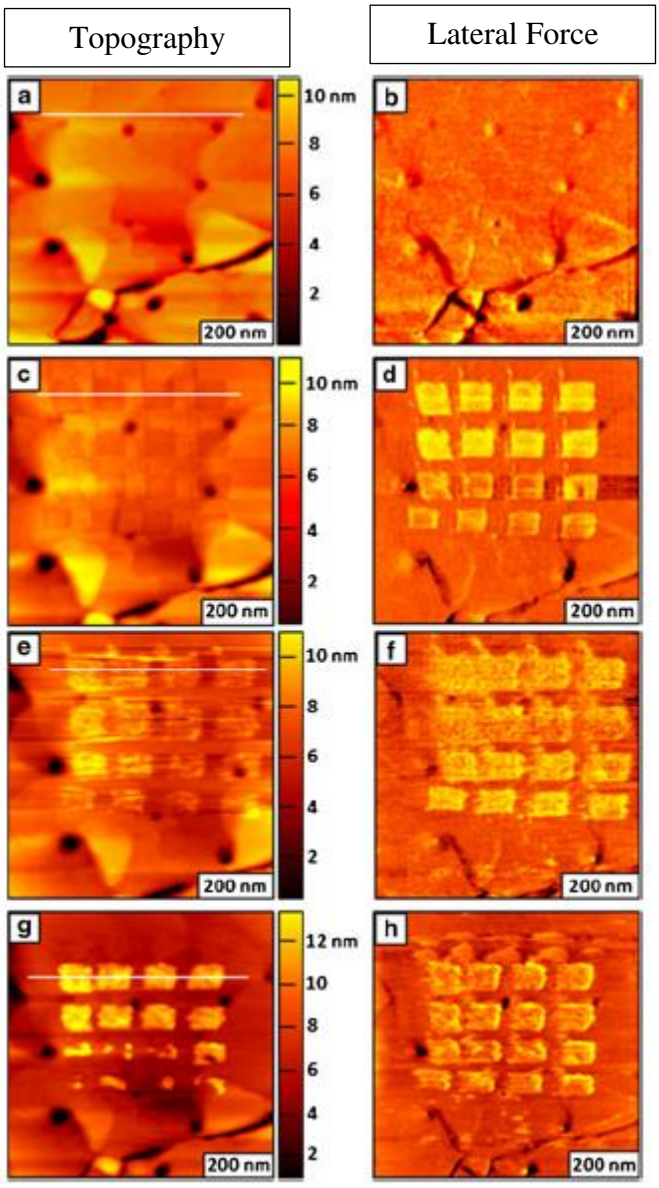

Figure 3.3: Steps of in situ nanografting and protein patterning viewed with liquid AFM. (A) Surface of an octadecanethiol SAM deposited on gold, before fabrication steps, topography frame. (B) Simultaneously aquired lateral force image of **A**. (C) Nanografted patterns of 11-mercaptoundecanoic acid within the octadecanethiol monolayer. (D) Correspondign lateral force image of **C**. (E) Binding of staphylococcal protein A after activation of MUA nanopatterns with EDC/NHS coupling. (F) Lateral force image of **E**. (G) Covalent attachment of immunoglobulin G onto the staphylococcal protein A. (H) Simultaneously acquired lateral force image of **G**. Used with permission from reference 2.[2]

Nanografting was used by Bano et al. to pattern single stranded DNA and then to bind a protein with a complimentary DNA tag.[216] First a thin film of an ethylene glycol-terminated

alkythiol was prepared on a gold substrate. Next, nanografting was done in a solution of single stranded DNA. A streptavidin conjugate protein attached to the complimentary single stranded DNA was then immersed on the substrates. The single stranded DNA bound to the complimentary single stranded DNA on the surface which covalently bonded the protein to the surface. Further modification with ant streptavidin was found to bind to the modified streptavidin areas. An SPM-based method to pattern proteins at the nanoscale using an AFM probe was done using oxidative lithography, reported by Martinez et al.[217] Ferritin was patterned at the nanoscale using oxidative lithography. A silicon oxide substrate was coated with a monolayer of OTS. During imaging, a voltage was applied to the tip to oxidize the surface. In the oxidation step, the OTS was removed leaving areas of bare substrate.[218-220] Subsequent immersion in an amine-terminated silane provided sites for the ferritin to bind. Lines of protein nanopatterns as small as 10 nm were formed using oxidative lithography.

Scanning probe based lithography can be used to pattern proteins at the nanoscale for high resolutions studies of biochemical reactions. In situ studies can be accomplished in liquid media to investigate biological processes. However, with SPL, patterns have to be written sequentially, one at a time.

3.10 Conclusion

A number of methods have been developed to pattern proteins at the micro- and nanoscale. Depending on the desired pattern geometry, surface chemistry and proteins selected for patterning methods can be done using organothiol and organosilane chemistries. Approached with electron beam and photolithography approaches provide high throughput for wider areas of the surface. Methods with scanning probe lithography, nanoimprint, stencil methods provide local areas of small patterns. Particle lithography, microcontact printing, and microfluidic lithography

can provide arrays of nanopatterns over wider areas of the surface. Studies of protein patterning can be applied to cellular level studies as well as for studies of protein-protein dynamics.

CHAPTER 4. NANOPATTERNS OF GREEN FLUORESCENT PROTEIN PRODUCED WITH PARTICLE LITHOGRAPHY

4.1 Introduction

Controlling the orientation, surface density and the self-aggregation of proteins is increasingly becoming a consideration for the design of biosensors. The interface for biosensors is often a film of protein prepared by drying a drop of protein suspension on a glass surface. The dried sample may contain multiple layers of proteins, thus it is difficult to assess protein orientation and binding efficiency. For this strategy of sample preparation the self-aggregation of proteins and the lack of unfilled areas of the surface do not provide a measurement baseline. With the drop-deposition approach, not all of the proteins are available for binding other biomolecules for assay due to the high density of adsorbates.

Patterning strategies have been applied to improve the design of biosensors based on proteins. Protein patterns have been made using electron beam lithography, [221-223] microcontact printing, [224, 225] microfluidic channels, [226, 227] and photolithography.[169, 228] Additionally the application of self-assembled monolayers (SAMs) as linker groups and matrix films have been used with scanning probe based methodologies such as with dip-pen nanolithography,[229-232] bias-induced oxidation lithography,[233] imprint lithography[96, 234] and nanografting.[2, 163, 235-237] Nanopatterning protocols based on scanning probe lithography can be time consuming and cannot be easily replicated over broad areas of a substrate. For high throughput, methods of particle lithography have been developed to pattern proteins for areas that span millimeter to centimeter dimensions.[1, 70, 107, 238-241]

Green fluorescent protein (GFP) has been isolated from the jellyfish *Aequorea victoria* and is useful in studies of cellular processes and the interactions of proteins.[242-245] The crystal structure of GFP was reported and solved in 1996 to be an 11-stranded β-barrel with an α-helix that runs up

the axis of the cylinder.[246] Studies with micro and nanometer scale patterns of fluorescent proteins have included strategies with block copolymers,[247] colloidal lithography,[241] photocatalytic patterning,[248] and electron beam lithography.[249]

Although GFP is widely used in fluorescence studies with proteins, there are relatively few studies reported with characterizations using atomic force microscopy (AFM). Histidine tagged GFP was bound to mica to form a monolayer as reported in a study by Liu et al.[250] Conditions were established to determine the minimum amount of time and concentration that were needed to prepare a single layer of protein. The intra-molecular mechanics of a single GFP molecule was investigated using atomic force spectroscopy by Wang et al.[251] The C-terminus end of the protein was attached to the AFM tip while the N-terminus end of the protein was attached to a modified glass slide. As tensile force was applied the protein was stretched. Reproducible force versus extension curves were found and the intermolecular strength was measured.

With studies that use AFM to characterize biomolecules, the method of preparing samples should be robust and reproducible, and enable the protein to withstand forces applied by the tip. Sample preparation protocols with nanopatterning offer control of the surface coverage of protein and can provide a way to limit adsorption to a single layer with designed linker chemistries. Using particle lithography only small volumes of reagents are needed for making protein nanopatterns. Millions of regularly spaced nanopatterns of organosilanes can be made with exquisitely uniform geometries at the nanoscale.[252, 253] The size of the particles used as a surface mask defines the packing density of nanopatterns. With sufficiently small nanopatterns, studies of individual proteins can be done with AFM.

Protein patterning can be accomplished by designing a surface template of organosilanes with reactive sites for binding biomolecules and well-defined areas that resist binding of protein.

For successful patterning, an effective resist layer is required to prevent nonspecific binding of protein on areas throughout the surface. Methoxy groups of MPT-silane have been widely used for resisting protein adsorption however this poses a problem for protocols with particle lithography using immersion steps. Oligo(ethylene glycol) terminated silanes become sites that react with other organosilanes to form multilayers rather than provide selectivity for inserting a second molecule. For this reason, a protocol was developed to pattern the reactive sites for binding as the first step, and then in a separate step the sites between the reactive nanopatterns were backfilled with the MPT-silane matrix after UV-ozone treatment.

In our strategy for defining a biointerface at the nanoscale, green fluorescent protein was selectively patterned onto glass slides. We chose GFP because the structure has been previously reported and due to the fluorescent properties. Using particle lithography to design the biointerface, discrete areas of mercaptosilane were prepared for binding protein within a resist layer of the MPT-silane. Nanopatterns of mercaptosilane furnished sites to bind sulfo-SMCC that can link to the primary amine of lysine residues of GFP. Studies with AFM were used to evaluate the efficiency and selectivity of linking proteins after key steps in preparing GFP nanopatterns.

4.2 Experimental Section

4.2.1 Materials and Methods

Glass coverslips were used as substrates for preparing protein patterns (12 mm, VWR). Substrates were cleaned with piranha solution made with sulfuric acid (ACS reagent 95%) and hydrogen peroxide (30%). Anhydrous toluene (Sigma-Aldrich) was used for preparing solutions of organosilanes. Silica mesoparticles (500 nm) were obtained from Fisher Scientific. Ethanol (ACS reagent grade) was used for rinsing samples (Pharmco-Aaper, TX). Deionized water was used both for rinsing and to make phosphate buffered saline (PBS, pH 7.4) from a Direct-Q3

system (18 MΩ; Millipore, Bedford, MA). Green fluorescent protein was obtained from Molecular Probes (Eugene, OR). The organosilane reagents 2-[methoxy (polyethyleneoxy)6-9propyl] trichlorosilane (MPT-silane) and (3-mercapto propyl)trimethoxysilane (MPTMS), were used as received (Thermo Fisher Scientific, Inc., Rockford, IL). Sulfosuccinimidyl-4-(N-maleimidomethyl)cyclohexane-1-carboxylate (sulfo-SMCC) was used as a linker to bind GFP to glass substrates.

4.2.2 Preparation of the substrates

Glass substrates were first rinsed in ultrapure water and dried with nitrogen. The substrates were then placed in piranha solution (3:1 solution of sulfuric acid to hydrogen peroxide) for 90 min. Piranha solution is highly corrosive and should be handled with care. Next substrates were rinsed copiously with high purity water and dried with nitrogen. The clean slides were used immediately for patterning organosilanes.

4.2.3 Steps of particle lithography used to pattern organosilanes

A film of MPTMS was prepared on glass slides using vapor deposition [Figure 4.1A]. The thiol terminated layer of MPTMS will be used for attaching protein. Substrates were placed on a platform inside a sealed reaction vessel. A small volume (400 μL) of neat MPTMS was added. The vessel was heated in an oven at 70 °C to generate a vapor of MPTMS. After 4 h the samples were removed and rinsed with ultrapure water, sonicated in ethanol for 30 min and then dried with nitrogen.

In the second step, an aqueous solution (0.1%) of 500 nm silica spheres was placed on the surface of the MPTMS film [Figure 4.1B]. Samples were dried in a refrigerator (4 °C) for 16 h. Next, the samples were placed in a UV-ozone chamber for 30 min. With UV-ozone treatment, areas of MPTMS are decomposed to form silanol functional groups which can be rinsed away.[254]

However, areas of MPTMS which are covered with silica spheres are protected from irradiation and persist on the surface to form circular nanopatterns. After UV-ozone treatment, the samples were immediately placed into a solution of MPT-silane in anhydrous toluene (1%) for 5 h. The areas that were etched away with UV-ozone were filled with MPT-silane to form a resist layer with methoxy terminated MPT-silane surrounding the MPTMS nanopatterns [Figure 4.1C]. After 5 h of immersion, the substrates were rinsed in ultrapure water. To remove the mesosphere mask, samples were rinsed and sonicated in ethanol for 30 min. In the final step, the samples were rinsed and sonicated in water for 30 min and dried with nitrogen.

4.2.4 Selective attachment of GFP to nanopatterns of MPTMS

The surface templates prepared with defined nanopatterns of organosilanes were used to attach single layers of GFP [Figure 4.1D]. The samples were placed into a 1 mM solution of sulfo-SMCC prepared in PBS buffer (pH 7.4) for 1 h. Next, the samples were rinsed with PBS to remove any unbound sulfo-SMCC linker that might be remaining on the surface. The samples were then placed in a jar containing a solution of GFP (0.5 mg/mL in PBS) for 50 min. Lysine residues of GFP bind to the N-hydroxysulfosuccinimide ester (NHS-ester) of the sulfo-SMCC linker presented at the areas of nanopatterns. For scanning probe studies, the samples with GFP were rinsed with PBS followed by a solution of 0.1% Tween 20 detergent and ultrapure water. Rinsing steps are critical for analysis of samples at the nanoscale to remove possible contaminants.

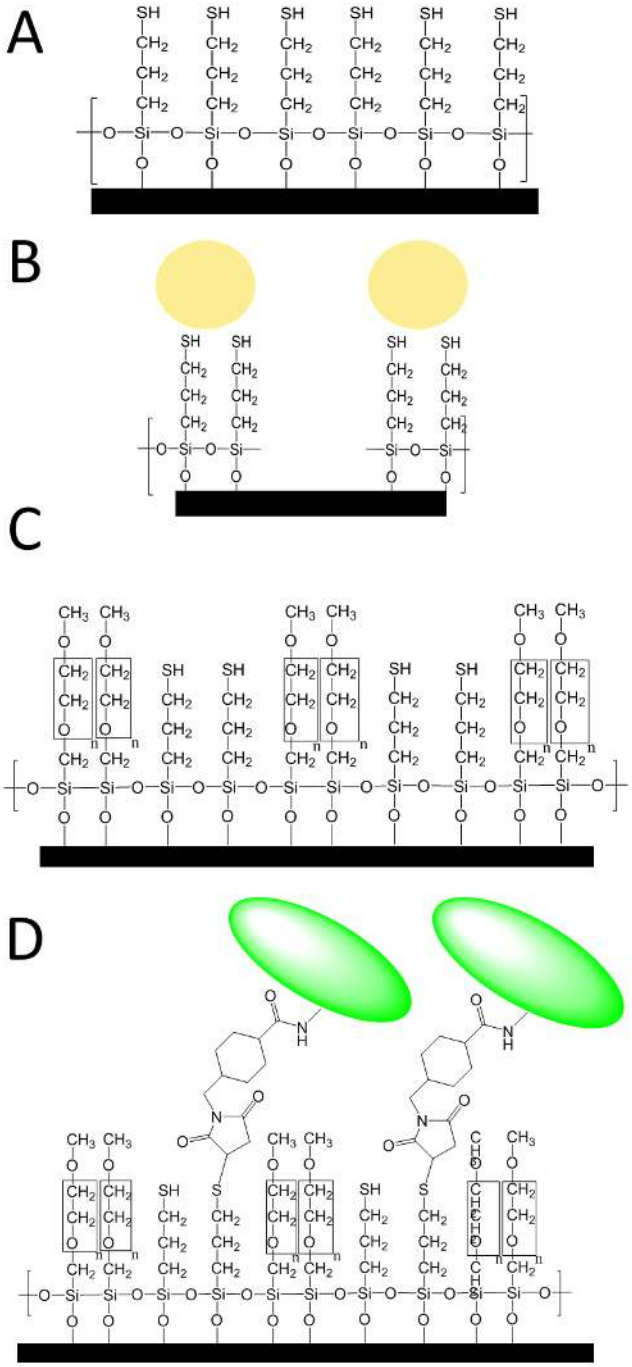

Figure 4.1: Steps for preparing a spatially selective template for patterning GFP with particle lithography. (A) A film of MPTMS was formed on a clean glass substrate using vapor deposition. (B) A mask of silica spheres was placed on top of the prepared MPTMS film. (C) After treatment with UV-ozone the samples were immersed in a solution of MPT-silane to backfill areas that were etched away. (D) A sulfo-SMCC linker was used to attach GFP selectively to areas with –SH groups at the interface. Image is not drawn to scale.

4.2.5 Atomic Force Microscopy

Scanning probe microscopy studies were done after successive steps of sample preparation. A model 5500 atomic force microscope (AFM) was used for imaging, equipped with PicoView v. 1.18 software (Keysight Technologies, Santa Rosa, CA). Contact mode in ambient conditions was used for imaging organic thin films. A commercially available soft probe was used for contact mode studies, (Budget Sensors) with a resonance frequency around 13 kHz and an average spring constant of 0.2 N/m. Tapping mode in ambient air was used for imaging the protein nanopatterns to preserve the sample structure. Probes for tapping mode had a resonance frequency around 300 kHz and an average spring constant of 40 N/m (Budget Sensors). Minimal image processing was done using Gwyddion (v. 2.44) which is freely available and is supported by the Czech Metrology Institute.[255] Surface coverage of the nanopatterns was estimated using pixel counting with FIJI software which converts the images to black and white with a user-defined threshold.[256]

4.3 Results

4.3.1 Characterization of orgaosilane nanopatterns

Images of the nanopatterns surrounded by a MPT-silane resist that were acquired using contact mode AFM are shown in Figure 4.2. Approximately 40 nanopatterns can be viewed in the topography image of Figure 4.2(A), which would scale to ~10^8 patterns per cm^2. The nanopatterns are the sites where the silica spheres were displaced, and are filled with MPTMS. Multiple areas of the sample were imaged, and the AFM frames that are shown are representative of the sample morphology throughout the entire sample. The dark areas reveal the location of holes containing MTPMS surrounded by the lighter colored areas of MPT-silane.

The arrangement of nanopatterns is more clearly evident in the corresponding lateral force image shown in Figure 4.2(B). The spacing between nanopatterns measures ~500 nm, which is attributable to the size of the silica particles used as a surface mask. The differences in surface groups are shown in the lateral force frame, the bright spots have –SH groups for binding GFP, and the darker areas are regions of the MPT-silane matrix which will resist protein adsorption. The mechanisms and resistivity of proteins to the methoxy groups of MPT-silane have been previously reported.[257-261] The circular nanopatterns of MPTMS will provide discrete sites for linking GFP to form single layers of protein.

An individual nanopattern of MPTMS is shown in Figure 4.3, acquired with tapping mode AFM in ambient conditions. With a close-up view, the heights of the matrix and nanopatterns are mostly indistinguishable. The wider areas clearly show that the circular nanopatterns are shallower than the matrix. The depth of the nanopatterns measured 1.6 ± 0.5 nm (n = 63) for cursor measurements of multiple areas. The error term is the value of the standard deviation. The circular shape of the area of MPTMS is apparent in the topography frame in Figure 4.3(A), this is the region of MPTMS that was protected from UV-ozone irradiation by a silica sphere.

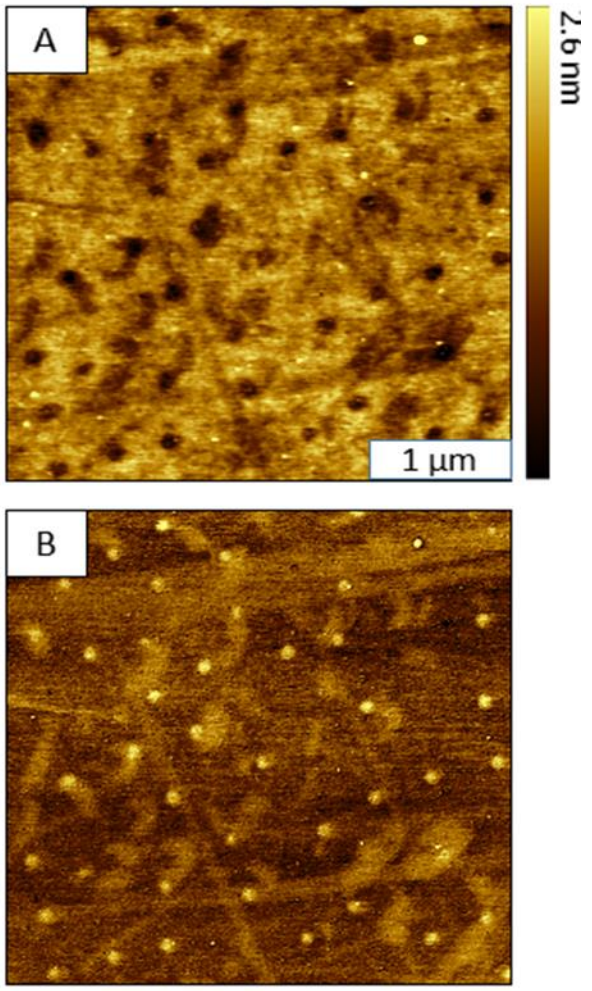

Figure 4.2: Nanopatterns of MPTMS within a film of MPT-silane prepared using particle lithography, as viewed with contact mode AFM images.(A) Wide area of the sample viewed with a topography frame (4×4 µm^2); (B) simultaneously acquired lateral force image.

Differences in the surface chemistry of the nanopatterns and matrix area are revealed in the simultaneously acquired lateral force image [Figure 4.3B]. There are distinct differences in tip-surface interactions between matrix areas and the –SH nanopatterns of MPTMS. An example height profile along the white line drawn across the nanopattern is shown in Figure 4.3C. The average diameter of the nanopores measured 94 ± 20 nm which is much smaller than the size of the silica spheres used as a surface mask. The size of the nanopatterns of MPTMS represents the actual area of contact of the spheres with the surface. The spacing between nanopatterns is

determined by the size of the particles used to form a surface mask. An estimate of surface coverage was obtained by pixel counting, approximately 4.4% of the surface is covered with MPTMS nanopatterns as active areas for binding GFP. The small holes surrounding the nanopattern result from natural defects in the glass cover slides.

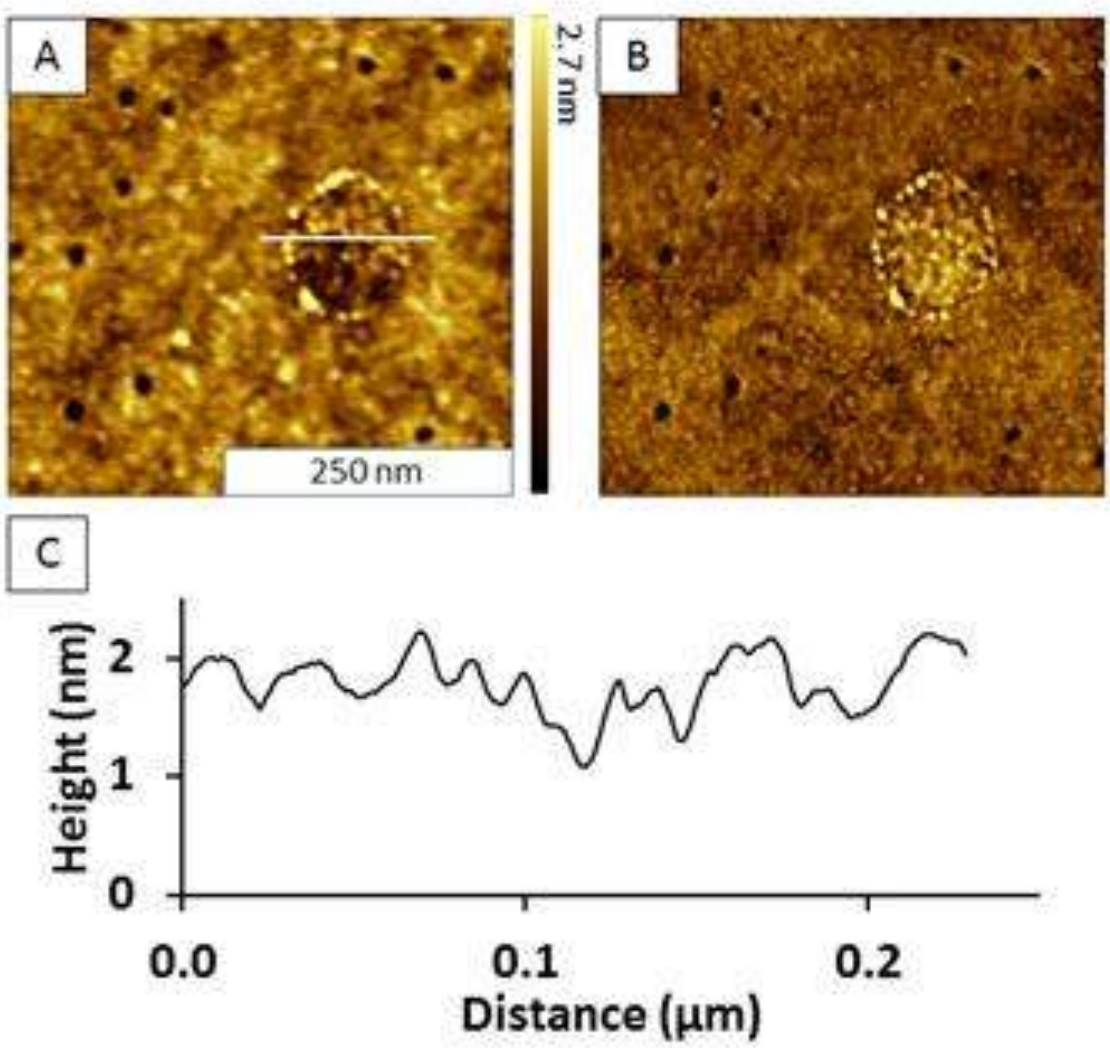

Figure 4.3: Single nanopattern of MPTMS characterized with contact mode AFM.(A) Close up topography view of a single nanopattern of MPTMS; (B) corresponding lateral force image; (C) cursor profile for the white line in (A).

4.3.2 Evaluating the selectivity of nanopatterns for binding GFP

The samples prepared with MPTMS nanopatterns within a matrix of MPT-silane were used as a surface template for attaching a linker molecule to bind GFP. Samples were immersed in a solution of sulfo-SMCC in PBS and then transferred to a solution of GFP. After attaching protein, the nanopatterns of GFP were imaged with tapping mode AFM [Figure 4.4] to evaluate the selectivity of protein binding. Taller features are apparent in the topography frame [Figure 4.4(A)] for most of the sites of MPTMS nanopatterns. There are approximately 98 nanopatterns within the $6 \times 6\ \mu m^2$ frame.

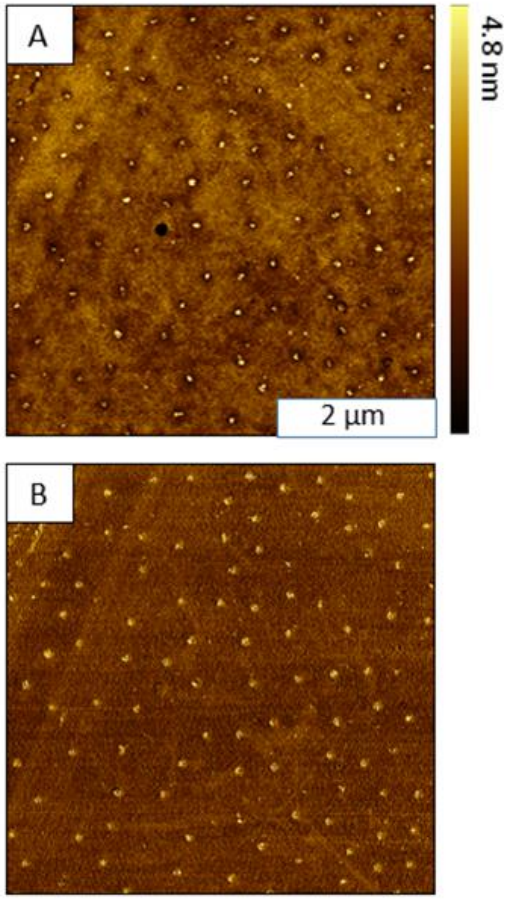

Figure 4.4: Surface changes after binding GFP to MPTMS nanopatterns. (A) Nanopatterns of GFP viewed with tapping mode, 6 × 6 µm2 topography frame; (B) simultaneously acquired phase image.

Green fluorescent protein appears to bind predominantly to the nanopatterns sites of MPTMS. Any nonspecific adsorption of GFP on the areas of MPT-silane in between the nanopatterns is not discernable at this magnification. The arrangement of circular GFP nanopatterns is apparent in the phase image shown in Figure 4.4(B). Phase images are acquired simultaneously with topography images, and sensitively disclose the elastic response of surface features. Differences in softness between the matrix film and GFP are mapped for corresponding areas shown in the topography frame. The size and shape of the nanopatterns is quite regular for such small-sized patterns and the spacing between patterns corresponds to the periodicity and packing of the mask of silica spheres used for particle lithography.

Close-up views of an individual nanopattern after binding GFP are presented in Figure 4.5(A). The nanopattern appears to have a cluster of GFP, the morphology of the proteins resemble nanoparticles, with a spherical shape. The spherical shapes are attributable to AFM imaging artifacts, because the shape of the apex of the AFM tip is convoluted with the shape of very small surface features. Sharper probes will provide images which more closely resemble the true protein morphology. At this magnification the nonspecific adsorption of a few isolated proteins can be detected in areas around the MPTMS nanopatterns. Intricate details of the shapes and arrangement of GFP within a single nanopattern are revealed in the phase image of Figure 4.5(B). The bright colored areas are GFP and have distinct differences in morphology compared to the surrounding areas of the oligo(ethylene glycol) terminated silane matrix.

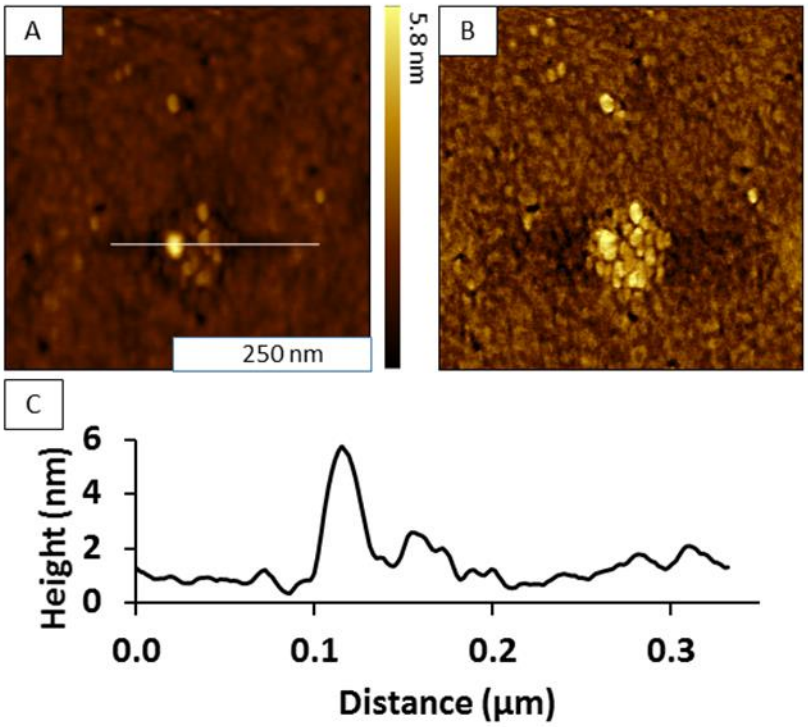

Figure 4.5: Magnified views of an individual GFP nanopattern acquired with tapping mode AFM. (A) Close up of an MPTMS nanopattern with GFP attached, topograph 500 × 500 nm^2; (B) corresponding phase image; (C) Example cursor profile for the line in A.

4.3.3 Analysis of protein dimensions with GFP nanopatterns

There are two lines of evidence that GFP was bound to MPTMS nanopatterns. First, the surface morphology of the MPTMS nanopatterns has changed. The size and shape of adsorbates was larger for the areas of nanopatterns after treatment with the linker chemistry and GFP. Second, the height of the nanopatterns is greater after binding protein. The height of the nanopatterns increased after treatment with linker chemistry and GFP to reveal clusters of adsorbates that are taller than the matrix film. The distribution of the height measurements of nanopatterns before and after binding protein is detailed in Figure 4.6. The average height of the nanopatterns was derived using AFM cursor measurements of multiple areas. The depth of the nanopores are fairly uniform [Figure 4.6(A)] which suggests that the MPT-silane matrix is relatively homogeneous in thickness.

There is a broader range of heights for the nanopatterns after binding GFP [Figure 4.6(B)] because the proteins assemble with different orientations such as side-on or end-on.

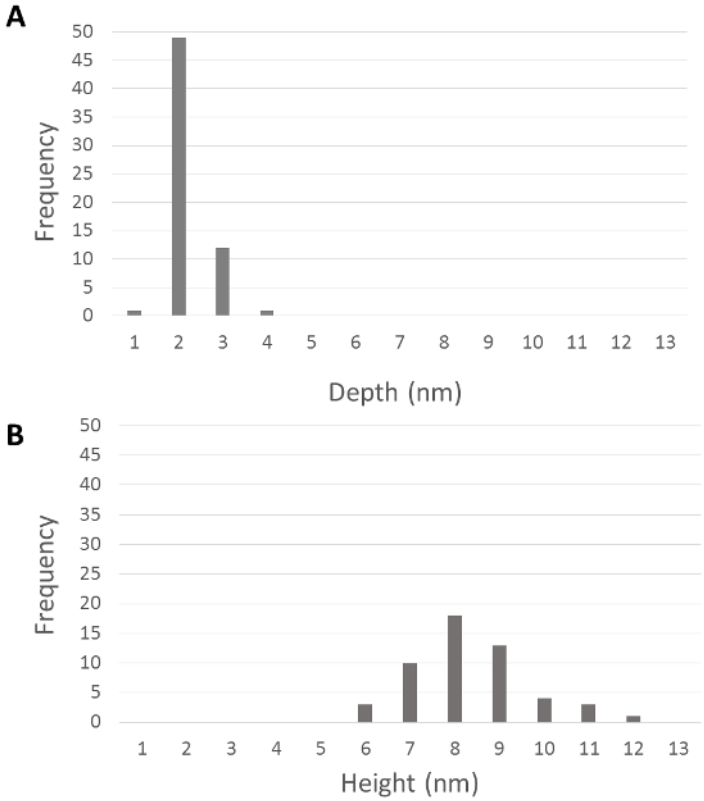

Figure 4.6: Size analysis of nanopatterns. (A) Depth of nanopatterns of MPTMS; (B) change in height

The average depth of the nanopores containing MPTMS measured 1.6 ± 0.5 nm (n = 63). After treatment with a linker molecule (sulfo-SMCC, 0.83 nm) and attaching GFP, the height of the nanopatterns measured 6.8 ± 1.3 nm (n = 52). The dimensions reported for GFP measure 4.2 nm in length and 2.4 nm in diameter.[262, 263] Taking into consideration the length of the linker molecule, the height of the nanopatterns correspond to an end-on orientation for GFP, with the longer portion of the protein oriented vertically with respect to the substrate. The variability in measured values in Figure 4.6 can be attributed partially to the roughness of the glass substrate. Also, the protein may not be oriented fully in the vertical direction, there may be proteins that have

a side-on or canted orientation depending on the self-aggregation and surface density of protein within the MPTMS sites.

4.4 Summary and Conclusions

Nanopatterns of organosilanes prepared with particle lithography can be used effectively to direct the adsorption of proteins onto selected areas of glass surfaces. Nanopatterns of GFP were prepared using a linker group and a spatially selective surface template. The selectivity of the biointerface at the nanoscale was evaluated with *ex situ* AFM studies, revealing that a single layer of protein was bound preferentially to areas of MPTMS nanopatterns. The designed surface with defined nanopatterns of protein provide an excellent platform for measuring the dimensions of GFP, assessing surface orientation, and viewing surface density using AFM. Future studies will be developed with smaller size particles for the surface mask, as well as *in situ* studies of protein binding reactions in buffer.

CHAPTER 5. PREPARATION OF OCTADECYLTRICHLOROSILANE NANOPATTERNS USING PARTICLE LITHOGRAPHY: AN ATOMIC FORCE MICROSCOPY LABORATORY

5.1 Introduction

Scanning probe microscopy (SPM) has increasingly become integrated in undergraduate laboratories and research activities.[264-266] However, it can be challenging to find very small size samples for SPM studies to provide an interesting "hands-on" experience with nanoscience. We have found that undergraduates can easily prepare nanostructures of organosilanes on surfaces using lab protocols based on particle lithography to demonstrate chemistry reactions at the nanoscale. To accomplish nanoscale lithography, a film of latex or silica spheres is used as a surface mask to make nanopatterns of organic thin films, such as octadecyltrichlorosilane (OTS).[267] Using either vapor deposition or immersion protocols of particle lithography, molecules of OTS bind to masked substrates in areas between the spheres to form regular circular patterns that are suitable for scanning probe analysis. Experiments with SPM provide students with training and experience with nanoscience, molecular self-assembly, chemistry lab protocols, instrumental analysis, digital image processing, as well as data interpretation.

Particle lithography offers high throughput as well as control of surface density, which is ideal for patterning organic thin films. The dimensions of nanopatterns prepared with particle lithography are at the level of a few nanometers to the molecular thickness of films, providing an excellent model sample for undergraduate studies. The steps for sample preparation provide students with basic chemistry skills, and generate highly reproducible results at the nanoscale.

To evaluate the samples of organosilane nanopatterns, instruments are needed that have resolution beyond the optical microscope to view features that are smaller than the wavelength of light. Analysis with an atomic force microscope (AFM) requires little sample preparation and can provide results with nanometer resolution.[268-270] The benefits of using an AFM in the

undergraduate teaching curriculum have been reported previously.[271-275] To demonstrate interdisciplinary topics in surface science and chemistry, nanofabrication of organic thin films offers practical and relatively inexpensive methods for undergraduate studies.

In the experiments described, particle lithography was used to prepare nanopatterns with octadecyltrichlorosilane (OTS). To produce regularly spaced patterns of uniform geometry at the nanoscale, monodispersed latex or silica beads were used as a surface mask. Two methods of depositing OTS are demonstrated to make ring-shaped nanopatterns or nanoholes within an OTS matrix film. Undergraduates enjoy characterizing the nanopatterns that they have prepared and learning how to image their samples with AFM. Nanoscience is an interdisciplinary field, therefore the laboratory introduces concepts in chemistry and surface science, as well as instrumental approaches for instrumental analysis of samples.

5.2 Experimental Methods and results

Two preparation methods will be described for preparing OTS nanopatterns on silicon substrates. An overview of the process for vapor deposition of OTS is shown at the top of Figure 5.1, and the steps for an immersion method are shown in the bottom panels. In both methods, trace amounts of water are important in determining the shape of OTS nanopatterns.[276] Water is essential for initiating the hydrolysis of OTS, however if too much water is present on the surface then self-polymerization takes place to generate multilayers. The location of small amounts of water on the surface surrounding the particle mask determines the reaction sites for hydrolysis and condensation of OTS.[253]

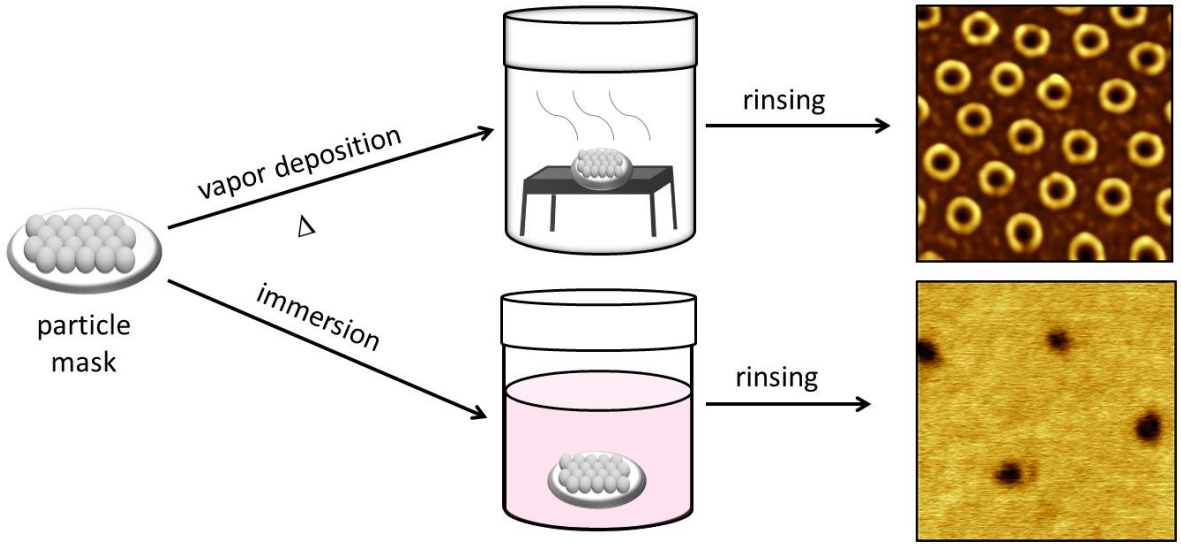

Figure 5.1: Nanopatterns prepared using particle lithography combined with (top) vapor deposition and (bottom) immersion of a particle mask in an OTS solution. The AFM topography frames (1×1 μm^2) were acquired in ambient air.

Undergraduate students prepared samples using silicon substrates. Silicon wafers were cleaned with Piranha solution, rinsed with ultra-pure water and dried. For nanoscale studies with AFM, samples must be free of contaminants so the cleaning procedure is critical for successfully preparing samples for experiments. Organochlorosilanes spontaneously form cross-linked films on surfaces of mica, glass, metal oxides and silicon [Figure 5.2]. When siloxane films are formed from OTS there is a competition for the Si-O bridges to form links to the substrate, cross-links to adjacent molecules and for producing free hydroxyl groups. Self-polymerization can occur when excess water is present to generate multilayered surface structures.

Two methods for particle lithography will be demonstrated to show how small changes in the procedure for depositing OTS can dramatically influence the shapes of the nanopatterns that are made. With vapor deposition of OTS, ring-shaped nanopatterns were formed with a multilayer formed at the edges of the nanoholes. With a solution immersion step for silane deposition,

nanoholes within a film of OTS were produced. Both methods produce areas of uncovered substrate that can be filled with new molecules to prepare more complex patterns.

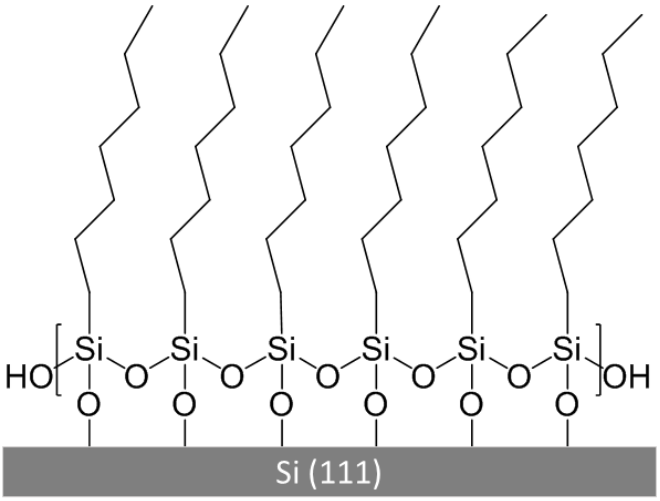

Figure 5.2: Self-assembly of organosilanes forms a cross-linked film on a silicon surface.

5.3 Preparation of a Surface Mask with Size-Sorted Latex or Silica Particles

The first step of sample preparation is the same for both procedures of particle lithography, preparation of a mask of monodisperse spheres on a flat substrate. An aliquot of the latex or silica spheres was cleaned by centrifugation in water. After centrifuging, the pellet was resuspended in high purity water for three washing cycles. Next a drop of the mesosphere solution was placed onto each substrate so that the entire surface was covered by the solution. A droplet of 20 µL will cover an area of 1×1 cm^2. The solution was dried on the substrates for at least 6 h. A view of a surface mask prepared with 495 nm latex spheres is shown in Figure 5.3. The latex beads

spontaneously pack into a hexagonal arrangement on flat surfaces, and furnish a suitable mask for producing uniform nanopatterns of organosiloxanes.

The area of the sample shown in Figure 5.3 is a view of the topmost layer of latex for the

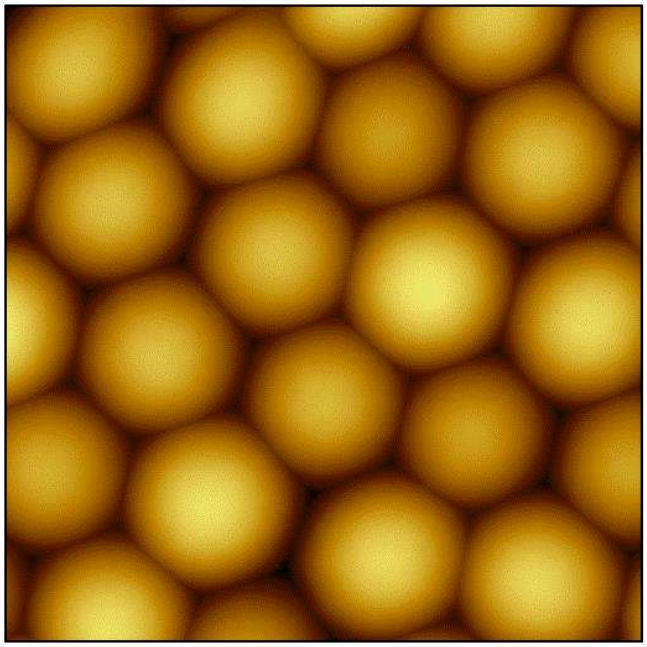

Figure 5.3: Arrangement of spheres for a surface mask of 495 nm diameter latex viewed with an AFM topography frame (2×2 μm^2).

surface mask, however the layer at the bottom of a multilayered film is the template for particle lithography. When an aqueous suspension of monodisperse latex or silica beads is dried, a close-packed arrangement of spheres forms spontaneously to form a periodic arrangement. The spacing between nanopatterns can be selected by changing the diameter of particles used as a surface mask.

5.4 Hazards

Personal protective equipment should be used throughout the experiment, including apron or lab coat, goggles and gloves. Samples should be prepared in a well-ventilated area such as fume hoods. Chemical waste should be disposed according to the material safety data sheet specifications found for each material. Piranha solution is corrosive. Care should be taken when handling Piranha solution to avoid skin contact.

5.5 Particle Lithography Combined with Vapor Deposition of OTS

To prepare samples using particle lithography with vapor deposition of OTS, the masked substrates were placed on a platform in a sealed container with neat silane. The reaction vessel was sealed and placed in a 70 °C oven for 15 h. In the final step, the latex mask was removed by rinsing and sonication. Ring shaped nanopatterns were formed with a multilayer of OTS surrounding the edges of the nanoholes where latex spheres were displaced.

A sample was prepared using 300 nm latex as a surface mask, as shown in Figure 5.4. The ring shapes are formed by the self-polymerization of OTS in areas of the water meniscus surrounding the base of the spheres. The arrangement of regularly shaped rings is apparent in the topography frame ($4\times4\ \mu m^2$) of Figure 5.4A. The locations of each ring nanopattern are sites where a latex particle was displaced. The area of contact between a sphere and a planar surface is quite small, however the spacing between nanopatterns corresponds to the 300 nm diameter of the latex mask. Within the frame of Figure 5.4 A, there are 664 nanopatterns, which scales to $2.64\ \sim10^9$ nanostructures for a $1\times1\ cm^2$ sample.

A hexagonal arrangement of the nanorings is evident in the magnified view of Figure 5.4B. The center of the rings are deeper than the areas surrounding the nanopatterns. The area of actual contact between the latex spheres and the surface produces sites of uncovered substrate as a baseline for cursor measurements of film thickness.

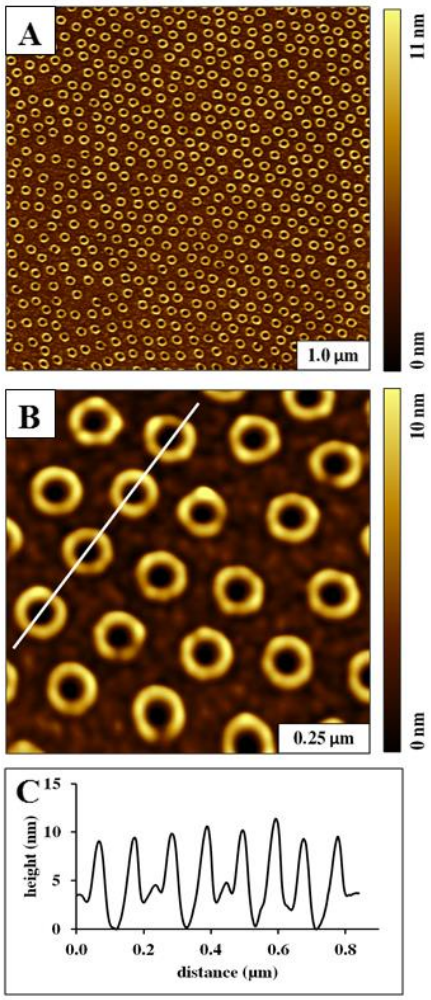

Figure 5.4: Nanostructures of OTS prepared using particle lithography combined with vapor deposition.(A) Arrangement of ring nanostructures viewed with a topography image (5×5 μm^2); (B) Magnified view (1×1 μm^2); (C) cursor profile for the white line in B.

The heights for the nanopatterns is indicated with an example line profile (Figure 5.4C) drawn across four nanopatterns. The layer of OTS forming the rings is taller than the matrix film formed in between the circles. The thickness of the rings measured 9.1 ± 0.7 nm (n= 50). The theoretical height of OTS oriented perpendicular to the substrate is 2.1 ± 0.3 nm.[277] Considering this value, the height of the nanorings corresponds to approximately 3-4 layers of polymerized OTS in the meniscus areas of the latex mask. The regions of OTS between the ring nanopatterns has a relatively uniform thickness and matches the thickness of a monolayer. The area of uncovered

substrate within the rings measures 64.3 ± 9.2 nm (n=84) in diameter, furnishing exquisitely small, uniform holes for depositing new molecules or nanomaterials.[278-280]

5.6 Immersion Particle Lithography

When a masked substrate is placed into a solution of ethanol or water, we have observed that latex and silica beads will rapidly detach from the surface. To accomplish particle lithography with an immersion step the particle mask can be temporarily annealed to the surface by heating. With further sonication and rinsing the particles can be removed later on. Immersion of substrates in organosilane solutions is the optimal procedure to prepare high quality monolayer films. Immersion steps enable optimization of parameters such as concentration, duration of exposure, and trace amounts of water in the solvents,

For immersion particle lithography a substrate masked with silica spheres was placed into an oven at 150° C overnight, to temporarily anneal the beads to the surface. After cooling, the annealed sample was placed into solution of OTS (0.1%) in toluene and left to react for 8 h. The samples were then rinsed with ultrapure water and alternately washed in ethanol and water for 10 min each to remove the silica particles.

With immersion particle lithography, a film of OTS punctuated with small holes was produced as shown with a representative topography image in Figure 5.5. Multilayers of OTS did not form, the thickness of the film appears to be homogeneous throughout the sample [Figure 5.5A]. The dark circular areas of nanoholes are sites of the uncovered substrate where the silica particles were displaced. The absence of a ring of multilayered OTS reveals that there was no water meniscus surrounding the particles of the mask, indicating that the heating step removed trace residues of water. There are 104 nanoholes visible within the 5× 5 μm^2 frame of Figure 5.5A, this

scales to 4.16×10^9 nanopatterns per cm^2 for the surface density. A few bright spots of adsorbates are present on areas of the matrix film, these can mostly be removed by additional rinsing steps.

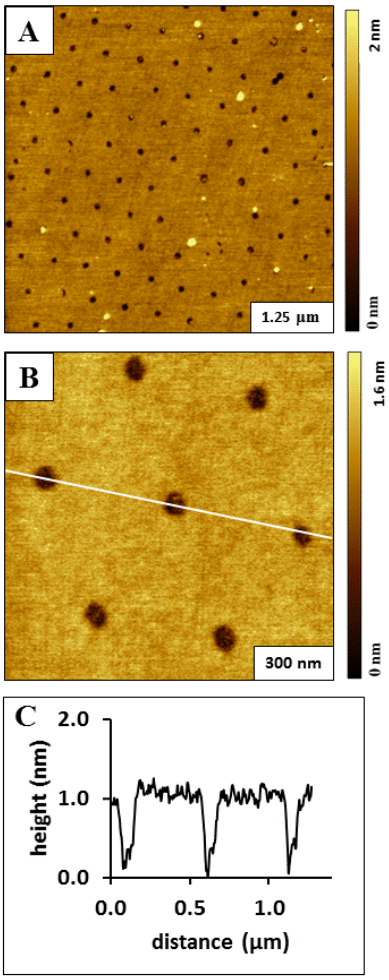

Figure 5.5: Nanoholes within a film of OTS produced by immersion particle lithography. (A) Location of nanoholes over a 5×5 μm^2 area, topography image acquired in air; (B) Zoom-in view of the hexagonal arrangement of nanoholes (1.3×1.3 μm^2); (C) Cursor profile for the white line in B.

A close-up view of the arrangement of seven nanohole patterns is shown in Figure 5.5B. Unlike the ring nanopatterns in Figure 5.4, with an immersion step nanoholes were formed when the particle mask was removed. The bottom of the nanoholes are uncovered areas of the silicon substrate which were protected by the silica particles of the surface mask. The nanoholes are

surrounding by a film of methyl-terminated OTS which furnishes an excellent resist layer for further chemical steps. The average thickness of the OTS film measured 1.2 nm ± 0.2 nm (n=50) Considering that the theoretical height of a densely packed OTS monolayer when it is oriented perpendicular to the surface is 2.1 ± 0.3 nm,[277] the average value indicates incomplete surface coverage. An example cursor profile drawn across three nanohole patterns is shown in Figure 5.5C. The spacing (center to-center) between nanoholes measures ~500 nm which matches the diameter of the silica spheres used as a surface mask.

5.7 Changes in Nanopatterns with an Immersion Step versus Vapor Deposition of OTS

A side-by-side comparison of nanopatterns prepared with particle lithography is shown in Figure 5.6 for samples made with steps of immersion or vapor deposition. The images disclose remarkable uniformity for the shapes and periodicity of the nanopatterns. However, the deposition method produces somewhat different morphologies for either ring shapes [Figure 5.6A] or nanoholes [Figure 5.6B] within a film of OTS. The results shown are representative images of areas throughout the sample, and the shapes of the nanopatterns are reproducible for preparing multiple samples. When preparing nanorings with vapor deposition, the heights of the rings will change according to the size of the particle masks. Larger particles produce taller rings because there is more liquid in the sites of the meniscus surrounding the base of the spheres. However, with immersion particle lithography the size and geometry of the nanoholes is consistent even when changing the diameter of the particle mask.

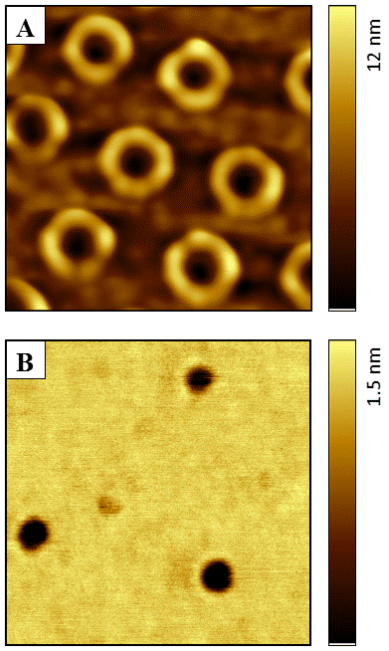

Figure 5.6: Comparison of samples prepared with particle lithography using (A) vapor deposition of OTS (600×600 nm^2); (B) immersion of masked substrates in solution. Topography views were acquired in air (1.3×1.3 μm^2).

5.8 Conclusion

Experiments using particle lithography were described for teaching skills of sample preparation and instrumental analysis to undergraduates. Students gain valuable hands-on experience with an AFM as well as learn chemistry and nanoscience concepts about how molecules arrange on surfaces. The experiments can be used as an independent study for undergraduates or for laboratory experiments. Undergraduates at Louisiana State University have tested the protocols in physical chemistry labs, learning the techniques in a single afternoon session. Students enjoyed the activities of visualizing the nanopatterns that they prepared themselves as well as having an opportunity for characterizing samples with advanced instrumentation.

CHAPTER 6. THICKNESS-DEPENDENT THERMAL DEWETTING OF Au FILMS ON GLASS

6.1 Introduction

It is well known that the microstructure of metal films are sensitive to a variety of deposition parameters, including deposition method (thermal vs. sputtering), deposition rate, substrate surface characteristics, and substrate temperature.[281] Post deposition processing can also have profound effects on the film morphology. For instance, annealing the films at elevated temperatures can completely change their microstructure.[282-287] Annealing has been used to processes thin metal films for purposes of nanostructuring, determining the interfacial energies, as well as small scale mechanical testing.[8]

Thermal annealing works by producing lateral mass diffusion in the metal film in order for the system to lower the surface free energy.[282-287] Solid state mass diffusion can change the microstructure of the film and, under the proper conditions, can induce a film to de-wet from the substrate. Typically voids at grain-boundaries, pinholes and even gas bubbles are the site of pore nucleation.[288] From pinhole formation thermal de-wetting proceeds by the formation of tiny clusters that evolve into well-defined islands thus exposing the underlying substrate. Indeed, solid state de-wetting has been extensively studied in gold films deposited on a variety of substrates. [281, 282, 288-296]

One of the earliest reports of de-wetting during thermal annealing was by Faraday in 1857.[291] He found that when gold leaf was examined under a microscope after being annealed at high temperature, a greater amount of white light was transmitted from holes that were present in pre-annealed gold leaf. Typically, voids in solid films start at one of three areas: grain-boundaries,[293, 297-300] from pore nucleation at the film-substrate interface,[301-303] or from areas of high stress at grain boundary triple junctions.[304] After voids have been nucleated in the film, they

can grow[285, 301] and form islands.[305] As the void regions spread, material that is displaced is incorporated into the island structures. Of course, the details of thermally induced island growth depends on many physical parameters such as the surface tension in the film, the adhesion between the film and the substrate, and the vapor pressure of the film.[281, 285, 290, 306-309]

The optical properties of thin gold films can also change after annealing.[294, 310-312] Indeed, the morphological characteristics of the films can be probed using surface-enhanced infrared absorption (SEIRA) and surface-enhanced Raman scattering.[313-315] For example, by measuring the change in the surface plasmon resonance in gold films, the adsorption of sub-monolayer organic thin films on the gold surface can be detected.[296, 312, 316]

In the present work we present a detailed study of the effects of thermal annealing on Au films on glass as a function of the nominal pre-annealed film thickness. Surface morphology before and after annealing was monitored using atomic force microscopy. Surface plasmon of the films were also monitored before and after annealing of the thin films. To further investigate island development a time dependent study was conducted on two 100 Å films was imaged after subsequent annealing every fifteen minutes.

6.2 Experimental Details

6.2.1 Preparation of the Thin Films

Cover glass slides (Thomas Scientific, Red Label) were cleaned via 5 minutes of sonication in boiling ultrapure water followed by sonication in methanol. Just prior to the Au deposition the clean glass slides were fire-polished in a propane flame. Gold films ranging in thicknesses from 2.0 nm to 15 nm were deposited at room temperature in a vacuum of ~1 μTorr via electron beam evaporation of 99.999% Au. Typical deposition rates were ~ 0.1 nm/s. The films were annealed

by placing them in a horizontal tube furnace at 550 C for 60 minutes in an argon/hydrogen gas flow.

6.2.2 Atomic Force Microscopy

Both the pristine and annealed gold films were characterized using contact mode atomic force microscopy on a 5420 Agilent scanning probe microscope (Agilent Technologies, Chandler, AZ). Triangular MSCT tips from Bruker were used with force constants ranging from 0.030- 0.60 N/m and resonance frequencies ranging from 4-160 kHz (Burker, Camarillo, CA). Images were processed using Gwyddion 2.31 open source software, which is supported by the Czech Metrology Institute.[317] Surface coverage as well as average height measurements were also conducted in Gwyddion by masking the gold islands with a height filter.

6.2.3 UV-Vis-NIR Analysis.

Surface plasmon changes from pre- and post-annealed films were monitored using a Cary 5000 UV-Vis-NIR spectrophotometer (Chandler, AZ). Spectra were collected from 300-2000 nm range under a nitrogen environment. The detector crossover from NIR to UV-Vis was set to 800 nm. All samples were measured using a double beam design with a fire-polished glass slide as the blank.

6.2.4 Kinetic Study of Film Development

Two films, 100 Å thick were placed in a tube furnace. Both films were heated and annaled for 15, 30, 45, 60, and 120 minutes. After each successive annealing the two films were imaged by atomic force microscopy. Three topography images ($2 \times 2\ \mu m^2$) from each film during each annealing were imported into FIJI.[318] The image was converted to 8-bit format and then made into a binary image using the thresholding tool. Grain analysis was then completed using built in

software in FIJI and surface coverage was calculated. Particles on the edges of the frame were excluded from analysis due to variability.

6.3 Results and Discussion

Shown in Figure 6.1 are AFM images of pristine Au films of varying thickness. The 2.5 nm thick film has significant voids but otherwise shows little spheroid granularity. The bare substrate can be seen in parts of the image between the grains as evidenced by the lateral force image. Large clumps of gold can also be seen speckled throughout the topograph image. In contrast, the 15 nm film has a relatively well-defined spheroid granular texture with a typical grain diameter of approximately 40 nm. These grains are somewhat larger than those observed in the unnealed 2.5 nm film. The 10 nm film microstructure appears to be a convolution of the 2.5 nm and 15 nm film morphologies. Although all three films appear to almost completely cover the substrate surface, none of them, in fact, were electrically continuous.[319] As can be seen in the AFM images, the gaps between the grains in the 10 nm and 15 nm films, are very small and beyond the resolution of the instrument. Because we were unable to image the substrate between the grains, the profile traces represent the surface roughness rather than the actual grain heights. It is well known that the morphological details of a pristine film can greatly influence the formation of the post-annealed microstructure[281, 282, 288-296] and the post-anneal electrical properties.[38,39] In this regard one might expect the effects of annealing will be substantially different between the 2.5 nm film and the 15 nm film, and, indeed this is what we observed.

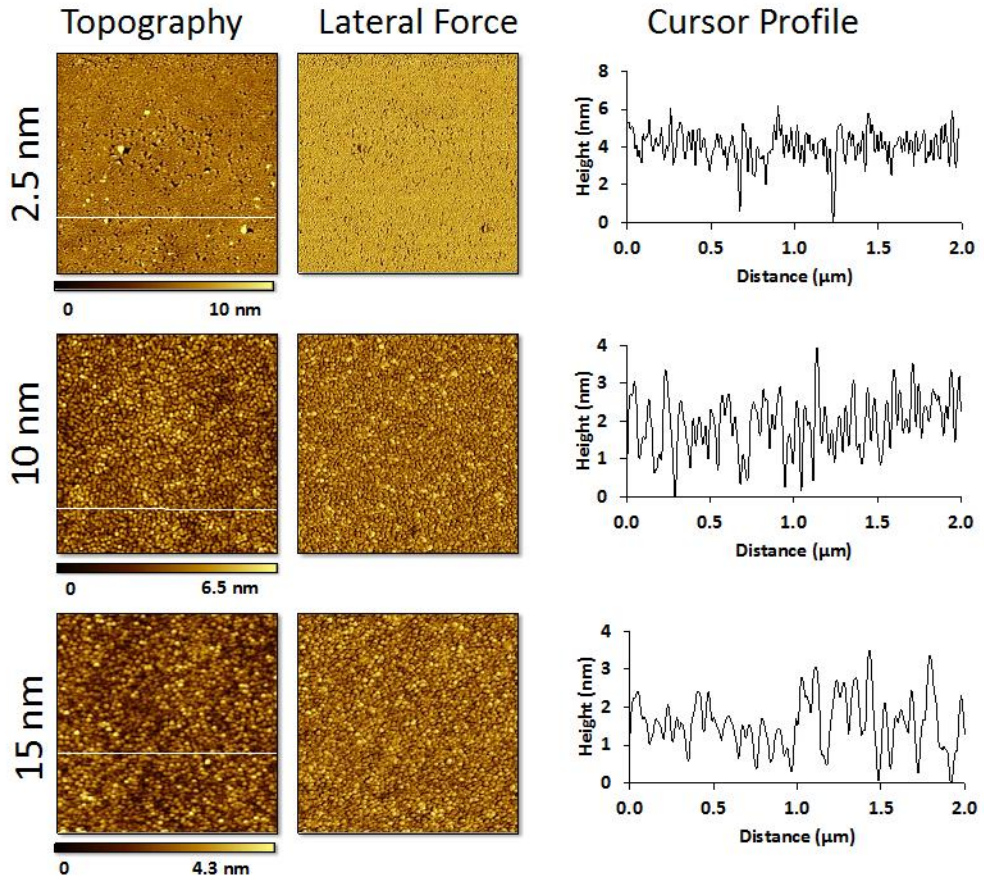

Figure 6.1: Un-annealed gold films on fire-polished glass obtained in contact mode. The films were thermally deposited at room temperature.

In Figure 6.2 we present AFM images of annealed Au films of varying initial thickness. The pre-anneal film thickness was determined from a quartz crystal deposition monitor during the deposition of the Au. Note that annealing generally enhances the granularity of all of the films as is evident by the increased circularity of the grains. Interestingly, the surface coverage of the two thinnest films (2.5 nm and 5 nm) is ~99%, suggesting that the Au did not completely de-wet the glass substrate during the high-temperature anneal. When these two films are viewed with the simultaneously acquired lateral force images, edges of the grains can be seen, but the surface of the substrate cannot be distinguished. In contrast, the post-anneal coverage decreases abruptly for films with initial thickness greater than ~5 nm. Indeed, these thicker films exhibit well-separated

Au islands with little or no Au material remaining in the intra-grain gaps as evidenced by the contrast in the corresponding lateral force images. By increasing the initial film thickness by only 2.5 nm, the surface area coverage of the gold islands fell from ~99% in the 5 nm film to ~66% in the 7.5 nm film. Films with initial thicknesses greater than 5.0 nm show islands with relatively flatter tops after annealing.[312, 320]

In Figure 6.3 we plot the surface coverage as a function of the initial film thickness for all of the films in this study. The coverage data suggests that the films exhibit a de-wetting threshold at a critical thickness of about 6 nm. Films thinner than this will not de-wet under the the particular annealing conditions used in this study. Thicker films clearly do de-wet and ironically, the plot clearly shows that the surface coverage of these annealed films decreases with increasing initial thickness.[312] The height of the islands must simultaneously increase with increasing initial thickness in order to conserve mass, unless, of course, mass is lost to evaporation during the anneal. The latter possibility can be ruled out by the fact that, at the annealing temperature of 550 C, the vapor pressure of Au is of the order of 10^{-14} Torr.[321] In Figure 6.4 we plot the average Au island height as a function of initial thickness. As expected, there is a positive correlation between the island heights and the initial film thickness.[312, 320]

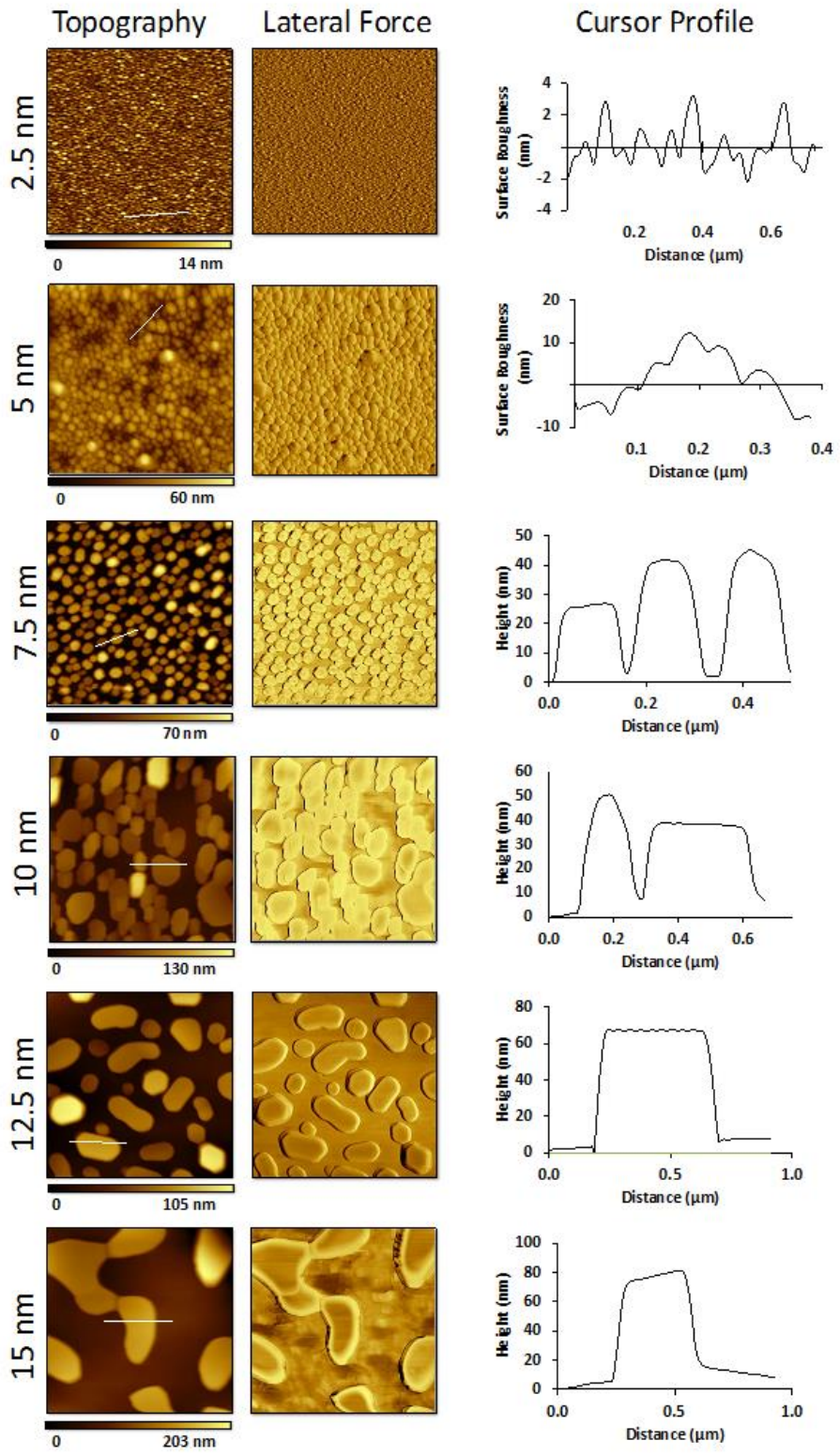

Figure 6.2: Annealed Au films of varying initial deposition thickness obtained in contact mode. Topographs with corresponding lateral force, and cursor profile of the white line drawn in the topograph.

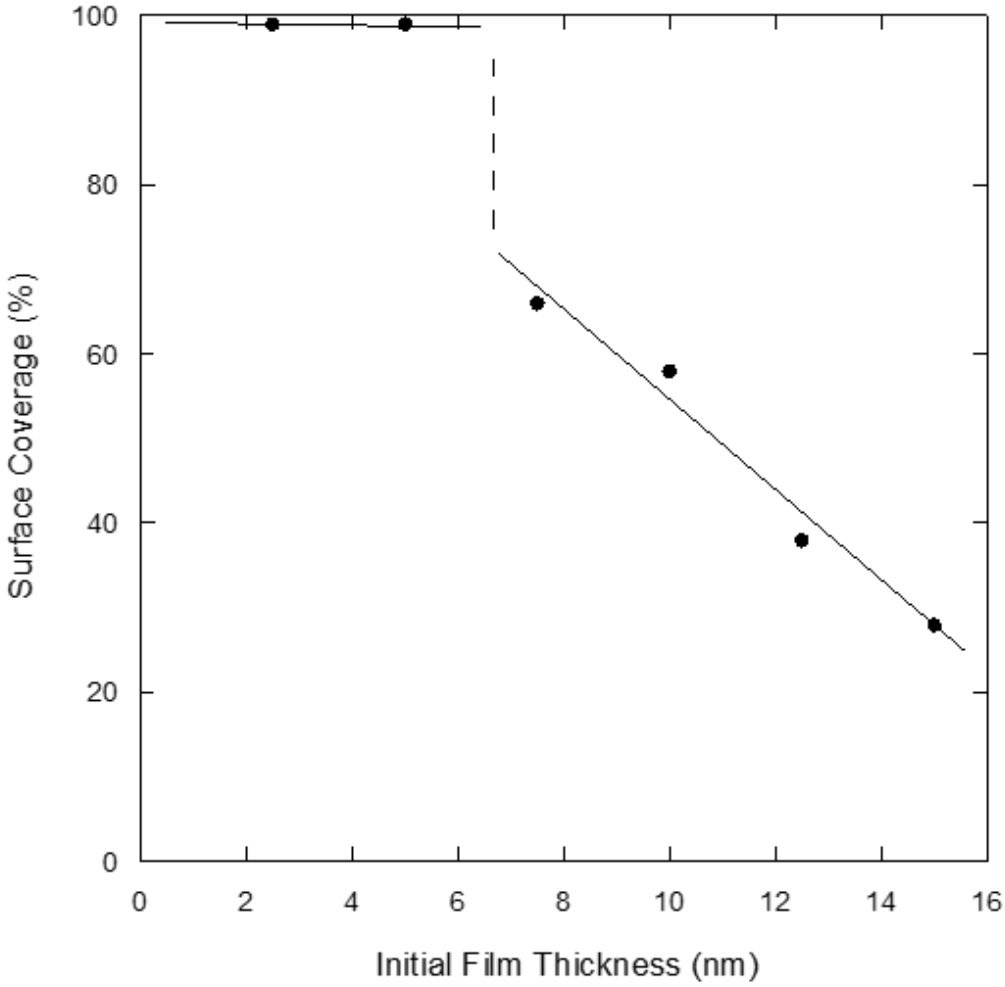

Figure 6.3: Surface coverage of annealed Au films as a function of the initial un-annealed film thickness.The lines are provided as a guide to the eye.

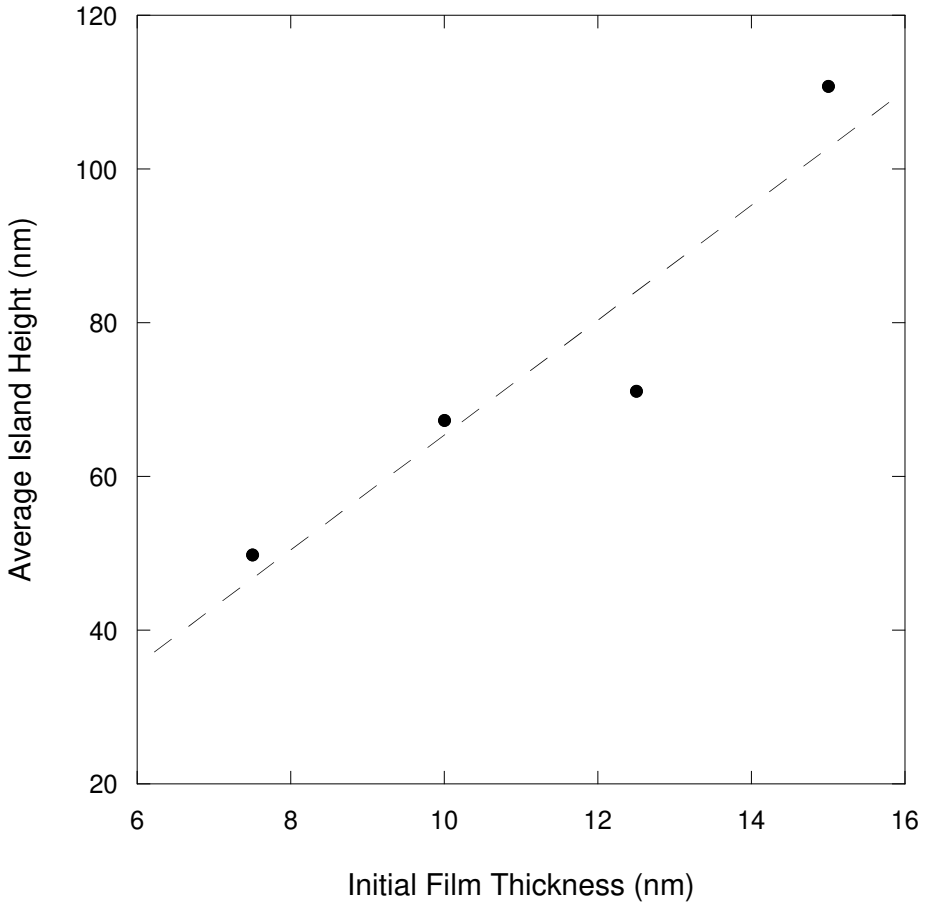

Figure 6.4: Average island height in annealed Au films as a function of the pre-anneal film thickness. The dashed line is provided as a guide to the eye.

The Au film morphology was also explored using surface plasmon resonance spectroscopy in the UV-Vis-NIR spectral range. Shown in Figure 6.5 are the extinction spectra of several Au films before and after annealing. Note that the un-annealed films all exhibit a broad absorption peak centered at a wavelength of ~700 nm and have an extended near infrared absorption tail. The un-annealed films also show a local adsorption minimum in the 500-550 nm range. In contrast, the annealed films show a much sharper absorption peak near 550 nm and very little absorption beyond 800 nm. Interestingly, the spectra of the annealed 2.7 nm and 5.3 nm are almost identical. Note, however, that films thicker than ~ 6 nm have a significantly stronger overall absorption than those

of the two thinner films. We believe that this abrupt increase in the amplitude of the absorption peak reflects the de-wetting transition. In addition to the enhancement of the absorption peak, increasing film thickness shifts the peak to shorter wavelengths.[322,41] Rycenga *et. al.* and Mayer *et. al.* have attributed this to a charge separation in islands with sharper corners.[323, 324] Indeed, when observed through the AFM data, as the initial film thickness increases, the islands become rounder with fewer sharp corners.

In order to verify that post-annealed film images reflected the steady-state morphologies of the system we performed a series of AFM scans at preset annealing durations. Two gold films, each 10 nm thick, were annealed under the conditions used in this study for 15, 30, 45, 60, and 120 minutes. Shown in Figure 6.6 are the topographs of the films after the stated annealing times. Each film was removed at the stated annealing times and then imaged. The films were then returned to the furnace for further annealing. As can be seen from the two upper panels, the Au islands are well formed after only 15 minutes of annealing at 550 C. Although there are some minor changes in the island distributions as the annealing time is increased, the dewetting transition occurs quite early in these relatively thick films and their structure remains relatively constant from thereon. These measurements show that even if Au films with thicknesses less than 6 nm eventually dewet and form microstructure similar to their thicker counterparts, the dewetting timescale is least an order of magnitude longer than that of the films in Figure 6.6.

6.4 Conclusions

We have shown that thermally-induced island formation in thin gold films deposited on fire-polished glass slides is sensitive to the film thickness. Films having thicknesses less than ~6 nm do not thermally de-wet when annealed at 550 C. In contrast, thicker films exhibit a well-defined de-wetting behavior in as little as 15 min of annealing. We have demonstrated that by

varying the preanneal Au film thickness, islands of differing sizes and separation can be formed using identical anneal protocols. It should prove interesting to see if similar thickness dependencies of the de-wetting behavior of Au films occurs on other substrates.

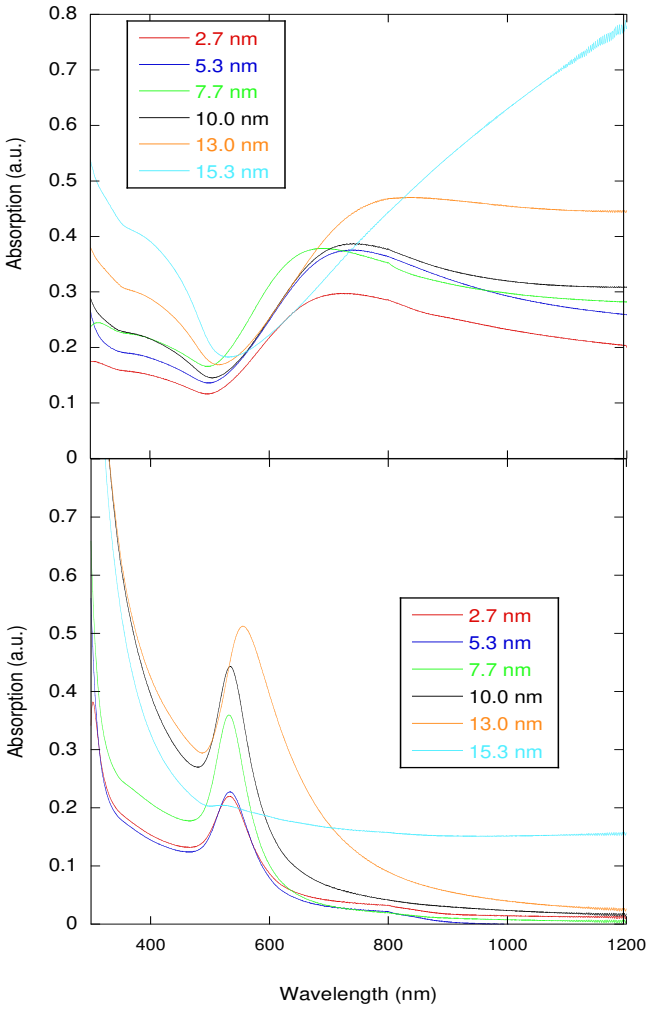

Figure 6.5: UV-vis spectra of Au films of varying initial thickness before (upper panel) and after (lower panel) annealing.

Figure 6.6: AFM images of two 10 nm-thick Au films after the indicated annealing times. The annealing temperature was 550C.

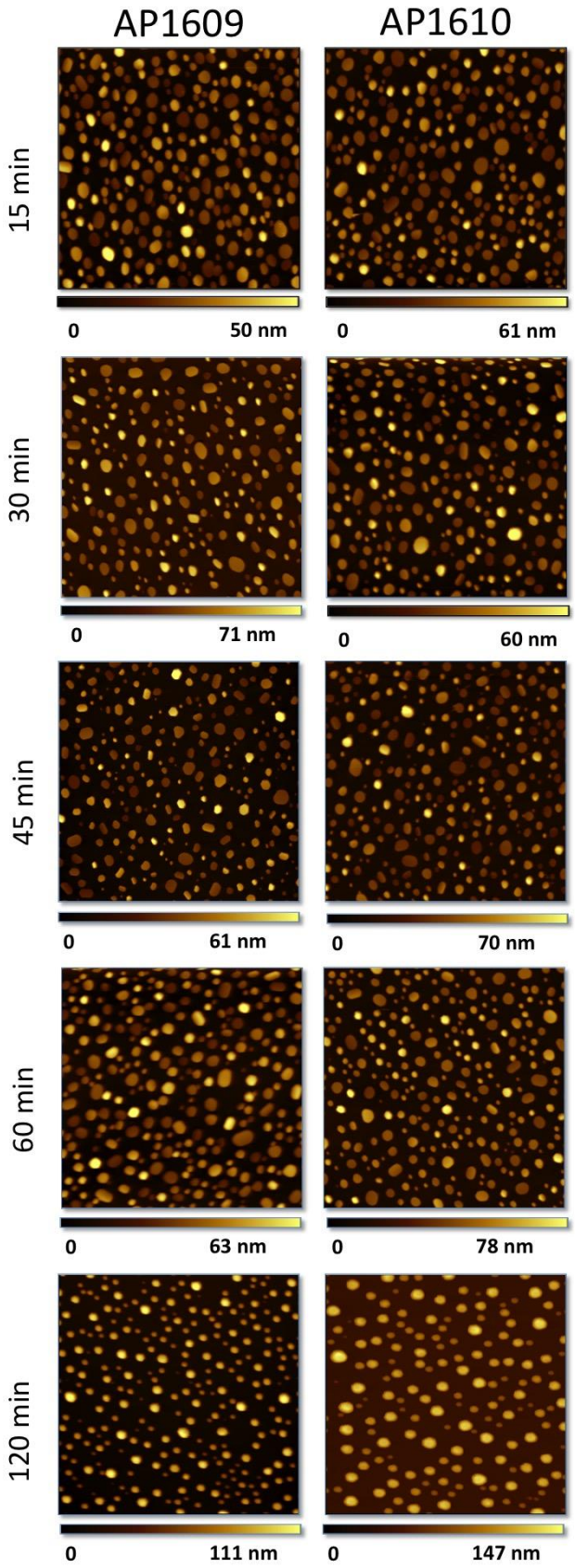
AP1609
AP1610
15 min
0
50 nm
0
61 nm
30 min
0
71 nm
0
60 nm
45 min
0
61 nm
0
70 nm
60 min
0
63 nm
0
78 nm
120 min
0
111 nm
0
147 nm

CHAPTER 7. CONCLUSIONS AND FUTURE DIRECTIONS

Particle lithography with organosilanes can be used to prepare nanopatterns for a range of silicon based substrates such as mica, glass, and silicon wafers. The shape of nanopatterns that are produced depends on the protocol for applying organosilanes, such as heated vapor deposition or immersion protocols. The protocols for particle lithography are highly reproducible, once the method parameters have been optimized.

Proteins can be precisely positioned onto surfaces using patterning techniques of particle lithography and silane deposition. Nanopores within a thin film of silane were used as reaction sites for the selective binding of green fluorescent protein. When investigated with AFM, high spatial selectivity of the protein was observed for binding within the nanopores rather than the matrix film of MPT-silane. The nanopatterns were used to assess the orientation of proteins at the molecular level.

Future studies will focus on protein binding using *in situ* AFM in buffer solutions using a liquid sample cell. During *in situ* imaging, the sulfo-SMCC solution will be introduced in the sample chamber to react for 1 h. During incubation of the sulfo-SMCC the maleimide functional group will bind to the –SH group of MPTMS nanopatterns. Next, ultrapure water will be introduced to clean the surface of excess sulfo-SMCC that did not react. Once the excess sulfo-SMCC chemical is rinsed away, a dilute solution of GFP in PBS will be introduced to the sample cell. Imaging will be accomplished concurrently throughout the steps of binding protein, to directly view the changes in surface topography. Care should be given during the imaging steps to not lose the area of interest during successive imaging and with the introduction of new solvents.

To further advance the study of fluorescent proteins, samples can be prepared with multiple densities of nanopatterns on a single substrate. When the protein nanopatterns are produced on

glass or quartz slides, fluorescent proteins can be detected with microscopy and fluorometry to determine the relationship between packing density of the nanopatterns of protein and fluorescence intensity. A brighter fluorescent protein or quantum dots should be used for fluorescence studies.

Studies of protein-protein interactions can be accomplished with protein nanopatterns using AFM studies. After a target protein is bound to the substrate, *in situ* AFM studies can be done to determine binding kinetics of protein-protein interactions. With particle lithography, multiple test sites can be visualized within the same experiment to view the binding of a second protein, antibody, or small molecule as it is introduced. Platforms can be developed to investigate immune-response of proteins. After patterning a recognition protein, a receptor protein can then be introduced to test activity for binding. By patterning a fluorescently tagged recognition protein on the surface, a biological analyte can be bound to the recognition protein. Changes in the fluorescence signal will be altered. With this design, a biological sensing device can be made based on the patterning technology of particle lithography and organosilane deposition.

Advanced AFM imaging modes of force modulation microscopy and dynamic lateral force modulation microscopy can be used to investigate the surface properties of proteins that have been bound to organic thin films. Using dynamic lateral force modulation, shear forces between the tip and sample can be minimized. Samples which are "stickier" can be imaged in tapping mode as well as with force modulation AFM. The intermittent tapping of the AFM probe minimizes the forces of shear and stress that can damage fragile proteins. Studies can be designed using dynamic lateral force modulation (DLFM). Quantitative information can be acquired with DLFM to elucidate the Young's modulus of proteins.

Particle lithography with organosilanes can be used for lab methods for teaching undergraduate students about nanoscience. Nanopatterns of rings or nanopores can be prepared

and used in the teaching laboratories of undergraduates. The high reproducibility of protocols with particle lithography will help for students learning basic bench top methods of chemistry. The patterns provide a robust and interesting sample for students to image when they are beginning to learn to use an AFM. Experiments were described for use in undergraduate teaching laboratories. During the experiment students gain valuable hands on experience with organosilanes, atomic force microscopy, and the preparation of samples for nanoscience experiments. The procedures can be done with basic laboratory equipment found in most chemistry laboratories.

At Louisiana State University, undergraduates have successfully prepared nanopatterns using methods of particle lithography. In addition, students in the physical chemistry laboratory receive hands on demonstrations and instruction with AFM. Exit surveys from the class show that students enjoyed the experience and learned from hands on exposure to AFM and surface science. By providing laboratory training with AFM, students will be better prepared for a career in science and the rapidly advancing fields of surface science and nanoscience. The goal of the laboratory is to generate interest in the nanoscience and inspire students to become involved in chemistry studies.

The formation of gold islands was studied on gold thin films after annealing for two hours. Films with an initial thickness of less than 5.0 nm were found to not form distributed islands. However, films that were initially 7.5 nm to 15 nm did form well dispersed islands after annealing. Further investigations conducted annealing on 10 nm thickness films after 15 min of annealing. Surface plasmon resonance spectra were observed to shift to a shorter wavelength as the island height increased.

Future studies will be conducted to determine the effect of longer annealing times on gold thin films. It is hypothesized, based on the correlation observed, that thicker films will yield taller

and more dispersed islands after annealing. Additional studies will also be conducted on other metal thin films. Aluminum and silver will also be investigated. By understanding the nature of the thin film and how it behaves under annealing conditions, surface characteristics can be investigated for further development for superconducting films and electronic devices. Finally, a mixture of metal thin films in different ratios will be investigated for dewetting characteristics and will be investigated for superconductivity behavior.

Additionally, metal films can be studied using advanced imaging modes of atomic force microscopy. Conductive probe measurements will be done with thin metal films before and after annealing to determine how the conductivity of the substrates changes and deduce if surface coverage of the islands has an effect on conductivity properties of the films. Correlations can also be investigated between island height and the conductivity of the islands.

Kelvin probe microscopy studies can also be performed on the substrates to determine the work function of the material and the surface potential. Correlations will be investigated between the initial height of the thin film before annealing and after annealing as well as a height of the formed islands compared with the surface potential and work function. Furthermore, mixed films will be studied to see how the work function will change with varying degrees of annealing. Studies with AFM will be used to evaluate the effect of ratios in metal films and thickness on surface potential and the work function.

REFERENCES

1. Ngunjiri, J. N.; Daniels, S. L.; Li, J.-R.; Serem, W. K.; Garno, J. C., Controlling the surface coverage and arrangement of proteins using particle lithography. *Nanomedicine* **2008,** *3* (4), 529-541.

2. Ngunjiri, J. N.; Stark, D. J.; Tian, T.; Briggman, K. A.; Garno, J. C., Immobilization of proteins on carboxylic acid functionalized nanopatterns. *Anal. Bioanal. Chem.* **2013,** *405* (6), 1985-1993.

3. Yagati, A. K.; Min, J.; Choi, J. W., Recombinant protein-based nanoscale biomemory devices. *J. Nanosci. Nanotechnol.* **2014,** *14* (1), 433-446.

4. Reimhult, E.; Hook, F., Design of surface modifications for nanoscale sensor applications. *Sensors* **2015,** *15* (1), 1635-1675.

5. Mendes, P. M.; Yeung, C. L.; Preece, J. A., Bio-nanopatterning of surfaces. *Nanoscale Res. Lett.* **2007,** *2* (8), 373-384.

6. Lord, M. S.; Foss, M.; Besenbacher, F., Influence of nanoscale surface topography on protein adsorption and cellular response. *Nano Today* **2010,** *5* (1), 66-78.

7. Zhou, Y.; Andersson, O.; Lindberg, P.; Liedberg, B., Reversible hydrophobic barriers introduced by microcontact printing: Application to protein microarrays. *Microchimica Acta* **2004,** *146* (3-4), 193-205.

8. Das, T.; Mallick, S. K.; Paul, D.; Bhutia, S. K.; Bhattacharyya, T. K.; Maiti, T. K., Microcontact printing of Concanavalin A and its effect on mammalian cell morphology. *J. Coll. Interf. Sci.* **2007,** *314* (1), 71-79.

9. Pattani, V. P.; Li, C. F.; Desai, T. A.; Vu, T. Q., Microcontact printing of quantum dot bioconjugate arrays for localized capture and detection of biomolecules. *Biomed. Microdevices* **2008,** *10* (3), 367-374.

10. Wu, C. C.; Reinhoudt, D. N.; Otto, C.; Velders, A. H.; Subramaniam, V., Protein immobilization on Ni(II) ion patterns prepared by microcontact printing and dip-pen nanolithography. *ACS Nano* **2010,** *4* (2), 1083-1091.

11. Maury, P.; Escalante, M.; Peter, M.; Reinhoudt, D. N.; Subramaniam, V.; Huskens, J., Creating nanopatterns of his-tagged proteins on surfaces by nanoimprint lithography using specific NiNTA-Histidine interactions. *Small* **2007,** *3* (9), 1584-1592.

12. Schvartzman, M.; Nguyen, K.; Palma, M.; Abramson, J.; Sable, J.; Hone, J.; Sheetz, M. P.; Wind, S. J., Fabrication of nanoscale bioarrays for the study of cytoskeletal protein binding interactions using nanoimprint lithography. *J. Vac. Sci. Technol. B* **2009,** *27* (1), 61-65.

13. Trabadelo, V.; Retolaza, A.; Merino, S.; Cruz, A.; Heredia, P.; Foelske, A.; Schift, H.; Padeste, C., Protein patterning by thermal nanoimprint lithography and NH(3)-plasma functionalization of polystyrene. *J. Vac. Sci. Technol. B* **2009,** *27* (3), 1060-1062.

14. Zhang, G. J.; Tanii, T.; Kanari, Y.; Ohdomari, I., Production of nanopatterns by a combination of electron beam lithography and a self-assembled monolayer for an antibody nanoarray. *J. Nanosci. Nanotechnol.* **2007,** *7* (2), 410-417.

15. Chen, S.; Svedendahl, M.; Antosiewicz, T. J.; Kall, M., Plasmon-enhanced enzyme-linked immunosorbent assay on large arrays of individual particles made by electron beam lithography. *ACS Nano* **2013,** *7* (10), 8824-8832.

16. Lau, U. Y.; Saxer, S. S.; Lee, J.; Bat, E.; Maynard, H. D., Direct write protein patterns for multiplexed cytokine detection from live cells using electron beam lithography. *ACS Nano* **2016,** *10* (1), 723-729.

17. Prachayasittikul, V.; Isarankura-Na-Ayudhya, C.; Tantimongcolwat, T.; Galla, H. J., Nanoscale orientation and lateral organization of chimeric metal-binding green fluorescent protein on lipid membrane determined by epifluorescence and atomic force microscopy. *Biochem. Biophys. Res. Commun.* **2005,** *326* (2), 298-306.

18. Wadu-Mesthrige, K.; Amro, N. A.; Garno, J. C.; Xu, S.; Liu, G. Y., Fabrication of nanometer-sized protein patterns using atomic force microscopy and selective immobilization. *Biophy. J.* **2001,** *80* (4), 1891-1899.

19. Zasadzinski, J. A.; Viswanathan, R.; Schwartz, D. K.; Garnaes, J.; Madsen, L.; Chiruvolu, S.; Woodward, J. T.; Longo, M. L., Applications of atomic-force microscopy to structural characterization of organic thin-films. *Colloids Surf., A* **1994,** *93*, 305-333.

20. Yu, A. A.; Stone, P. R.; Norville, J. E.; Vaughn, M.; Pacsial, E. J.; Bruce, B. D.; Baldo, M.; Raymo, F. M.; Stellacci, F., A simple atomic force microscopy method for the visualization of polar and non-polar parts in thin organic films. *J. Exp. Nanosci.* **2006,** *1* (1), 63-73.

21. de Santo, M. P.; Barberi, R.; Blinov, L. M.; Palto, S. P.; Yudin, S. G., A study of ultrathin dielectric films by atomic and electrostatic force microscopy. *Mole. Mat.* **2000,** *12* (4), 329-345.

22. Kelley, A. T.; Ngunjiri, J. N.; Serem, W. K.; Lawrence, S. O.; Yu, J.-J.; Crowe, W. E.; Garno, J. C., Applying AFM-based nanofabrication for measuring the thickness of nanopatterns: The role of head groups in the vertical self-assembly of omega-functionalized n-alkanethiols. *Langmuir* **2010,** *26* (5), 3040-3049.

23. Lyles, V. D.; Serem, W. K.; Hao, E.; Vicente, M. G. H.; Garno, J. C., Characterization of designed cobaltacarborane porphyrins using conductive probe atomic force microscopy. *Aims Mate. Sci.* **2016,** *3* (2), 380-389.

24. Glatzel, T.; Zimmerli, L.; Kawai, S.; Meyer, E.; Fendt, L. A.; Diederich, F., Oriented growth of porphyrin-based molecular wires on ionic crystals analysed by NC-AFM. *Beilstein J. Nanotechnol.* **2011,** *2*, 34-39.

25. Beinik, I.; Kratzer, M.; Wachauer, A.; Wang, L.; Piryatinski, Y. P.; Brauer, G.; Chen, X. Y.; Hsu, Y. F.; Djurisic, A. B.; Teichert, C., Photoresponse from single upright-standing ZnO nanorods explored by photoconductive AFM. *Beilstein J. Nanotechnol.* **2013,** *4*, 208-217.

26. Panda, A. K.; Manimaran, M.; Mitra, A.; Basu, S., AFM surface morphology and magnetic properties of nanocrystalline $Fe_{71}Nb_{3.7}Cu_1Al_3Mn_{0.8}Si_{13.5}B_7$ ribbons. *App. Surf. Sci.* **2004,** *235* (4), 475-486.

27. Daniels, S. L.; Ngunjiri, J. N.; Garno, J. C., Investigation of the magnetic properties of ferritin by AFM imaging with magnetic sample modulation. *Anal. Bioanal.Chem* **2009,** *394* (1), 215-223.

28. Highland, Z. L. G., J. C., Nanopatterns of green fluorescent protein produced with particle lithography. *In Submission, Biointerphases.*

29. Highland, Z. L. S., C. K.; Leegwater, C. N.; Girard, R. A.; Garno, J. C., Preparation of octadecyltrichlorosilane nanopatterns using particle lithography: An atomic force microscopy laboratory. *In Submission, J. Chem. Ed.*

30. Highland, Z. L., Malchow, P. M., Garno, J. C., Adams, P. W., Thickness-dependent Thermal Dewetting of Au Films on Glass. *In Submission, Thin Solid Films.*

31. Binnig, G.; Rohrer, H., Scanning tunneling microscopy. *Helvet. Phys. Acta* **1982,** *55* (6), 726-735.

32. Pohl, D. W.; Denk, W.; Lanz, M., Optical stethoscopy: Image recording with resolution λ/20. *Appl. Phys. Lett.* **1984,** *44* (7), 651-653.

33. Binnig, G.; Quate, C. F.; Gerber, C., Atomic force microscope. *Phys. Rev. Lett.* **1986,** *56* (9), 930-933.

34. Wang, X. H.; Wang, X.; Fernandez, R.; Ocola, L.; Yan, M. D.; La Rosa, A., Electric-field-assisted dip-pen nanolithography on poly(4-vinylpyridine) (P4VP) thin films. *ACS Appl. Mater. Interfaces* **2010,** *2* (10), 2904-2909.

35. Zhao, J. W.; Kan, R. R.; Zhang, Y.; Chen, H. Y., Applications of scanning probe microscopy in nanolithography on alkanethiol self-assembled monolayers. *Acta Physico-Chimica Sinica* **2006,** *22* (1), 124-130.

36. Johannes, M. S.; Kuniholm, J. F.; Cole, D. G.; Clark, R. L., Automated CAD/CAM-based nanolithography using a custom atomic force microscope. *IEEE Trans. Autom. Sci. Eng.* **2006,** *3* (3), 236-239.

37. Peachey, N. M.; Eckhardt, C. J., Structural studies of ordered monolayers using atomic-force microscopy. *Micron* **1994,** *25* (3), 271-292.

38. Jandt, K. D., Developments and perspectives of scanning probe microscopy (SPM) on organic materials systems. *Mat. Sci. Eng. R.* **1998,** *21* (5-6), 221-295.

39. Dazzi, A.; Prater, C. B.; Hu, Q. C.; Chase, D. B.; Rabolt, J. F.; Marcott, C., AFM-IR: Combining atomic force microscopy and infrared spectroscopy for nanoscale chemical characterization. *Applied Spectroscopy* **2012,** *66* (12), 1365-1384.

40. Taatjes, D. J.; Quinn, A. S.; Rand, J. H.; Jena, B. P., Atomic force microscopy: High resolution dynamic imaging of cellular and molecular structure in health and disease. *J Cell Physiol* **2013,** *228* (10), 1949-1955.

41. Gelmi, A.; Higgins, M. J.; Wallace, G. G., Quantifying fibronectin adhesion with nanoscale spatial resolution on glycosaminoglycan doped polypyrrole using atomic force microscopy. *Biochim Biophys Acta* **2013,** *1830* (9), 4305-4313.

42. Munz, M., Microstructure and roughness of photopolymerized poly(ethylene glycol) diacrylate hydrogel as measured by atomic force microscopy in amplitude and frequency modulation mode. *Appl. Surf. Sci.* **2013,** *279*, 300-309.

43. Motaung, D. E.; Mhlongo, G. H.; Kortidis, I.; Nkosi, S. S.; Malgas, G. F.; Mwakikunga, W.; Ray, S. S.; Kiriakidis, G., Structural and optical properties of ZnO nanostructures grown by aerosol spray pyrolysis: Candidates for room temperature methane and hydrogen gas sensing. *Appl. Surf. Sci.* **2013,** *279*, 142-149.

44. Binnig, G.; Gerber, C.; Stoll, E.; Albrecht, T. R.; Quate, C. F., Atomic resolution with atomic force microscope. *Euro. Phys. J.* **1987,** *3* (12), 1281-1286.

45. Ye, Q.; Cassell, A. M.; Liu, H. B.; Chao, K. J.; Han, J.; Meyyappan, M., Large-scale fabrication of carbon nanotube probe tips for atomic force microscopy critical dimension Imaging applications. *Nano Lett.* **2004,** *4* (7), 1301-1308.

46. Drake, B.; Prater, C.; Weisenhorn, A.; Gould, S.; Albrecht, T.; Quate, C.; Cannell, D.; Hansma, H.; Hansma, P., Imaging crystals, polymers, and processes in water with the atomic force microscope. *Science* **1989,** *243* (4898), 1586-1589.

47. Stahlberg, H.; Fotiadis, D.; Scheuring, S.; Remigy, H.; Braun, T.; Mitsuoka, K.; Fujiyoshi, Y.; Engel, A., Two-dimensional crystals: a powerful approach to assess structure, function and dynamics of membrane proteins. *Febs Letters* **2001,** *504* (3), 166-172.

48. Sauer, B. B.; McLean, R. S.; Thomas, R. R., Nanometer resolution of crystalline morphology using scanning probe microscopy. *Polym. Int.* **2000,** *49* (5), 449-452.

49. Maaloum, M., A close encounter with DNA. *Eur. Biophys. J. Biophy.* **2003,** *32* (6), 585-587.

50. Gaboriaud, F.; Dufrene, Y. F., Atomic force microscopy of microbial cells: Application to nanomechanical properties, surface forces and molecular recognition forces. *Colloids Surf., B* **2007,** *54* (1), 10-19.

51. Ebner, A.; Madl, J.; Kienberger, F.; Chtcheglova, L. A.; Puntheeranurak, T.; Zhu, R.; Tang, J. L.; Gruber, H. J.; Schutz, G. J.; Hinterdorfer, P., Single molecule force microscopy on cells and biological membranes. *Curr. Nanosci.* **2007,** *3* (1), 49-56.

52. Schon, P., Imaging and force probing RNA by atomic force microscopy. *Methods* **2016,** *103*, 25-33.

53. Wang, T.; Sakai, Y.; Nakajima, K.; Miyawaki, A.; Ito, K.; Hara, M., Nanorheology measurement on single circularly permuted green fluorescent protein molecule. *Colloids Surf., B* **2005,** *40* (3-4), 183-187.

54. Chung, H. J.; Song, J.; Vancso, G. J., Tip-surface interactions at redox responsive poly(ferrocenylsilane) (PFS) interface by AFM-based force spectroscopy. *Appl. Surf. Sci.* **2009,** *255* (15), 6995-6998.

55. Yamamoto, S.; Yamada, H.; Matsushige, K., Differentiation of Au islands on Ni film by friction force microscopy, force curve and new force modulation method. *Jpn. J. Appl. Phys., Part 1* **2000,** *39* (6B), 3717-3720.

56. Guleryuz, H.; Royset, A. K.; Kaus, I.; Filiatre, C.; Einarsrud, M. A., AFM measurements of forces between silica surfaces. *J. Sol-Gel Sci. Technol.* **2012,** *62* (3), 460-469.

57. Drelich, J.; Long, J.; Xu, Z.; Masliyah, J.; Nalaskowski, J.; Beauchamp, R.; Liu, Y., AFM colloidal forces measured between microscopic probes and flat substrates in nanoparticle suspensions. *J. Colloid Interface Sci.* **2006,** *301* (2), 511-522.

58. Elings, V. B. G., J. A. Tapping atomic force microscope. 5412980, 1992.

59. Zhong, Q.; Inniss, D.; Kjoller, K.; Elings, V. B., Fractured polymer silica fiber surface studied by tapping mode atomic-force microscopy. *Surf. Sci.* **1993,** *290* (1-2), L688-L692.

60. Hansma, P. K.; Cleveland, J. P.; Radmacher, M.; Walters, D. A.; Hillner, P. E.; Bezanilla, M.; Fritz, M.; Vie, D.; Hansma, H. G.; Prater, C. B.; Massie, J.; Fukunaga, L.; Gurley, J.; Elings, V., Tapping mode atomic-force microscopy in liquids. *Appl. Phys. Lett.* **1994,** *64* (13), 1738-1740.

61. Paul, J. K.; Nettikadan, S. R.; Ganjeizadeh, M.; Yamaguchi, M.; Takeyasu, K., Molecular imaging ofNa+, K+ atpase in purified kidney membranes. *Febs Letters* **1994,** *346* (2-3), 289-294.

62. Fritz, M.; Radmacher, M.; Cleveland, J. P.; Allersma, M. W.; Stewart, R. J.; Gieselmann, R.; Janmey, P.; Schmidt, C. F.; Hansma, P. K., Imaging globular and filamentous proteins in physiological buffer solutions with tapping mode atomic-force microscopy. *Langmuir* **1995,** *11* (9), 3529-3535.

63. Orsini, F.; Cremona, A.; Arosio, P.; Corsetto, P. A.; Montorfano, G.; Lascialfari, A.; Rizzo, A. M., Atomic force microscopy imaging of lipid rafts of human breast cancer cells. *Biochim. Biophys. Acta, Biomembr.* **2012,** *1818* (12), 2943-2949.

64. Lee, I.; Chan, K. Y.; Phillips, D. L., Atomic force microscopy of platinum nanoparticles prepared on highly oriented pyrolytic graphite. *Ultramicroscopy* **1998,** *75* (2), 69-76.

65. Ebenstein, Y.; Nahum, E.; Banin, U., Tapping mode atomic force microscopy for nanoparticle sizing: Tip-sample interaction effects. *Nano Lett.* **2002,** *2* (9), 945-950.

66. Umemura, K.; Arakawa, H.; Ikai, A., Imaging of neurons by atomic-force microscopy. *J. Vac. Sci. Technol., B* **1994,** *12* (3), 1470-1473.

67. Shibataseki, T.; Watanabe, W.; Masai, J., Imaging of cell with atomic-force microscopy operated at a tapping mode. *J. Vac. Sci. Technol., B* **1994,** *12* (3), 1530-1534.

68. Schaus, S. S.; Henderson, E. R., Cell viability and probe-cell membrane interactions of XR1 glial cells imaged by atomic force microscopy. *Biophys. J.* **1997,** *73* (3), 1205-1214.

69. Magonov, S. N.; Reneker, D. H., Characterization of polymer surfaces with atomic force microscopy. *Annu. Rev. Mater. Sci.* **1997,** *27*, 175-222.

70. Englade-Franklin, L. E.; Saner, C. K.; Garno, J. C., Spatially selective surface platforms for binding fibrinogen prepared by particle lithography with organosilanes. *Interface Focus* **2013,** *3* (3).

71. Deckman, H. W.; Dunsmuir, J. H., Natural lithography. *Appl. Phys. Lett.* **1982,** *41* (4), 377-379.

72. Saner, C. K.; Lusker, K. L.; LeJeune, Z. M.; Serem, W. K.; Garno, J. C., Self-assembly of octadecyltrichlorosilane: Surface structures formed using different protocols of particle lithography. *Beilstein J. Nano* **2012,** *3*, 114-122.

73. LeJeune, Z. M.; McKenzie, M. E.; Hao, E.; Vicente, M. G. H.; Chen, B.; Garno, J. C., COLL 216-Self-assembly of pyridyl-substituted porphyrins investigated in situ using AFM. *Abstr. Pap. Am. Chem. S.* **2008,** *235*.

74. Lusker, K. L.; Li, J.-R.; Garno, J. C., Nanostructures of functionalized gold nanoparticles prepared by particle lithography with organosilanes. *Langmuir* **2011,** *27* (21), 13269-13275.

75. Hulteen, J. C.; Treichel, D. A.; Smith, M. T.; Duval, M. L.; Jensen, T. R.; Van Duyne, R. P., Nanosphere lithography: Size-tunable silver nanoparticle and surface cluster arrays. *J. Phys. Chem. B* **1999,** *103* (19), 3854-3863.

76. Denis, F. A.; Hanarp, P.; Sutherland, D. S.; Dufrêne, Y. F., Fabrication of nanostructured polymer surfaces using colloidal lithography and spin-coating. *Nano Lett.* **2002,** *2* (12), 1419-1425.

77. Choi, W. M., Simple and rapid fabrication of large-area 2D colloidal crystals for nanopatterning of conducting polymers. *Microelectron. Eng.* **2013,** *110*, 1-5.

78. Brown, T. T.; Saner, C. K.; Garno, J. C., Particle lithography with organosilanes: A molecular toolkit for studying surface chemistry. *Abstr. Pap. Am. Chem. S.* **2011,** *242*.

79. Biswas, A.; Bayer, I. S.; Biris, A. S.; Wang, T.; Dervishi, E.; Faupel, F., Advances in top-down and bottom-up surface nanofabrication: Techniques, applications & future prospects. *Adv. Colloid Interface Sci.* **2012,** *170* (1-2), 2-27.

80. Chen, J.; Liao, W.-S.; Chen, X.; Yang, T.; Wark, S. E.; Son, D. H.; Batteas, J. D.; Cremer, P. S., Evaporation-induced assembly of quantum dots into nanorings. *ACS Nano* **2008,** *3* (1), 173-180.

81. Christman, K. L.; Schopf, E.; Broyer, R. M.; Li, R. C.; Chen, Y.; Maynard, H. D., Positioning multiple proteins at the nanoscale with electron beam cross-linked functional polymers. *JACS* **2009,** *131* (2), 521-527.

82. Li, J. R.; Lusker, K. L.; Yu, J. J.; Garno, J. C., Engineering the spatial selectivity of surfaces at the nanoscale using particle lithography combined with vapor deposition of organosilanes. *ACS Nano* **2009,** *3* (7), 2023-2035.

83. Taylor, Z. R.; Patel, K.; Spain, T. G.; Keay, J. C.; Jernigen, J. D.; Sanchez, E. S.; Grady, B. P.; Johnson, M. B.; Schmidtke, D. W., Fabrication of protein dot arrays via particle lithography. *Langmuir* **2009,** *25* (18), 10932-10938.

84. Strong, L.; Whitesides, G. M., Structures of self-assembled monolayer films of organosulfur compounds adsorbed on gold single crystals: electron diffraction studies. *Langmuir* **1988,** *4* (3), 546-558.

85. Delamarche, E.; Michel, B.; Gerber, C.; Anselmetti, D.; Guntherodt, H. J.; Wolf, H.; Ringsdorf, H., Real-space observation of nanoscale molecular domains in self-assembled monolayers. *Langmuir* **1994,** *10* (9), 2869-2871.

86. Li, J.-R.; Garno, J. C., Nanostructures of octadecyltrisiloxane self-assembled monolayers produced on Au(111) using particle lithography. *ACS Appl. Mater. Interfaces* **2009,** *1* (4), 969-976.

87. Sagiv, J., Organized monolayers by adsorption .1. Formation and structure of oleophobic mixed monolayers on solid-surfaces. *JACS* **1980,** *102* (1), 92-98.

88. Fadeev, A. Y.; McCarthy, T. J., Self-assembly is not the only reaction possible between alkyltrichlorosilanes and surfaces: Monomolecular and oligomeric covalently attached layers of dichloro- and trichloroalkylsilanes on silicon. *Langmuir* **2000,** *16* (18), 7268-7274.

89. Haddon, R. C.; Lamola, A. A., The molecular electronic device and the biochip computer - present status. *PNAS* **1985,** *82* (7), 1874-1878.

90. McAlear, J. H.; Wehrung, J. M., Microsubstrates and method for making micropattern devices. Google Patents: 1978.

91. Neeves, K. B.; Maloney, S. F.; Fong, K. P.; Schmaier, A. A.; Kahn, M. L.; Brass, L. F.; Diamond, S. L., Microfluidic focal thrombosis model for measuring murine platelet deposition and stability: PAR4 signaling enhances shear-resistance of platelet aggregates. *J. Thromb. Haemost.* **2008,** *6* (12), 2193-2201.

92. Nalayanda, D. D.; Kalukanimuttam, M.; Schmidtke, D. W., Micropatterned surfaces for controlling cell adhesion and rolling under flow. *Biomed. Microdevices* **2007,** *9* (2), 207-214.

93. Fosser, K. A.; Nuzzo, R. G., Fabrication of patterned multicomponent protein gradients and gradient arrays using microfluidic depletion. *Anal. Chem.* **2003,** *75* (21), 5775-5782.

94. Tuleuova, N.; Revzin, A., Micropatterning of aptamer beacons to create cytokine-sensing surfaces. *Cell. Mol. Bioeng.* **2010,** *3* (4), 337-344.

95. Kim, M.; Choi, J.-C.; Jung, H.-R.; Katz, J. S.; Kim, M.-G.; Doh, J., Addressable micropatterning of multiple proteins and cells by microscope projection photolithography based on a protein friendly photoresist. *Langmuir* **2010,** *26* (14), 12112-12118.

96. Falconnet, D.; Pasqui, D.; Park, S.; Eckert, R.; Schift, H.; Gobrecht, J.; Barbucci, R.; Textor, M., A novel approach to produce protein nanopatterns by combining nanoimprint lithography and molecular self-assembly. *Nano Lett.* **2004,** *4* (10), 1909-1914.

97. Zhang, G.-J.; Tanii, T.; Zako, T.; Hosaka, T.; Miyake, T.; Kanari, Y.; Funatsu, T.; Ohdomari, I., Nanoscale patterning of protein using electron beam lithography of organosilane self-assembled monolayers. *Small* **2005,** *1* (8-9), 833-837.

98. Bernard, A.; Renault, J. P.; Michel, B.; Bosshard, H. R.; Delamarche, E., Microcontact printing of proteins. *Adv. Mater. (Weinheim, Ger.)* **2000,** *12* (14), 1067-1070.

99. Renault, J. P.; Bernard, A.; Bietsch, A.; Michel, B.; Bosshard, H. R.; Delamarche, E.; Kreiter, M.; Hecht, B.; Wild, U. P., Fabricating arrays of single protein molecules on glass using microcontact printing. *J. Phys. Chem. B.* **2003,** *107* (3), 703-711.

100. Graber, D. J.; Zieziulewicz, T. J.; Lawrence, D. A.; Shain, W.; Turner, J. N., Antigen Binding Specificity of Antibodies Patterned by Microcontact Printing. *Langmuir* **2003,** *19* (13), 5431-5434.

101. Lee, K.-B.; Park, S.-J.; Mirkin, C. A.; Smith, J. C.; Mrksich, M., Protein nanoarrays generated by dip-pen nanolithography. *Science (Washington, DC, U. S.)* **2002,** *295* (5560), 1702-1705.

102. Lee, S. W.; Oh, B.-K.; Sanedrin, R. G.; Salaita, K.; Fujigaya, T.; Mirkin, C. A., Biologically active protein nanoarrays generated using parallel dip-pen nanolithography. *Adv. Mater. (Weinheim, Ger.)* **2006,** *18* (9), 1133-1136.

103. Garno, J. C.; Amro, N. A.; Wadu-Mesthrige, K.; Liu, G.-Y., Production of periodic arrays of protein nanostructures using particle lithography. *Langmuir* **2002,** *18* (21), 8186-8192.

104. Blattler, T. M.; Binkert, A.; Zimmermann, M.; Textor, M.; Voros, J.; Reimhult, E., From particle self-assembly to functionalized sub-micron protein patterns. *Nanotechnology* **2008,** *19* (7), 075301.

105. Cai, Y.; Ocko, B. M., Large-scale fabrication of protein nanoarrays based on nanosphere lithography. *Langmuir* **2005,** *21* (20), 9274-9279.

106. Taylor, Z. R.; Sanchez, E. S.; Keay, J. C.; Johnson, M. B.; Schmidtke, D. W., Patterning of quantum dot bioconjugates via particle lithography. *Langmuir* **2010,** *26* (24), 18938-18944.

107. Taylor, Z. R.; Keay, J. C.; Sanchez, E. S.; Johnson, M. B.; Schmidtke, D. W., Independently controlling protein dot size and spacing in particle lithography. *Langmuir* **2012,** *28* (25), 9656-9663.

108. Maivald, P.; Butt, H. J.; Gould, S. A. C.; Prater, C. B.; Drake, B.; Gurley, J. A.; Elings, V. B.; Hansma, P. K., Using force modulation to image surface elasticities with the atomic force microscope. *Nanotechnology* **1991,** *2* (2), 103.

109. Fritz, M.; Radmacher, M.; Petersen, N.; Gaub, H. E., Visualization and identification of intracellular structures by force modulation microscopy and drug-induced degradation. *J. Vac. Sci. Technol., B* **1994,** *12* (3), 1526-1529.

110. Sahoo, N.; Thakur, S.; Senthilkumar, M.; Das, N. C., Surface viscoelasticity studies of Gd2O3, SiO2 optical thin films and multilayers using force modulation and force-distance scanning probe microscopy. *App. Surf. Sci.* **2003,** *206* (1-4), 271-293.

111. Sasaki, S.; Morimoto, M.; Haga, H.; Kawabata, K.; Ito, E.; Ushiki, T.; Abe, K.; Sambongi, T., Elastic properties of living fibroblasts as imaged using force modulation mode in atomic force microscopy. *Arch. Histol. Cytol.* **1998,** *61* (1), 57-63.

112. Jourdan, J. S.; Cruchon-Dupeyrat, S. J.; Huan, Y.; Kuo, P. K.; Liu, G. Y., Imaging nanoscopic elasticity of thin film materials by atomic force microscopy: Effects of force modulation frequency and amplitude. *Langmuir* **1999,** *15* (19), 6495-6504.

113. Lu, L.; Xu, S.; Zhang, D.; Garno, J. C., Sample stage designed for force modulation microscopy using a tip-mounted AFM scanner. *Analyst* **2016,** *141* (5), 1753-1760.

114. Kimura, K.; Kobayashi, K.; Yamada, H.; Matsushige, K., High resolution molecular chain imaging of a poly(vinylidenefluoride-trifluoroethylene) crystal using force modulation microscopy. *Nanotechnology* **2007,** *18* (30).

115. Kimura, K.; Kobayashi, K.; Yamada, H.; Matsushige, K., Submolecular resolution viscoelastic imaging of a poly(p-toluene-sulfonate) single crystal using force modulation microscopy. *Nanotechnology* **2008,** *19* (6).

116. Lin, H. N.; Hung, T. T.; Chang, E. C.; Chen, S. A., Force modulation microscopy study of phase separation on blend polymer films. *Appl. Phys. Lett.* **1999,** *74* (19), 2785-2787.

117. Overney, R. M.; Takano, H.; Fujihira, M., Elastic compliances measured by atomic-force microscopy. *Europhys. Lett.* **1994,** *26* (6), 443-447.

118. Overney, R. M.; Meyer, E.; Frommer, J.; Guntherodt, H. J.; Fujihira, M.; Takano, H.; Gotoh, Y., Force microscopy study of friction and elastic compliance of phase-separated organic thin-films. *Langmuir* **1994,** *10* (4), 1281-1286.

119. Radmacher, M.; Tilmann, R. W.; Gaub, H. E., Imaging viscoelasticity by force modulation with the atomic force microscope. *Biophys. J.* **1993,** *64* (3), 735-742.

120. Li, J.-R.; Garno, J. C., Indirect modulation of nonmagnetic probes for force modulation atomic force microscopy. *Anal. Chem.* **2009,** *81* (4), 1699-1706.

121. Yamanaka, K.; Tomita, E., Lateral force modulation atomic-force microscope for selective imaging of friction forces. *Jpn. J. Appl. Phys., Part 1* **1995,** *34* (5B), 2879-2882.

122. Zhang, Y.; Ge, S.; Rafailovich, M. H.; Sokolov, J. C.; Colby, R. H., Surface characterization of cross-linked elastomers by shear modulation force microscopy. *Polymer* **2003,** *44* (11), 3327-3332.

123. Haugstad, G., Contrasting static-to-kinetic friction transitions on layers of an autophobically dewetted polymer film using Fourier-analyzed shear modulation force microscopy. *Tribol. Lett.* **2005,** *19* (1), 49-57.

124. Ge, S.; Pu, Y.; Zhang, W.; Rafailovich, M.; Sokolov, J.; Buenviaje, C.; Buckmaster, R.; Overney, R. M., Shear modulation force microscopy study of near surface glass transition temperatures. *Phys. Rev. Lett.* **2000,** *85* (11), 2340-2343.

125. Hiratsuka, S.; Mizutani, Y.; Tsuchiya, M.; Kawahara, K.; Tokumoto, H.; Okajima, T., The number distribution of complex shear modulus of single cells measured by atomic force microscopy. *Ultramicroscopy* **2009,** *109* (8), 937-941.

126. Lelievre, S. A.; Weaver, V. M.; Nickerson, J. A.; Larabell, C. A.; Bhaumik, A.; Petersen, O. W.; Bissell, M. J., Tissue phenotype depends on reciprocal interactions between the extracellular matrix and the structural organization of the nucleus. *PNAS* **1998,** *95* (25), 14711-14716.

127. Mrksich, M.; Whitesides, G. M., Using self-assembled monolayers to understand the interactions of man-made surfaces with proteins and cells. *Annu. Rev. Biophys. Biomol. Struct.* **1996,** *25*, 55-78.

128. Chen, C. S.; Mrksich, M.; Huang, S.; Whitesides, G. M.; Ingber, D. E., Geometric control of cell life and death. *Science* **1997,** *276* (5317), 1425-1428.

129. Mrksich, M.; Whitesides, G. M., Using self-assembled monolayers to understand the interactions of man-made surfaces with proteins and cells. *Annu. Rev. Bioph. Biom.* **1996,** *25*, 55-78.

130. Abendroth, A.; Slobedman, B.; Springer, M. L.; Blau, H. M.; Arvin, A. M., Analysis of immune responses to varicella tester viral proteins induced by DNA vaccination. *Antiviral Res.* **1999,** *44* (3), 179-192.

131. Movshev, B. E.; Semenova, G. M.; Petrova, V. I.; Kalinin, N. N., Colloid osmotic-pressure and total protein in the evaluation of the safety of therapeutic plasmapheresis. *Terap. Arkhiv* **1991,** *63* (7), 30-33.

132. Menard, E.; Meitl, M. A.; Sun, Y.; Park, J. U.; Shir, D. J.; Nam, Y. S.; Jeon, S.; Rogers, J. A., Micro- and nanopatterning techniques for organic electronic and optoelectronic systems. *Chem. Rev.* **2007,** *107* (4), 1117-1160.

133. Whitesides, G. M., The origins and the future of microfluidics. *Nature* **2006,** *442* (7101), 368-373.

134. Bettinger, C. J.; Langer, R.; Borenstein, J. T., Engineering substrate topography at the micro- and nanoscale to control cell function. *Angew. Chem. Int. Edit.* **2009,** *48* (30), 5406-5415.

135. El-Ali, J.; Sorger, P. K.; Jensen, K. F., Cells on chips. *Nature* **2006,** *442* (7101), 403-411.

136. Lin, J. N.; Andrade, J. D.; Chang, I. N., The Influence of Adsorption of Native and Modified Antibodies on Their Activity. *J Immunol Methods* **1989,** *125* (1-2), 67-77.

137. Soderquist, M. E.; Walton, A. G., Structural-changes in proteins adsorbed on polymer surfaces. *J. Colloid Interf. Sci.* **1980,** *75* (2), 386-397.

138. Norde, W.; Lyklema, J., Why proteins prefer interfaces. *J. Biomater. Sci. Polym. Ed.* **1991,** *2* (3), 183-202.

139. Sigal, G. B.; Mrksich, M.; Whitesides, G. M., Effect of surface wettability on the adsorption of proteins and detergents. *JACS* **1998,** *120* (14), 3464-3473.

140. Prime, K. L.; Whitesides, G. M., Self-assembled organic monolayers - model systems for studying adsorption of proteins at surfaces. *Science* **1991,** *252* (5009), 1164-1167.

141. Prime, K. L.; Whitesides, G. M., Adsorption of proteins onto surfaces containing end-attached oligo(ethylene oxide) - a model system using self-assembled monolayers. *JACS* **1993,** *115* (23), 10714-10721.

142. Singhvi, R.; Kumar, A.; Lopez, G. P.; Stephanopoulos, G. N.; Wang, D. I.; Whitesides, G. M.; Ingber, D. E., Engineering cell shape and function. *Science* **1994,** *264* (5159), 696-698.

143. Gombotz, W. R.; Wang, G. H.; Horbett, T. A.; Hoffman, A. S., Protein adsorption to poly(ethylene oxide) surfaces. *J. Biomed. Mater. Res.* **1991,** *25* (12), 1547-1562.

144. Deng, L.; Mrksich, M.; Whitesides, G. M., Self-assembled monolayers of alkanethiolates presenting tri(propylene sulfoxide) groups resist the adsorption of protein. *JACS* **1996,** *118* (21), 5136-5137.

145. Blawas, A. S.; Reichert, W. M., Protein patterning. *Biomaterials* **1998,** *19* (7–9), 595-609.

146. Li, Y.; Zhang, J.; Fang, L.; Jiang, L.; Liu, W.; Wang, T.; Cui, L.; Sun, H.; Yang, B., Polymer brush nanopatterns with controllable features for protein pattern applications. *J. Mat. Chem.* **2012,** *22* (48), 25116-25122.

147. Mooney, J. F.; Hunt, A. J.; McIntosh, J. R.; Liberko, C. A.; Walba, D. M.; Rogers, C. T., Patterning of functional antibodies and other proteins by photolithography of silane monolayers. *PNAS* **1996,** *93* (22), 12287-12291.

148. Geissler, M.; Xia, Y. N., Patterning: Principles and some new developments. *Advanced Materials* **2004,** *16* (15), 1249-1269.

149. Kolodziej, C. M.; Kim, S. H.; Broyer, R. M.; Saxer, S. S.; Decker, C. G.; Maynard, H. D., Combination of integrin-binding peptide and growth factor promotes cell adhesion on electron-beam-fabricated patterns. *JACS* **2012,** *134* (1), 247-255.

150. Zhang, G. J.; Tanii, T.; Zako, T.; Hosaka, T.; Miyake, T.; Kanari, Y.; Funatsu, T. W.; Ohdomari, I., Nanoscale patterning of protein using electron beam lithography of organosilane self-assembled monolayers. *Small* **2005,** *1* (8-9), 833-837.

151. Bernard, A.; Renault, J. P.; Michel, B.; Bosshard, H. R.; Delamarche, E., Microcontact printing of proteins. *Adv. Mater.* **2000,** *12* (14), 1067-1070.

152. Das, T.; Mallick, S. K.; Paul, D.; Bhutia, S. K.; Bhattacharyya, T. K.; Maiti, T. K., Microcontact printing of Concanavalin A and its effect on mammalian cell morphology. *J. Colloid Interface Sci.* **2007,** *314* (1), 71-79.

153. Filipponi, L.; Livingston, P.; Kaspar, O.; Tokarova, V.; Nicolau, D. V., Protein patterning by microcontact printing using pyramidal PDMS stamps. *Biomed. Microdevices* **2016,** *18* (1).

154. Mrksich, M.; Dike, L. E.; Tien, J.; Ingber, D. E.; Whitesides, G. M., Using microcontact printing to pattern the attachment of mammalian cells to self-assembled monolayers of alkanethiolates on transparent films of gold and silver. *Exp. Cell. Res.* **1997,** *235* (2), 305-313.

155. Huang, M.; Galarreta, B. C.; Artar, A.; Adato, R.; Aksu, S.; Altug, H., Reusable nanostencils for creating multiple biofunctional molecular nanopatterns on polymer substrate. *Nano Lett.* **2012,** *12* (9), 4817-4822.

156. Vazquez-Mena, O.; Gross, L.; Xie, S.; Villanueva, L. G.; Brugger, J., Resistless nanofabrication by stencil lithography: A review. *Microelectron. Eng.* **2015,** *132*, 236-254.

157. Gu, J. H.; Yam, C. M.; Li, S.; Cai, C. Z., Nanometric protein arrays on protein-resistant monolayers on silicon surfaces. *JACS* **2004,** *126* (26), 8098-8099.

158. Choi, I.; Kang, S. K.; Lee, J.; Kim, Y.; Yi, J., In situ observation of biomolecules patterned on a PEG-modified Si surface by scanning probe lithography. *Biomaterials* **2006,** *27* (26), 4655-4660.

159. Pavlovic, E.; Oscarsson, S.; Quist, A. P., Nanoscale site-specific immobilization of proteins through electroactivated disulfide exchange. *Nano Lett.* **2003,** *3* (6), 779-781.

160. Naujoks, N.; Stemmer, A., Using local surface charges for the fabrication of protein patterns. *Colloids Surf., A* **2004,** *249* (1-3), 69-72.

161. Case, M. A.; McLendon, G. L.; Hu, Y.; Vanderlick, T. K.; Scoles, G., Using nanografting to achieve directed assembly of de novo designed metalloproteins on gold. *Nano Lett.* **2003,** *3* (4), 425-429.

162. Case, M. A.; McLendon, G. L.; Scoles, G.; Vanderlick, T. K.; Hu, Y., Self-assembly squared. Nanografting metal-assembled modular proteins into C18 monolayers. *J. Chem. Soc. Abstr.* **2003,** *225*, U411-U411.

163. Hu, Y.; Das, A.; Hecht, M. H.; Scoles, G., Nanografting de novo proteins onto gold surfaces. *Langmuir* **2005,** *21* (20), 9103-9109.

164. Ngunjiri, J.; Dukes, R.; Serem, W.; Garno, J. C., Protein immobilization on activated SAM nanopatterns produced by nanografting. *J. Chem. Soc. Abstr.* **2006,** *231*.

165. Staii, C.; Wood, D. W.; Scoles, G., Verification of biochemical activity for proteins nanografted on gold surfaces. *JACS* **2008,** *130* (2), 640-646.

166. Hong, S. H.; Zhu, J.; Mirkin, C. A., Multiple ink nanolithography: Toward a multiple-pen nano-plotter. *Science* **1999,** *286* (5439), 523-525.

167. Choi, D.-S.; Yun, S.-H.; An, Y.-C.; Lee, M.-J.; Kang, D.-G.; Chang, S.-I.; Kim, H.-K.; Kim, K.-M.; Lim, J.-H., Nanopatterning proteins with a stamp tip for dip-pen nanolithography. *Biochip J* **2007,** *1* (3), 200-203.

168. Tsai, I. Y.; Crosby, A. J.; Russell, T. P., Surface patterning. In *Cell Mechanics*, Wang, Y. L.; Discher, D. E., Eds. Elsevier Academic Press Inc: San Diego, 2007; Vol. 83, pp 67-87.

169. Blawas, A. S.; Oliver, T. F.; Pirrung, M. C.; Reichert, W. M., Step-and-repeat photopatterning of protein features using caged/biotin-BSA: Characterization and resolution. *Langmuir* **1998,** *14* (15), 4243-4250.

170. Bhatia, S. K.; Shriverlake, L. C.; Prior, K. J.; Georger, J. H.; Calvert, J. M.; Bredehorst, R.; Ligler, F. S., Use of thiol-terminal silanes and heterobifunctional crosslinkers for immobilization of antibodies on silica surfaces. *Anal. Biochem.* **1989,** *178* (2), 408-413.

171. Das, T.; Mallick, S. K.; Paul, D.; Bhutia, S. K.; Bhattacharyya, T. K.; Maiti, T. K., Microcontact printing of Concanavalin A and its effect on mammalian cell morphology. *J. Colloid Interface Sci.* **2007,** *314* (1), 71-79.

172. Pritchard, D. J.; Morgan, H.; Cooper, J. M., Patterning and regeneration of surfaces with antibodies. *Anal. Chem.* **1995,** *67* (19), 3605-3607.

173. Pillai, V. N. R., Photo-removable protecting groups in organic-synthesis. *Synthesis-Stuttgart* **1980,** (1), 1-26.

174. Fodor, S. P.; Read, J. L.; Pirrung, M. C.; Stryer, L.; Lu, A. T.; Solas, D., Light-directed, spatially addressable parallel chemical synthesis. *Science* **1991,** *251* (4995), 767-773.

175. Pirrung, M. C.; Huang, C. Y., A general method for the spatially defined immobilization of biomolecules on glass surfaces using "caged" biotin. *Bioconjug. Chem.* **1996,** *7* (3), 317-321.

176. Blawas, A. S.; Huang, C.-Y.; Pirrung, M. C.; Reichert, W. M., *Patterning antibodies for a multiple analyte sensor via photodeprotection chemistry*. Society of Photo-Optical Instrumentation Engineers: Bellingham, WA, ETATS-UNIS, 1996; Vol. 2680, p 10.

177. Sigrist, H.; Collioud, A.; Clemence, J. F.; Gao, H.; Luginbuhl, R.; Sanger, M.; Sundarababu, G., Surface Immobilization of Biomolecules by Light. *Opt Eng* **1995,** *34* (8), 2339-2348.

178. Gao, H.; Sanger, M.; Luginbuhl, R.; Sigrist, H., Immunosensing with photoimmobilized immunoreagents on planar optical-wave guides. *Biosens Bioelectron* **1995,** *10* (3-4), 317-328.

179. Vazquez-Mena, O.; Gross, L.; Xie, S.; Villanueva, L. G.; Brugger, J., Resistless nanofabrication by stencil lithography: A review. *Microelectron. Eng.* **2015,** *132*, 236-254.

180. Wright, D.; Rajalingam, B.; Karp, J. M.; Selvarasah, S.; Ling, Y.; Yeh, J.; Langer, R.; Dokmeci, M. R.; Khademhosseini, A., Reusable, reversibly sealable parylene membranes for cell and protein patterning. *J. Biomed. Mater. Res. A.* **2008,** *85* (2), 530-538.

181. Denis, F. A.; Hanarp, P.; Sutherland, D. S.; Gold, J.; Mustin, C.; Rouxhet, P. G.; Dufrene, Y. F., Protein adsorption on model surfaces with controlled nanotopography and chemistry. *Langmuir* **2002,** *18* (3), 819-828.

182. Haynes, C. L.; Van Duyne, R. P., Nanosphere lithography: A versatile nanofabrication tool for studies of size-dependent nanoparticle optics. *J. Phys. Chem. B* **2001,** *105* (24), 5599-5611.

183. Chen, J.; Liao, W.-S.; Chen, X.; Yang, T.; Wark, S. E.; Son, D. H.; Batteas, J. D.; Cremer, P. S., Evaporation-induced assembly of quantum dots into nanorings. *ACS Nano* **2009,** *3* (1), 173-180.

184. Ngunjiri, J. N.; Daniels, S. L.; Li, J. R.; Serem, W. K.; Garno, J. C., Controlling the surface coverage and arrangement of proteins using particle lithography. *Nanomedicine* **2008,** *3* (4), 529-541.

185. Singh, G.; Gohri, V.; Pillai, S.; Arpanaei, A.; Foss, M.; Kingshott, P., Large-area protein patterns generated by ordered binary colloidal assemblies as templates. *ACS Nano* **2011,** *5* (5), 3542-3551.

186. Arnold, M.; Cavalcanti-Adam, E. A.; Glass, R.; Blummel, J.; Eck, W.; Kantlehner, M.; Kessler, H.; Spatz, J. P., Activation of integrin function by nanopatterned adhesive interfaces. *Chemphyschem* **2004,** *5* (3), 383-388.

187. Agheli, H.; Malmstroem, J.; Larsson, E. M.; Textor, M.; Sutherland, D. S., Large Area Protein Nanopatterning for Biological Applications. *Nano Lett.* **2006,** *6* (6), 1165-1171.

188. Broers, A. N.; Hoole, A. C. F.; Ryan, J. M., Electron beam lithography - Resolution limits. *Microelec. Eng.* **1996,** *32* (1-4), 131-142.

189. Schmidt, R. C.; Healy, K. E., Controlling biological interfaces on the nanometer length scale. *J. Biomed. Mater. Res. Part A* **2009,** *90* (4), 1252-1261.

190. Mancini, R. J.; Lee, J.; Maynard, H. D., Trehalose glycopolymers for stabilization of protein conjugates to environmental stressors. *JACS* **2012,** *134* (20), 8474-8479.

191. Lee, J.; Ko, J. H.; Lin, E.-W.; Wallace, P.; Ruch, F.; Maynard, H. D., Trehalose hydrogels for stabilization of enzymes to heat. *Polym. Chem.* **2015,** *6* (18), 3443-3448.

192. Lee, J.; Lin, E.-W.; Lau, U. Y.; Hedrick, J. L.; Bat, E.; Maynard, H. D., Trehalose Glycopolymers as Excipients for Protein Stabilization. *Biomacromolecules* **2013,** *14* (8), 2561-2569.

193. Horzum, U.; Ozdil, B.; Pesen-Okvur, D., Differentiation of Normal and Cancer Cell Adhesion on Custom Designed Protein Nanopatterns. *Nano Lett.* **2015,** *15* (8), 5393-5403.

194. Xia, Y. N.; Whitesides, G. M., Soft lithography. *Angew. Chem. Int. Edit.* **1998,** *37* (5), 550-575.

195. Renault, J. P.; Bernard, A.; Bietsch, A.; Michel, B.; Bosshard, H. R.; Delamarche, E.; Kreiter, M.; Hecht, B.; Wild, U. P., Fabricating Arrays of Single Protein Molecules on Glass Using Microcontact Printing. *J. Phys. Chem. B.* **2002,** *107* (3), 703-711.

196. Bernard, A.; Renault, J. P.; Michel, B.; Bosshard, H. R.; Delamarche, E., Microcontact printing of proteins. *Adv. Mater.* **2000,** *12* (14), 1067-1070.

197. Filipponi, L.; Livingston, P.; Kaspar, O.; Tokarova, V.; Nicolau, D. V., Protein patterning by microcontact printing using pyramidal PDMS stamps. *Biomed. Microdevices* **2016,** *18* (1), 9.

198. Duffy, D. C.; McDonald, J. C.; Schueller, O. J.; Whitesides, G. M., Rapid Prototyping of Microfluidic Systems in Poly(dimethylsiloxane). *Anal. Chem.* **1998,** *70* (23), 4974-4984.

199. Segerer, F. J.; Rottgermann, P. J. F.; Schuster, S.; Alberola, A. P.; Zahler, S.; Radler, J. O., Versatile method to generate multiple types of micropatterns. *Biointerphases* **2016,** *11* (1).

200. Liu, W. D.; Li, Y. F.; Yang, B., Fabrication and applications of the protein patterns. *Science China-Chemistry* **2013,** *56* (8), 1087-1100.

201. Jin, C. R.; Qiao, Q. C., Deformation of Pyramidal PDMS Stamps During Microcontact Printing. *J. Appl. Mech.-T. Asme* **2016,** *83* (7).

202. Hoff, J. D.; Cheng, L. J.; Meyhofer, E.; Guo, L. J.; Hunt, A. J., Nanoscale protein patterning by imprint lithography. *Nano. Lett.* **2004,** *4* (5), 853-857.

203. Kim, E.; Xia, Y. N.; Whitesides, G. M., Polymer Microstructures Formed by Molding in Capillaries. *Nature* **1995,** *376* (6541), 581-584.

204. Delamarche, E.; Bernard, A.; Schmid, H.; Bietsch, A.; Michel, B.; Biebuyck, H., Microfluidic networks for chemical patterning of substrate: Design and application to bioassays. *JACS* **1998,** *120* (3), 500-508.

205. Delamarche, E.; Bernard, A.; Schmid, H.; Michel, B.; Biebuyck, H., Patterned delivery of immunoglobulins to surfaces using microfluidic networks. *Science* **1997,** *276* (5313), 779-781.

206. He, X.; Dandy, D. S.; Henry, C. S., Microfluidic protein patterning on silicon nitride using solvent extracted poly(dimethylsiloxane) channels. *Sens Actuators B Chem* **2008,** *129* (2), 811-817.

207. Gu, J.; Yam, C. M.; Li, S.; Cai, C., Nanometric protein arrays on protein-resistant monolayers on silicon surfaces. *JACS* **2004,** *126* (26), 8098-8099.

208. Naujoks, N.; Stemmer, A., Using local surface charges for the fabrication of protein patterns. *Colloid Surface A* **2004,** *249* (1-3), 69-72.

209. Ngunjiri, J. N.; Stark, D. J.; Tian, T.; Briggman, K. A.; Garno, J. C., Immobilization of proteins on carboxylic acid functionalized nanopatterns. *Anal. Bioanal.Chem.* **2013,** *405* (6), 1985-1993.

210. El Zubir, O.; Barlow, I.; Leggett, G. J.; Williams, N. H., Fabrication of molecular nanopatterns at aluminium oxide surfaces by nanoshaving of self-assembled monolayers of alkylphosphonates. *Nanoscale* **2013,** *5* (22), 11125-11131.

211. Piner, R. D.; Zhu, J.; Xu, F.; Hong, S. H.; Mirkin, C. A., "Dip-pen" nanolithography. *Science* **1999,** *283* (5402), 661-663.

212. Lee, S. W.; Oh, B. K.; Sanedrin, R. G.; Salaita, K.; Fujigaya, T.; Mirkin, C. A., Biologically active protein nanoarrays generated using parallel dip-pen nanolithography. *Adv. Mater.* **2006,** *18* (9), 1133-1136.

213. Lee, K. B.; Kim, E. Y.; Mirkin, C. A.; Wolinsky, S. M., The use of nanoarrays for highly sensitive and selective detection of human immunodeficiency virus type 1 in plasma. *Nano Lett.* **2004,** *4* (10), 1869-1872.

214. Fabie, L.; Agostini, P.; Stopel, M.; Blum, C.; Lassagne, B.; Subramaniam, V.; Ondarcuhu, T., Direct patterning of nanoparticles and biomolecules by liquid nanodispensing. *Nanoscale* **2015,** *7* (10), 4497-4504.

215. Xu, S.; Liu, G.-y., Nanometer-Scale Fabrication by Simultaneous Nanoshaving and Molecular Self-Assembly. *Langmuir* **1997,** *13* (2), 127-129.

216. Bano, F.; Fruk, L.; Sanavio, B.; Glettenberg, M.; Casalls, L.; Niemeyer, C. M.; Scoles, G., Toward Multiprotein Nanoarrays Using Nanografting and DNA Directed Immobilization of Proteins. *Nano Lett.* **2009,** *9* (7), 2614-2618.

217. Martinez, R. V.; Martinez, J.; Chiesa, M.; Garcia, R.; Coronado, E.; Pinilla-Cienfuegos, E.; Tatay, S., Large-scale Nanopatterning of Single Proteins used as Carriers of Magnetic Nanoparticles. *Adv. Mater.* **2010,** *22* (5), 588-+.

218. Sugimura, H.; Nakagiri, N., Degradation of a trimethylsilyl monolayer on silicon substrates induced by scanning probe anodization. *Langmuir* **1995,** *11* (10), 3623-3625.

219. Zheng, J. W.; Zhu, Z. H.; Chen, H. F.; Liu, Z. F., Nanopatterned assembling of colloidal gold nanoparticles on silicon. *Langmuir* **2000,** *16* (10), 4409-4412.

220. Wouters, D.; Willems, R.; Hoeppener, S.; Flipse, C. F. J.; Schubert, U. S., Oxidation conditions for octadecyl trichlorosilane monolayers on silicon: A detailed atomic force microscopy study of the effects of pulse height and duration on the oxidation of the monolayer and the underlying Si substrate. *Adv. Funct. Mat.* **2005,** *15* (6), 938-944.

221. Ballav, N.; Thomas, H.; Winkler, T.; Terfort, A.; Zharnikov, M., Making Protein Patterns by Writing in a Protein-Repelling Matrix. *Angew. Chem. Int. Ed.* **2009,** *48* (32), 5833-5836.

222. Jeyachandran, Y. L.; Zharnikov, M., Comprehensive Analysis of the Effect of Electron Irradiation on Oligo(ethylene glycol) Terminated Self-Assembled Monolayers Applicable for Specific and Nonspecific Patterning of Proteins. *J. Phys. Chem. C* **2012,** *116* (28), 14950-14959.

223. Kolodziej, C. M.; Kim, S. H.; Broyer, R. M.; Saxer, S. S.; Decker, C. G.; Maynard, H. D., Combination of Integrin-Binding Peptide and Growth Factor Promotes Cell Adhesion on Electron-Beam-Fabricated Patterns. *J. Am. Chem. Soc.* **2012,** *134* (1), 247-255.

224. Kane, R. S.; Takayama, S.; Ostuni, E.; Ingber, D. E.; Whitesides, G. M., Patterning proteins and cells using soft lithography. *Biomaterials* **1999,** *20* (23-24), 2363-2376.

225. Renault, J. P.; Bernard, A.; Bietsch, A.; Michel, B.; Bosshard, H. R.; Delamarche, E.; Kreiter, M.; Hecht, B.; Wild, U. P., Fabricating arrays of single protein molecules on glass using microcontact printing. *J. Phys. Chem. B* **2003,** *107* (3), 703-711.

226. Delamarche, E.; Bernard, A.; Schmid, H.; Bietsch, A.; Michel, B.; Biebuyck, H., Microfluidic networks for chemical patterning of substrate: Design and application to bioassays. *J. Am. Chem. Soci.* **1998,** *120* (3), 500-508.

227. Patel, N.; Sanders, G. H. W.; Shakesheff, K. M.; Cannizzaro, S. M.; Davies, M. C.; Langer, R.; Roberts, C. J.; Tendler, S. J. B.; Williams, P. M., Atomic force microscopic analysis of highly defined protein patterns formed by microfluidic networks. *Langmuir* **1999,** *15* (21), 7252-7257.

228. Dontha, N.; Nowall, W. B.; Kuhr, W. G., Generation of biotin/avidin/enzyme nanostructures with maskless photolithography. *Anal. Chem.* **1997,** *69* (14), 2619-2625.

229. Zhou, H.-L.; Shi, W.-J., Construction of Bovine Serum Albumin Nanostructure by Scanning Probe Nanolithography. *Chin. J. Anal. Chem.* **2009,** *37* (6), 884-887.

230. Lee, K. B.; Park, S. J.; Mirkin, C. A.; Smith, J. C.; Mrksich, M., Protein nanoarrays generated by dip-pen nanolithography. *Science* **2002,** *295* (5560), 1702-1705.

231. Lee, K. B.; Lim, J. H.; Mirkin, C. A., Protein nanostructures formed via direct-write dip-pen nanolithography. *J. Am. Chem. Soc.* **2003,** *125* (19), 5588-5589.

232. Choi, D.-S.; Yun, S.-H.; An, Y.-C.; Lee, M.-J.; Kang, D.-G.; Chang, S.-I.; Kim, H.-K.; Kim, K.-M.; Lim, J.-H., Nanopatterning proteins with a stamp tip for dip-pen nanolithography. *Biochip J.* **2007,** *1* (3), 200-203.

233. Qin, G.; Gu, J.; Liu, K.; Xiao, Z.; Yam, C. M.; Cai, C., Conductive AFM patterning on oligo(ethylene glycol)-terminated alkyl monolayers on silicon substrates: Proposed mechanism and fabrication of avidin patterns. *Langmuir* **2011,** *27* (11), 6987-6994.

234. Hoff, J. D.; Cheng, L.-J.; Meyhofer, E.; Guo, L. J.; Hunt, A. J., Nanoscale protein patterning by imprint lithography. *Nano Lett.* **2004,** *4* (5), 853-857.

235. Wadu-Mesthrige, K.; Amro, N. A.; Garno, J. C.; Xu, S.; Liu, G.-Y., Fabrication of nanometer-sized protein patterns using AFM and selective immobilization. *Biophys. J.* **2001,** *80*, 1891-1899.

236. Wadu-Mesthrige, K.; Xu, S.; Amro, N. A.; Liu, G. Y., Fabrication and imaging of nanometer-sized protein patterns. *Langmuir* **1999,** *15* (25), 8580-8583.

237. Sanavio, B.; Scaini, D.; Grunwald, C.; Legname, G.; Scoles, G.; Casalis, L., Oriented immobilization of prion protein demonstrated via precise interfacial nanostructure measurements *ACS Nano* **2010,** *4* (11), 6607-6616.

238. Garno, J. C.; Amro, N. A.; Wadu-Mesthrige, K.; Liu, G. Y., Production of periodic arrays of protein nanostructures using particle lithography. *Langmuir* **2002,** *18* (21), 8186-8192.

239. Li, J. R.; Henry, G. C.; Garno, J. C., Fabrication of nanopatterned films of bovine serum albumin and staphylococcal protein A using latex particle lithography. *Analyst* **2006,** *131* (2), 244-250.

240. Cai, Y. G.; Ocko, B. M., Large-scale fabrication of protein nanoarrays based on nanosphere lithography. *Langmuir* **2005,** *21* (20), 9274-9279.

241. Satriano, C.; Fragala, M. E.; Aleeva, Y., Ultrathin and nanostructured ZnO-based films for fluorescence biosensing applications. *J. Colloid Interface Sci.* **2012,** *365* (1), 90-96.

242. Heim, R.; Prasher, D. C.; Tsien, R. Y., Wavelength mutations and posttranslational autoxidation of green fluorescent protein. *Proc. Natl. Acad. U.S.A.* **1994,** *91* (26), 12501-12504.

243. Chalfie, M.; Tu, Y.; Euskirchen, G.; Ward, W. W.; Prasher, D. C., Grenn fluorescent protein as a marker for gene expression. *Science* **1994,** *263* (5148), 802-805.

244. Heim, R.; Cubitt, A. B.; Tsien, R. Y., Improved green fluorescence. *Nature* **1995,** *373* (6516), 663-664.

245. Delagrave, S.; Hawtin, R. E.; Silva, C. M.; Yang, M. M.; Youvan, D. C., Red-shifted excitation mutants of the green fluorescent protein. *Bio-Technol.* **1995,** *13* (2), 151-154.

246. Yang, F.; Moss, L. G.; Phillips, G. N., The molecular structure of green fluorescent protein. *Nat. Biotechnol.* **1996,** *14* (10), 1246-1251.

247. Groll, J.; Albrecht, K.; Gasteier, P.; Riethmueller, S.; Ziener, U.; Moeller, M., Nanostructured ordering of fluorescent markers and single proteins on substrates. *Chembiochem* **2005,** *6* (10), 1782-1787.

248. Moxey, M.; Johnson, A.; El-Zubir, O.; Cartron, M.; Dinachali, S. S.; Hunter, C. N.; Saifullah, M. S. M.; Chong, K. S. L.; Leggett, G. J., Fabrication of self-cleaning, reusable titania

templates for nanometer and micrometer scale protein patterning. *ACS Nano* **2015,** *9* (6), 6262-6270.

249. Zhang, G.-J.; Tanii, T.; Kanari, Y.; Ohdomari, I., Production of nanopatterns by a combination of electron beam lithography and a self-assembled monolayer for an antibody nanoarray. *J. Nanosci. Nanotechnol.* **2007,** *7* (2), 410-417.

250. Liu, Z. G.; Zu, Y. G.; Fu, Y. J.; Zhang, Z. H.; Meng, R. H., Assembling and Imaging of His-Tag Green Fluorescent Protein on Mica Surfaces Studied by Atomic Force Microscopy and Fluorescence Microscopy. *Microscopy Research and Technique* **2008,** *71* (11), 802-809.

251. Wang, T.; Nakajima, K.; Miyawaki, A.; Hara, M., Probing intra-molecular mechanics of single circularly permuted green fluorescent protein with atomic force microscopy. *Ultramicroscopy* **2005,** *105* (1-4), 90-95.

252. Li, J.-R.; Lusker, K. L.; Yu, J.-J.; Garno, J. C., Engineering the spatial selectivity of surfaces at the nanoscale using particle lithography combined with vapor deposition of organosilanes. *Acs Nano* **2009,** *3* (7), 2023-2035.

253. Saner, C. K.; Lusker, K. L.; LeJeune, Z. M.; Serem, W. K.; Garno, J. C., Self-assembly of octadecyltrichlorosilane: Surface structures formed using different protocols of particle lithography. *Beilstein J. Nanotechnol.* **2012,** *3*, 114-122.

254. Uosaki, K.; Quayum, M. E.; Nihonyanagi, S.; Kondo, T., Decomposition processes of an organic monolayer formed on Si(111) via a silicon-carbon bond induced by exposure to UV irradiation or ozone. *Langmuir* **2004,** *20* (4), 1207-1212.

255. Necas, D.; Klapetek, P., Gwyddion: an open-source software for SPM data analysis. *Cent. Eur. J. Phys.* **2012,** *10* (1), 181-188.

256. Schindelin, J.; Arganda-Carreras, I.; Frise, E.; Kaynig, V.; Longair, M.; Pietzsch, T.; Preibisch, S.; Rueden, C.; Saalfeld, S.; Schmid, B.; Tinevez, J.-Y.; White, D. J.; Hartenstein, V.; Eliceiri, K.; Tomancak, P.; Cardona, A., Fiji: an open-source platform for biological-image analysis. *Nat. Methods* **2012,** *9* (7), 676-682.

257. Jo, S.; Park, K., Surface modification using silanated poly(ethylene glycol)s. *Biomaterials* **2000,** *21* (6), 605-616.

258. Prime, K. L.; Whitesides, G. M., Adsorption of Proteins onto Surfaces Containing End-Attached Oligo(Ethylene Oxide) - A Model System Using Self-Assembled Monolayers. *J Am. Chem. Soc.* **1993,** *115* (23), 10714-10721.

259. Chapman, R. G.; Ostuni, E.; Takayama, S.; Holmlin, R. E.; Yan, L.; Whitesides, G. M., Surveying for surfaces that resist the adsorption of proteins. *J Am. Chem. Soc.* **2000,** *122* (34), 8303-8304.

260. Holmlin, R. E.; Chen, X. X.; Chapman, R. G.; Takayama, S.; Whitesides, G. M., Zwitterionic SAMs that resist nonspecific adsorption of protein from aqueous buffer. *Langmuir* **2001,** *17* (9), 2841-2850.

261. Luk, Y. Y.; Kato, M.; Mrksich, M., Self-assembled monolayers of alkanethiolates presenting mannitol groups are inert to protein adsorption and cell attachment. *Langmuir* **2000,** *16* (24), 9604-9608.

262. Hink, M. A.; Griep, R. A.; Borst, J. W.; van Hoek, A.; Eppink, M. H. M.; Schots, A.; Visser, A., Structural dynamics of green fluorescent protein alone and fused with a single chain Fv protein. *J Biol Chem* **2000,** *275* (23), 17556-17560.

263. Brejc, K.; Sixma, T. K.; Kitts, P. A.; Kain, S. R.; Tsien, R. Y.; Ormo, M.; Remington, S. J., Structural basis for dual excitation and photoisomerization of the Aequorea victoria green fluorescent protein. *Proc. Natl. Acad. Sci. USA* **1997,** *94*, 2306-2311.

264. Brown, T. T.; LeJeune, Z. M.; Liu, K.; Hardin, S.; Li, J.-R.; Rupnik, K.; Garno, J. C., Automated scanning probe lithography with n-alkanethiol self-assembled monolayers on Au(111): Application for teaching undergraduate laboratories. *J. Am. Lab Assoc.* **2011,** *16*, 112-125.

265. Sanders, W. C.; Valcarce, R.; Iles, P.; Smith, J. S.; Glass, G.; Gomez, J.; Johnson, G.; Johnston, D.; Morham, M.; Befus, E.; Oz, A.; Tomaraei, M., Printing silver nanogrids on glass. *J. Chem. Ed.* **2017,** *ASAP*.

266. Ito, T., Observation of DNA molecules using fluorescence microscopy and atomic force microscopy an undergraduate instrumental analysis laboratory experiment. *J. Chem. Ed.* **2008,** *85* (5), 680-682.

267. Li, J.-R.; Garno, J. C., Nanostructures of octadecyltrisiloxane self-assembled monolayers produced on Au(111) using particle lithography. *ACS Appl Mater. Interfaces* **2009,** *1* (4), 969-976.

268. Binnig, G.; Quate, C. F.; Gerber, C., Atomic force microscope. *Phys Rev Lett* **1986,** *56* (9), 930-933.

269. Mohn, F.; Schuler, B.; Gross, L.; Meyer, G., Different tips for high-resolution atomic force microscopy and scanning tunneling microscopy of single molecules. *Appl. Phys. Lett.* **2013,** *102* (7).

270. Wastl, D. S., Ambient atomic resolution atomic force microscopy with qPlus sensors: Part 1. *Microsc. Res. Tech.* **2017,** *80* (1), 50-65.

271. Lyman, B. M.; Farmer, O. J.; Ramsey, R. D.; Lindsey, S. T.; Stout, S.; Robison, A.; Moore, H. J.; Sanders, W. C., Atomic Force Microscopy Analysis of Nanocrystalline Patterns Fabricated Using Micromolding in Capillaries. *J. Chem. Ed.* **2012,** *89* (3), 401-405.

272. Goss, V.; Brandt, S.; Lieberman, M., The analog atomic force microscope: Measuring, modeling, and graphing for middle school. *J. Chem. Ed.* **2013,** *90* (3), 358-360.

273. Heinz, W. F.; Hoh, J. H., Getting physical with your chemistry: Mechanically investigating local structure and properties of surfaces with the atomic force microscope. *J. Chem. Ed.* **2005,** *82* (5), 695.

274. Blonder, R.; Joselevich, E.; Cohen, S. R., Atomic Force Microscopy: Opening the Teaching Laboratory to the Nanoworld. *J. Chem. Ed.* **2010,** *87* (12), 1290-1293.

275. Maye, M. M.; Luo, J.; Han, L.; Zhong, C.-J., Chemical Analysis Using Scanning Force Microscopy. An Undergraduate Laboratory Experiment. *J. Chem. Ed.* **2002,** *79* (2), 207.

276. Li, J.-R.; Garno, J. C., Elucidating the role of surface hydrolysis in preparing organosilane nanostructures via particle lithography. *Nano Lett.* **2008,** *8* (7), 1916-1922.

277. Wasserman, S. R.; Tao, Y. T.; Whitesides, G. M., Structure and reactivity of alkylsiloxane monolayers formed by reaction of alkyltrichlorosilanes on silicon substrates. *Langmuir* **1989,** *5* (4), 1074-1087.

278. Li, J. R.; Ross, S. S.; Liu, Y.; Liu, Y. X.; Wang, K. H.; Chen, H. Y.; Liu, F. T.; Laurence, T. A.; Liu, G. Y., Engineered nanostructures of haptens lead to unexpected formation of membrane nanotubes connecting rat basophilic leukemia cells. *ACS Nano* **2015,** *9* (7), 6738-6746.

279. Li, J.-R.; Lewandowski, B. R.; Xu, S.; Garno, J. C., Detecting the magnetic response of iron oxide capped organosilane nanostructures using magnetic sample modulation and atomic force microscopy. *Anal Chem.* **2009,** *81* (12), 4792-4802.

280. Brownfield, A. L.; Causey, C. P.; Mullen, T. J., Effects of surface water on organosilane nanostructure fabrication using particle lithography. *Thin Solid Films* **2015,** *594*, 184-191.

281. Kosinova, A.; Klinger, L.; Kovalenko, O.; Rabkin, E., The role of grain boundary sliding in solid-state dewetting of thin polycrystalline films. *Scripta Mater.* **2014,** *82*, 33-36.

282. Mueller, C. M.; Spolenak, R., Microstructure evolution during dewetting in thin Au films. *Acta Mater.* **2010,** *58* (18), 6035-6045.

283. Presland, A. E.; Price, G. L.; Itrimm, D. L., Role of microstructure and surface-energy in hole growth and island formation in thin silver films. *Surf. Sci.* **1972,** *29* (2), 435.

284. Hummel, R. E.; Dehoff, R. T.; Mattsgoho, S.; Goho, W. M., Thermal grooving, thermotransport and electrotransport in doped and undoped thin gold-films. *Thin Solid Films* **1981,** *78* (1), 1-14.

285. Srolovitz, D. J.; Goldiner, M. G., The thermodynamics and kinetics of film agglomeration. *Jom-J. Min. Met. Mat. S.* **1995,** *47* (3), 31-&.

286. Giermann, A. L.; Thompson, C. V., Solid-state dewetting for ordered arrays of crystallographically oriented metal particles. *Appl. Phys. Lett.* **2005,** *86* (12).

287. Petersen, J.; Mayr, S. G., Dewetting of Ni and NiAg solid thin films and formation of nanowires on ripple patterned substrates. *J. Appl. Phys.* **2008,** *103* (2).

288. Zhao, X.; Lee, U.-J.; Lee, K.-H., Dewetting behavior of Au films on porous substrates. *Thin Solid Films* **2010,** *519* (2), 706-713.

289. Mueller, C. M.; Spolenak, R., Dewetting of Au and AuPt alloy films: A dewetting zone model. *J. Appl. Phys.* **2013,** (9).

290. Wang, D.; Schaaf, P., Solid-state dewetting for fabrication of metallic nanoparticles and influences of nanostructured substrates and dealloying. *Phys. Status Solidi A* **2013,** *210* (8), 1544-1551.

291. Faraday, M., Experimental relations of gold (and other metals) to light. *Phil Trans R Soc* **1857,** *147*, 145-181.

292. Danielson, D. T.; Sparacin, D. K.; Michel, J.; Kimerling, L. C., Surface-energy-driven dewetting theory of silicon-on-insulator agglomeration. *J. Appl. Phys.* **2006,** *100* (8).

293. Mullins, W. W., Theory of thermal grooving. *J. Appl. Phys.* **1957,** *28* (3), 333-339.

294. Kalyuzhny, G.; Vaskevich, A.; Schneeweiss, M. A.; Rubinstein, I., Transmission surface-plasmon resonance (T-SPR) measurements for monitoring adsorption on ultrathin gold island films. *Chem. Eur. J.* **2002,** *8* (17), 3850-3857.

295. Thompson, C. V., Solid-State Dewetting of Thin Films. *Annu. Rev. Mater. Res.* **2012,** *42*, 399-434.

296. Kalyuzhny, G.; Schneeweiss, M. A.; Shanzer, A.; Vaskevich, A.; Rubinstein, I., Differential plasmon spectroscopy as a tool for monitoring molecular binding to ultrathin gold films. *JACS* **2001,** *123* (13), 3177-3178.

297. Srolovitz, D. J.; Safran, S. A., Capillary instabilities in thin-films. 1. Energetics. *J. Appl. Phys.* **1986,** *60* (1), 247-254.

298. Miller, K. T.; Lange, F. F.; Marshall, D. B., The instability of polycrystalline thin-films - experiment and theory. *J. Mater. Res.* **1990,** *5* (1), 151-160.

299. Rha, J. J.; Park, J. K., Stability of the grain configurations of thin films - A model for agglomeration. *J. Appl. Phys.* **1997,** *82* (4), 1608-1616.

300. Genin, F. Y.; Mullins, W. W.; Wynblatt, P., Capillary instabilities in thin-films - a model of thermal pitting at grain-boundary vertices. *Acta Metall. Mater.* **1992,** *40* (12), 3239-3248.

301. Shaffir, E.; Riess, I.; Kaplan, W. D., The mechanism of initial de-wetting and detachment of thin Au films on YSZ. *Acta Mater.* **2009,** *57* (1), 248-256.

302. Agrawal, D. C.; Raj, R., Autonucleation of cavities in thin ceramic films. *Acta Metall.* **1989,** *37* (7), 2035-2038.

303. Kennefick, C. M.; Raj, R., Copper on sapphire - stability of thin-films at 0.7-tm. *Acta Metall.* **1989,** *37* (11), 2947-2952.

304. Kristensen, N.; Ericson, F.; Schweitz, J. A.; Smith, U., Hole formation in thin aluminum films under controlled variation of strain and temperature. *Thin Solid Films* **1991,** *197* (1-2), 67-83.

305. Szkutnik, D.; Karmous, A.; Bassani, F.; Ronda, A.; Berbezier, I.; Gacem, K.; El Hdiy, A.; Troyon, M., Ge nanocrystals formation on SiO_2 by dewetting: application to memory. *Eur Phys J-Appl Phys* **2008,** *41* (2), 103-106.

306. Vrij, A., Possible mechanism for spontaneous rupture of thin free liquid films. *Discuss. Faraday Soc.* **1966,** (42), 23-&.

307. Yadavali, S.; Khenner, M.; Kalyanaraman, R., Pulsed laser dewetting of Au films: Experiments and modeling of nanoscale behavior. *J. Mater. Res.* **2013,** *28* (13), 1715-1723.

308. Trice, J.; Favazza, C.; Thomas, D.; Garcia, H.; Kalyanaraman, R.; Sureshkumar, R., Novel self-organization mechanism in ultrathin liquid films: Theory and experiment. *Phys. Rev. Lett.* **2008,** *101* (1), 017802.

309. Trice, J.; Thomas, D.; Favazza, C.; Sureshkumar, R.; Kalyanaraman, R., Pulsed-laser-induced dewetting in nanoscopic metal films: Theory and experiments. *Phys. Rev. B.* **2007,** *75* (23).

310. Luo, Y.; Ruff, J.; Ray, R.; Gu, Y. L.; Ploehn, H. J.; Scrivens, W. A., Vapor-assisted remodeling of thin gold films. *Chem. Mater.* **2005,** *17* (20), 5014-5023.

311. Shankar, S. S.; Rai, A.; Ankamwar, B.; Singh, A.; Ahmad, A.; Sastry, M., Biological synthesis of triangular gold nanoprisms. *Nat. Mater.* **2004,** *3* (7), 482-488.

312. Kalyuzhny, G.; Vaskevich, A.; Ashkenasy, G.; Shanzer, A.; Rubinstein, I., UV/vis spectroscopy of metalloporphyrin and metallophthalocyanine monolayers self-assembled on ultrathin gold films. *J. Phys. Chem. B.* **2000,** *104* (34), 8238-8244.

313. Tessier, P.; Velev, O. D.; Kalambur, A. T.; Lenhoff, A. M.; Rabolt, J. F.; Kaler, E. W., Structured metallic films for optical and spectroscopic applications via colloidal crystal templating. *Adv. Mater.* **2001,** *13* (6), 396-400.

314. Miyake, H.; Ye, S.; Osawa, M., Electroless deposition of gold thin films on silicon for surface-enhanced infrared spectroelectrochemistry. *Electrochem. Commun.* **2002,** *4* (12), 973-977.

315. Sockalingum, G. D.; Beljebbar, A.; Morjani, H.; Angiboust, J. F.; Manfait, M., Characterization of island films as surface-enhanced Raman spectroscopy substrates for detecting low antitumor drug concentrations at single cell level. *Biospectroscopy* **1998,** *4* (5), S71-S78.

316. Doron-Mor, I.; Barkay, Z.; Filip-Granit, N.; Vaskevich, A.; Rubinstein, I., Ultrathin gold island films on silanized glass. Morphology and optical properties. *Chem. Mater.* **2004,** *16* (18), 3476-3483.

317. Klapetek, P. N., D. Gwyddion.

318. Schindelin, J.; Arganda-Carreras, I.; Frise, E.; Kaynig, V.; Longair, M.; Pietzsch, T.; Preibisch, S.; Rueden, C.; Saalfeld, S.; Schmid, B.; Tinevez, J.-Y.; White, D. J.; Hartenstein, V.; Eliceiri, K.; Tomancak, P.; Cardona, A., Fiji: an open-source platform for biological-image analysis. *Nat. Meth.* **2012,** *9* (7), 676-682.

319. Belser, R. B.; Hicklin, W. H., Temperature coefficients of resistance of metallic films in the temperature range 25 ^{0}C to 600 ^{0}C. *J. Appl. Phys.* **1959,** *30* (3), 313-322.

320. Malyi, O.; Klinger, L.; Srolovitz, D. J.; Rabkin, E., Size and shape evolution of faceted bicrystal nanoparticles of gold on sapphire. *Acta Mater.* **2011,** *59* (7), 2872-2881.

321. Hall, L. D., The vapor pressure of gold and the activities of gold in gold copper solid solutions. *JACS* **1951,** *73* (2), 757-760.

322. Chen, B.; Mokume, M.; Liu, C.; Hayashi, K., Structure and localized surface plasmon tuning of sputtered Au nano-islands through thermal annealing. *Vacuum* **2014,** *110*, 94-101.

323. Mayer, K. M.; Hafner, J. H., Localized surface plasmon resonance sensors. *Che. Rev.* **2011,** *111* (6), 3828-3857.

324. Rycenga, M.; Cobley, C. M.; Zeng, J.; Li, W. Y.; Moran, C. H.; Zhang, Q.; Qin, D.; Xia, Y. N., Controlling the Synthesis and Assembly of Silver Nanostructures for Plasmonic Applications. *Chem. Rev.* **2011,** *111* (6), 3669-3712.

325. Barbee, K. A.; Davies, P. F.; Lal, R., Shear stress-induced reorganization of the surface-topography of living endothelial-cells imaged by atomic-force microscopy. *Circulation Research* **1994,** *74* (1), 163-171.

326. Pietrement, O.; Beaudoin, J. L.; Troyon, M., A new calibration method of the lateral contact stiffness and lateral force using modulated lateral force microscopy. *Tribol. Lett.* **1999,** *7* (4), 213-220.

327. Wilcox, C. D., Dove, S. D.; McDavid, W. D.; Greer, D.B., ImageTool. University of Texas Health Science Center (UTHSCSA): San Antonio, TX, 1996-2002.

APPENDIX A: PROCEDURE FOR LATERAL FORCE MODULATION MICROSCOPY

Dynamic lateral force modulation microscopy (DLFM) is a type of force modulation microscopy. Instead of the tip or the sample vibrating in a perpendicular direction, for lateral force modulation the tip and sample are operated in a direction parallel to the sample. Surface properties such as shear stress can be calculated using this method.[325] Contact stiffness can also be deduced using this DLFM.[326] The DLFM mode of AFM can be used for samples that tend to be "sticky" to keep the tip from binding to the surface.

A.1 Hardware Set-up for Agilent 5500 SPM

A. For DLFM, connect BNC cables as shown in Figure A1.

B. Connect a BNC cable from the **AUX** output of the scanner electronics box to the **Phase** input of the MAC/AC controller.

C. Connect a second BNC cable from the **Amplitude** output of the MAC/AC controller to the **AUX IN** of the PicoSPM II controller. Make sure to use the DLFM nosecone shown in Figure A.1.

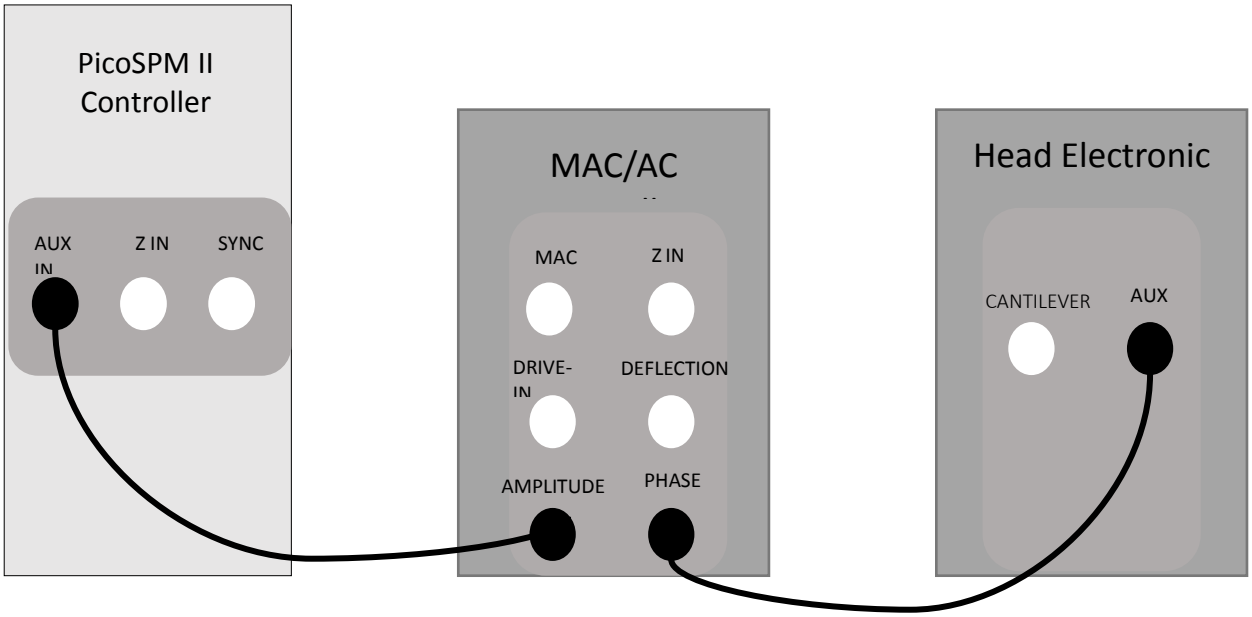

Figure A.1 Cable connections for DLFM.

D. Use the DLFM nosecone with the Keysight 5500 AFM multipurpose scanner for DLFM imaging (Figure A2).

E. Connect the two cables between the PicoSPM II controller, MAC/AC controller, head electronic box as show in Figure A1.

F. Use a silicon nitride contact cantilever (MSCT, Bruker Probes) with force constants of 0.01-0.6 N/m for DLFM imaging.

G. Place the scanner in AFM set up following contact mode instructions in the Keysight operation manual.

H. Adjust the photodiode so that the **Deflection** signal is -1 and the **LFM** is 0 on the scanhead electronics controller.

A.2 Software Set-up

A. Launch the Picoview v1.18 software. Under **main menu**, select contact mode parameters for the Keysight 5500 AFM multipurpose scanner.

B. Create eight channels on the second monitor including trace and retrace of topography, Aux BNC (amplitude) and HEB Aux (phase) on the top/bottom row. The last two channels can be set for deflection and friction of either the trace or retrace signal.

C. Open the AFM AC Mode Tune window and set up the frequency range between 0 to 500 kHz.

D. Enter 0 for the **Force Setpoint** and then start to approach.

E. Image the sample to find an area of interest.

A.3 Frequency Sweep

A. Under the **AC Tune** window, check the box for drive on. Make sure AAC is listed as the drive mechanism. Set drive percentage to 1%.

B. Click the **Manual Tune** button in the **AC Tune** window to acquire a frequency spectrum with the vibration of the tip lateral in relation to the surface.

C. Adjust the **Drive On** until significant, detectable peaks are observed for the frequency sweep, typically around 1 V. Save the frequency sweep as a .txt file for later import into Microsoft Excel for graphing purposes.

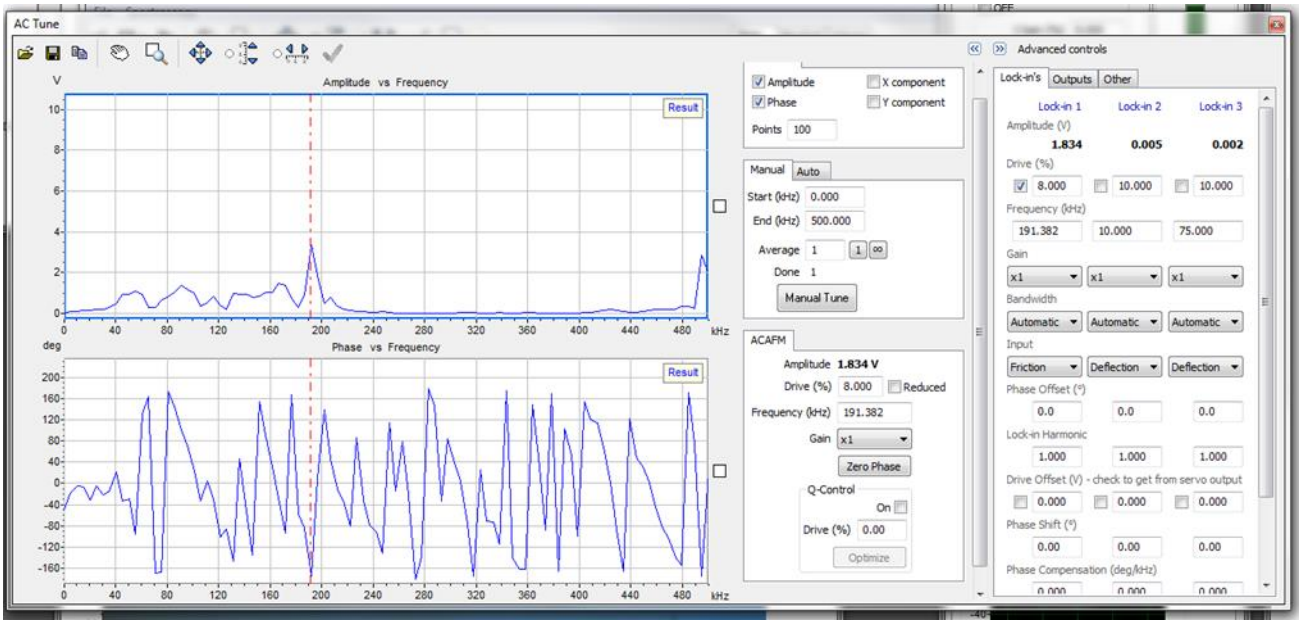

Figure A.2: Spectra obtained from DLFM. Frequency sweep from 0 to 500 kHz. One prominent peak is observed at 191.382 kHz in the frequency sweep (top panel). Corresponding phase spectra (bottom panel.) Drive percent was set to 8%.

D. Choose a resonance frequency in the frequency sweep by moving the vertical red line on top of the resonance peak that has good phase separation. A.4 DLFM imaging

A. Start acquiring DLFM images changing the Integral (I) Gain, the Proportional (P) Gain, the Driving Frequency and the Force Sepoint to tune the images.

B. When running experiments, compare spectra and images with the AC Drive on and the AC Drive off. This can be used to test the experimental setup.

C. During the course of the experiment, try changing resonance frequencies in the frequency sweep and compare the DLFM results.

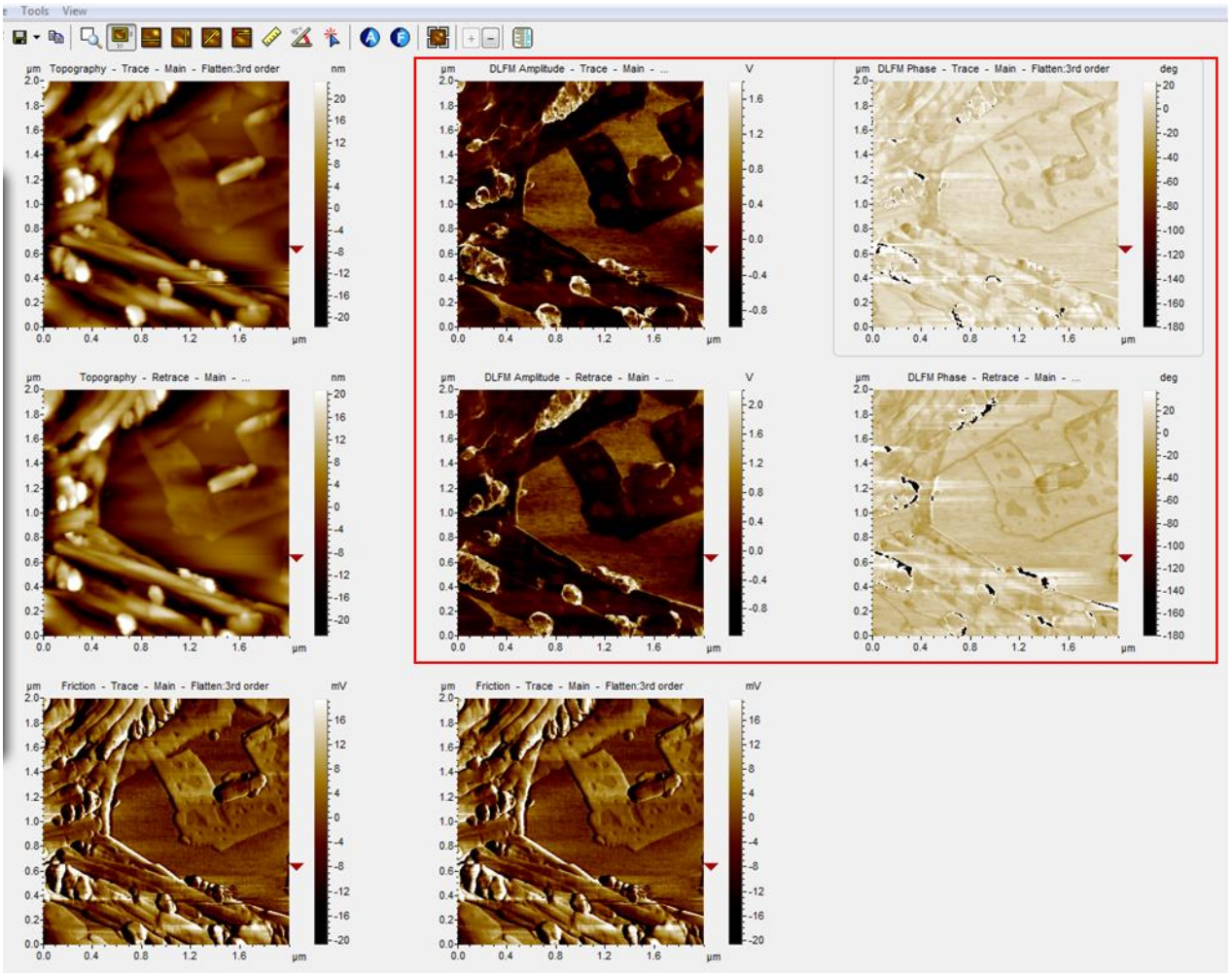

Figure A.3: Imaging window for DLFM AFM. The red box displays the DLFM amplitude (left) and DLFM phase (right) for the trace scan (top panel) and the retrace scan (bottom panel).

APPENDIX B: FORCE MODULATION AFM STUDIES OF PROTEINS

Dynamic lateral force modulation microscopy was used to image nanopatterns of green fluorescent protein bound to MPTMS nanopatterns within a film of 2-[methoxy (polyethyleneoxy)6-9propyl]trichlorosilane (MPT-silane). For DLFM imaging the tip is scanned across the surface in a raster pattern, as an AC bias is applied to a piezoceramic actuator within the nosecone of the scanner. The tip is driven to move in a direction which is perpendicular to the sample. Topography, amplitude, and phase information is acquired simultaneously with DLFM. Surface structures of green fluorescent protein (GFP) viewed with DLFM are shown in Figure B.1. The brighter areas are clusters of GFP in the topography frame (Figure B.1A). The shapes and arrangement of GFP are clearly apparent in the simultaneously acquired amplitude and phase images (Figures B.1B and B.1C).

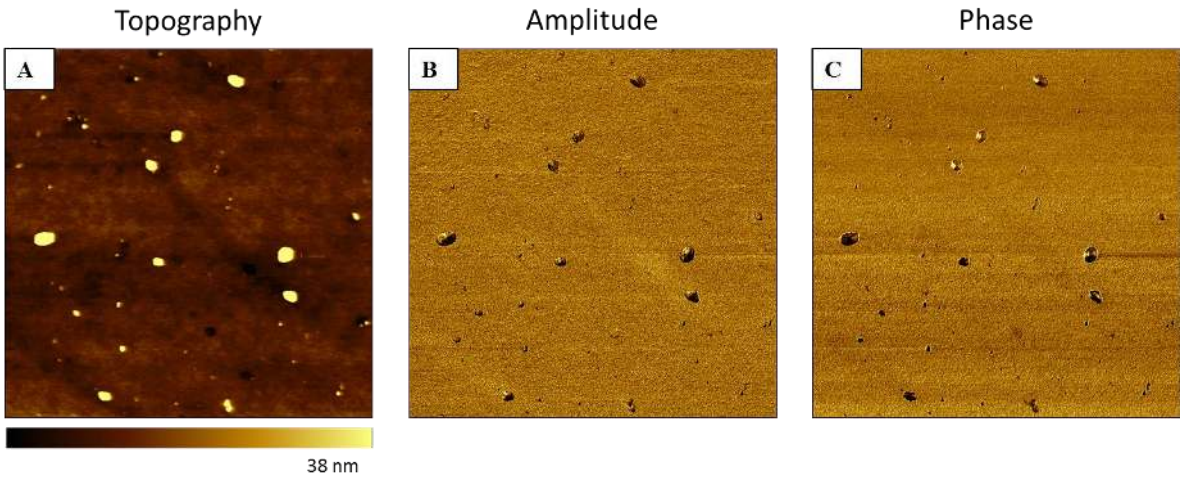

Figure B.1: Green fluorescent protein imagined with DLFM [A] Topography frame; [B] Corresponding amplitude and [C] phase image ($6 \times 6\ \mu m^2$).

Amplitude images do not detect differences in height, instead, changes in the amplitude of tip oscillation indicate the elastic response of tip-surface interactions. The phase images do not correlate with a specific surface property because it is difficult to interpret changes in the phase

angle of the tip-sample vibration. However, phase images can provide sensitive detection of edge effects and sample morphology.

A close up scan of a single GFP cluster is presented in Figure B.2. An individual protein cluster is observed in the topography frame (Figure B.2A). Height scaling differences in the topography frame make it difficult to visualize details of the sample morphology. However, detailed features of the sample are apparent in the simultaneously acquired phase and amplitude channels. The cluster has a round shape, which can be attributed to the convolution of the shape and size of the probe scanned over a very small surface feature.

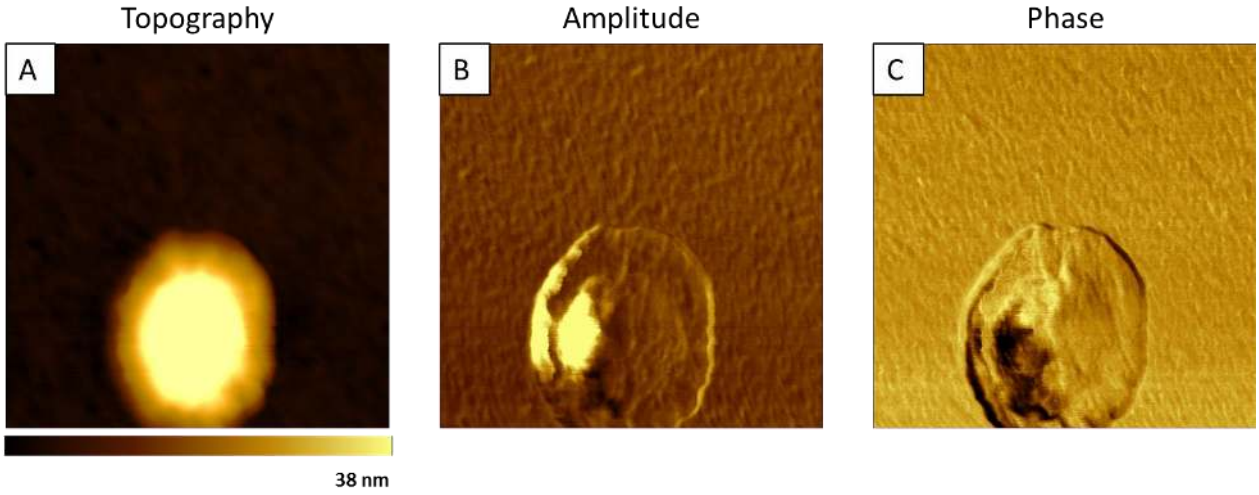

Figure B.2: An individual protein nanocluster imaged with force modulation AFM. [A] A nanocluster of protein shown with a topography frame; [B] Simultaneously acquired amplitude image; [C] Phase channel (500×500 nm^2).

.

APPENDIX C: ADDITIONAL INFORMATION FOR INSTRUCTORS[29]

C.1 Preparation of Substrates

Silicon wafers (1×1 cm2) (Ted Pella, Inc., Redding, CA) were rinsed with ultrapure water (18 MΩ, Millipore, Bedford, MA) then dried and placed in a clean glass jar containing Piranha solution. Piranha solution is a 3:1 (v/v) solution of sulfuric acid and hydrogen peroxide (30%). Peroxide should always be added very slowly to the acid because heat is released. You should handle Piranha solution with caution and use personal protective equipment. Be sure to dispose of the solution according to safety guidelines. Substrates were immersed in Piranha solution for 1.5 h, then rinsed with ultrapure water. After drying, the sample can be stored in a petri dish until needed. Glass slides can also be used as substrates and can be prepared using the same procedure as the silicon wafers. Freshly cleaved mica also is a suitable substrate for particle lithography.

C.2 Preparation of Mesosphere Masks

Monodisperse, size-sorted particles were used as a surface mask for particle lithography. The particles were washed to remove surfactants and possible contaminants using rinsing and centrifugation. A drop (300 μL) of an aqueous solution of latex or silica particles (Duke Scientific, Waltham, MA) was placed into a centrifuge tube, and then filled to a volume of 1 mL with ultrapure water. The solution was centrifuged for 10 min at 14,000 rpm to form a pellet. The supernatant was decanted to leave a precipitate at the bottom of the tube. Ultrapure water was used to refill the centrifuge tube and the pellet was resuspended with vortex mixing. The process was repeated four times. After the last rinsing step, the same quantity of water from the original droplet was added to maintain the initial concentration. In the next step, the solution of particles (10 μL) was deposited onto the Si substrate to ensure that the surface was fully covered by the solution. The substrate was then dried in ambient air.

C.3 Heated Vapor Deposition of OTS

After drying, the samples were placed on a platform in a container with neat OTS. A sealed glass jar or plastic container is suitable as a homebuilt vapor deposition chamber. We made a platform of aluminum foil to keep the OTS liquid from touching the samples. The sealed container was heated at least 8 h at 70° C to generate a vapor. In the next step, to remove the particle masks, samples were rinsed with water and then sonicated in ethanol for 3 min. Next samples were sonicated in fresh ethanol for 15 min, then further rinsed with ethanol and water. After drying, the sample can be imaged with AFM. If the surfaces appear dirty, further steps of cleaning and sonication can be used as needed. Samples prepared on mica substrates should not be sonicated, instead, the samples can be immersed in clean solvent to remove particles of the surface mask.

C.4 Immersion of Particle Masks in OTS Solution

A problem we have encountered when immersing a masked substrate in organosilane solutions is that the particles rapidly detach from the surface. We have solved this problem by heating the samples before the immersion step to temporarily anneal the spheres to the substrate. Latex spheres do not work well for an immersion step because the polymeric particles melt and become deformed. Silica spheres retain their original shape and work well for immersion particle lithography with an annealing step.

The silicon substrates masked with monodisperse silica particles was heated at 150°C for 12 h. After annealing, the samples were cooled to room temperature. The samples were then immersed in an OTS solution (0.1%) in toluene for 8 h. Afterwards, the samples were rinsed with successive steps of sonication in water and ethanol to remove the particle mask.

C.5 Atomic Force Microscopy

Samples were imaged using either contact mode or tapping mode AFM. A Keysight model 5420 or 5500 microscope (Keysight Technologies, Chandler, AZ) was used for AFM studies. Commercial soft tips were used for contact mode AFM which had an average spring constant of 0.5 N/m (Veeco Probes, Santa Barbara, California). For tapping mode experiments, the spring constant of the tip was 48 N/m with a resonant frequency of 190 KHz (Nanosensors PPP-NCL-20, Neuchatel, Switzerland). Digital image processing was done using Gwyddion, which is freely available on the internet and is supported by the Czech Metrology Institute.[255] Surface coverage estimates were done by converting the images into a black and white image and counting pixels with UTHSCA Image Tool.[327]

APPENDIX D: THERMAL K DETERMINATION OF THE TIP FORCE CONSTANT

To obtain quantitative measurements of the interaction forces between the AFM tip and the sample, the tip spring constant must be measured. Due to manufacturing differences, the average value of the tip spring constants reported by the manufacturer are not exactly precise for each probe. For accurate measurement of the spring constant of the tip, a software tool is built into the Keysight 5500 scanning probe microscope. The method models the tip as a thermal oscillator using a triple lock-in amplifier. The protocol for obtaining the spring constant of a tip is outlined as follows from imaging modes that apply contact mode. A force distance curve is used to obtain the deflection sensitivity of the photodiode.

A. Do the test with a sample that is a hard, clean surface, such as mica or bare silicon.
B. Set up the instrument for contact mode imaging. Deflection should be approximately -1 V and lateral force should be approximately 0.
C. With the **Spectroscopy** window, take a force distance curve. Set the max force to 4 and check the "relative" box. This will limit the amount of force that is measured to be approximately four volts to protect the tip from damage.
D. Once the force distance curve is obtained, right click the approach curve in the retractive regime and click "add ruler." This option is shown in Figure D.1.
E. Drag the top dot of the ruler along a straight part of the repulsive regime.
F. Once the ruler is added, right click again and click "Deflection Sensitivity" To calculate the deflection sensitivity of the cantilever.

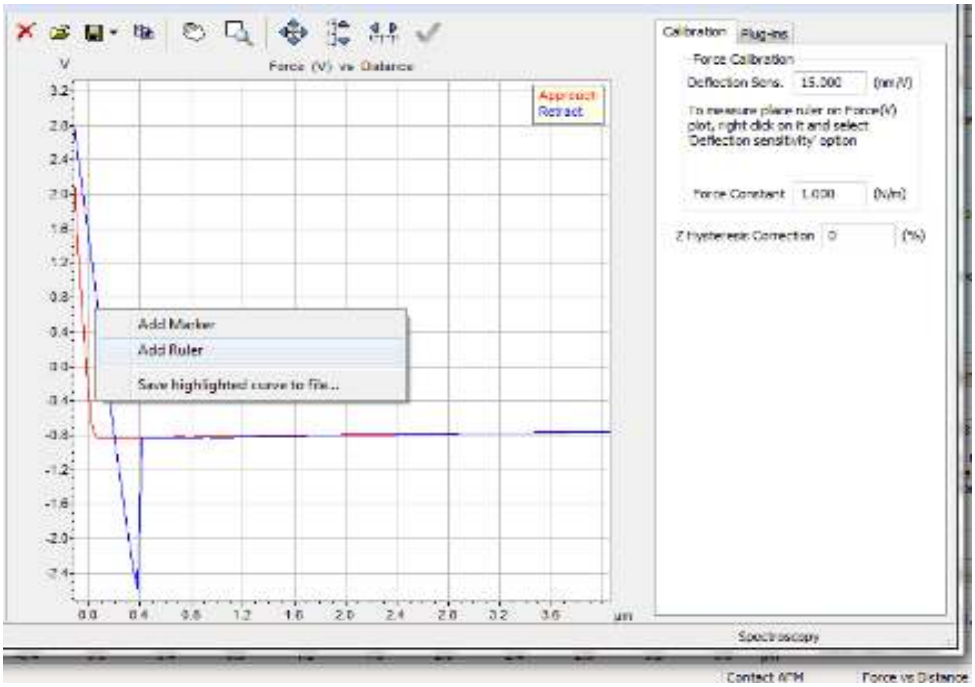

Figure D.1: Once the force distance curve is obtained, right click and select add ruler.

G. Once that is calculated, click on the **advanced** tab.

H. Click on Thermal K.

I. From the window, click **Full Span**, then **Optimize**, then **compute**. The full range of the cantilever will be acquired, then optimize the signal. Once the signal is optimized, the force constant can be computed. Once this process is done, click **apply**. Double check that the cantilever shape is the correct one of the probe you are using, i.e. rectangular or pyramid (Figure D.2).

J. Once the force constant has been applied, a force distance curve can be obtained on a feature of interest in the spectroscopy tab and model fitting can be applied as shown in Figure D.3

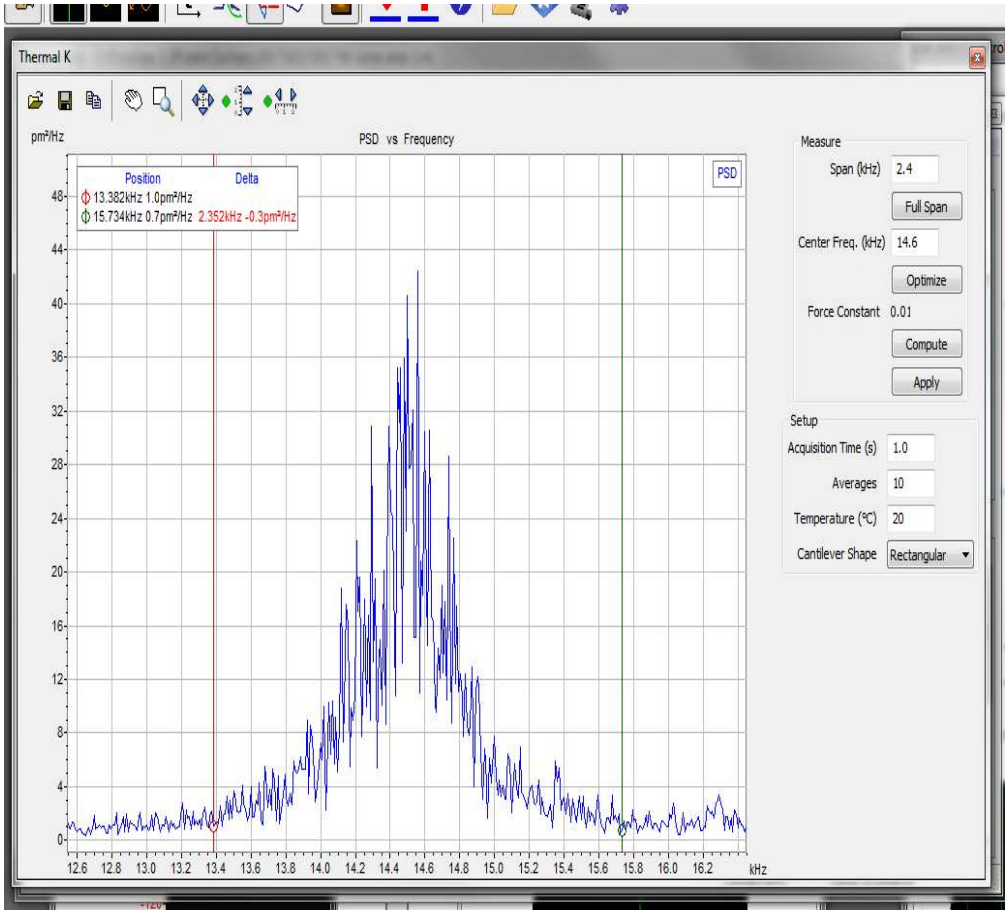

Figure D.2: Example spectra for Thermal K window.

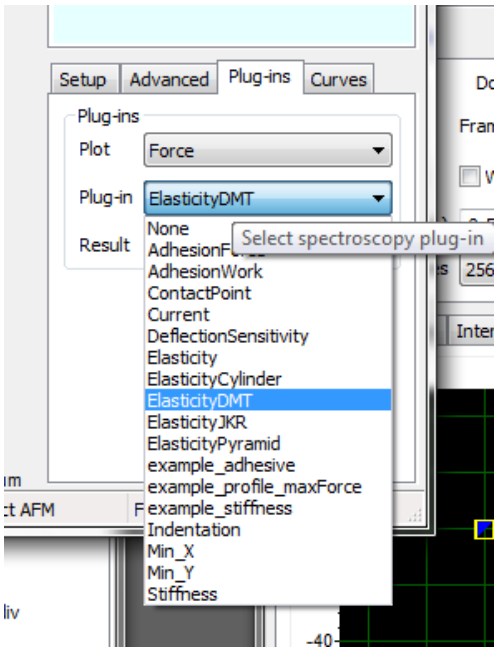

Figure D.3: Plug-ins to calculate different fits to the force distance curve.

APPENDIX E: PERMISSION TO REPUBLISH FIGURES

Permission for works used in reference for Figure 3.1 and Figure 3.2 as found at http://www.futuremedicine.com/page/Permissions.

"Are you planning on using our material in a Thesis/dissertation?

If you are using figure(s)/table(s), permission is granted for use in print and electronic versions of your thesis/dissertation

A full text article may be used only in print versions of a dissertation/thesis. Future Medicine Ltd does not permit the reproduction of full text articles in electronic versions of theses or dissertations."

Permission for works used in reference for Figure 3.3.

From: no-reply@copyright.com
Subject: Thank you for your order with RightsLink / Springer
Date: March 28, 2017 at 9:14 AM
To: zhighl1@lsu.edu

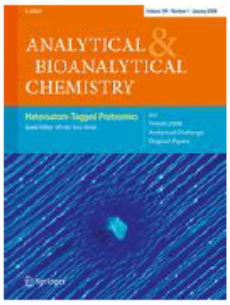

Thank you for your order!

Dear Mr. Zachary Highland,

Thank you for placing your order through Copyright Clearance Center's RightsLink® service.

Order Summary

Order Date:	Mar 28, 2017
Order Number:	4077670332253
Publication:	Analytical and Bioanalytical Chemistry
Title:	Immobilization of proteins on carboxylic acid functionalized nanopatterns
Type of Use:	Thesis/Dissertation
Order Total:	0.00 USD

View or print complete details of your order and the publisher's terms and conditions.

Sincerely,

Copyright Clearance Center

How was your experience? Fill out this survey to let us know.

Tel: +1-855-239-3415 / +1-978-646-2777
customercare@copyright.com
https://myaccount.copyright.com

Copyright Clearance Center RightsLink®

VITA

Zachary L. Highland is a native of Staunton, Virginia. He received his Bachelor of Science degree in Chemistry with a minor in Biology and a concentration in Pre-Pharmacy from Longwood University, Farmville, Virginia in May 2012. He is currently a Ph. D. candidate at Louisiana State University in the department of Chemistry. The Doctor of Philosophy degree is anticipated to be conferred at the May 2017 commencement. Mr. Highland is lead author on three journal articles and is currently coauthor on three more articles. Mr. Highland is an active participate within the American Chemical Society and Alpha Chi Sigma Fraternity. He has also been very active in the teaching of chemistry to undergraduate students throughout his Ph. D. career at Louisiana State University. He has taught a variety of classes and has won the graduate student teaching award three years out of his five year career. In addition, he has also developed online content that is used curriculum wide for the undergraduate general chemistry laboratories. In his research he has made advances in the nanoscale patterning of proteins towards the production of biosensing devices. In addition he has written a laboratory to teach nanoscience through a hands on project for undergraduates in chemistry. He is well sought after in the department for his analytical skills and his teaching abilities. Mr. Highland has made tremendous progress throughout his graduate career and it has set a great preface for his further accomplishments. When not in school Mr. Highland is very active in the Trinity Episcopal Church community serving in various capacities as sub deacon, ringer in the bell choir, and guest organist.